The Pennsylvania State University

The Graduate School

Eberly College of Science

STUDY OF CORRELATIONS IN FRACTIONAL QUANTUM HALL EFFECT

A Dissertation in
Physics
by
Chuntai Shi

© 2009 Chuntai Shi

Submitted in Partial Fulfillment
of the Requirements
for the Degree of

Doctor of Philosophy

August 2009

The dissertation of Chuntai Shi was reviewed and approved* by the following:

Jainendra K. Jain
Erwin W. Mueller Professor of Physics
Dissertation advisor, Chair of Committee

Milton W. Cole
Distinguished Professor of Physics

Nitin Samarth
Professor of Physics

Asok Ray
Distinguished Professor of Mechanical Engineering

Jayanth R. Banavar
Distinguished Professor of Physics
Head of the Department of Physics

*Signatures are on file in the Graduate School.

Abstract

Bulk two-dimensional electron systems in a strong perpendicular magnetic field exhibit the fascinating phenomenon of fractional quantum Hall effect. Composite fermion theory was developed in the process of understanding the fractional quantum Hall effect and was proven to work successfully for the FQHE and even beyond. In this dissertation, we explore the effect of the strong correlation between electrons in several cases. All of them belong to the category of 2DES in strong perpendicular magnetic field and they are listed below:

(i)A fractional quantum Hall island surrounded by a bulk fractional quantum Hall state with a different filling factor. Specifically, we study the resonant tunneling composite fermions through their quasibound states around the island. A rich set of possible transitions are found and the possible relevance to an interesting experiment is discussed. Also, we discuss the subtlety of separating the effect of fractional braiding statistics from other factors.

(ii) Correlated states of a quantum dot, at high magnetic fields, assuming four electrons with two components. Such a dot can be realized by reducing the two lateral dimensions of a 2DES tremendously. Both the liquid states and crystallites (the latter occurring at large angular momenta) of four electrons in terms of composite fermions

are considered. Residual interaction between composite fermions is shown to leads to complex spin correlations.

(iii) Bilayer quantum Hall effect at total filling $\nu_{\boldsymbol{T}} = 5$. This can accommodate an excitonic superfluid state at small layer separations just like at $\nu_{\boldsymbol{T}} = 1$. At large layer separations, however, $\nu_{\boldsymbol{T}} = 5$ state evolves into uncorrelated $\nu = 5/2$ fractional quantum Hall states in both layers, in contrast to uncorrelated composite Fermi sea in $\nu_{\boldsymbol{T}} = 1$ case. We focus on finding the critical layer separation at which the correlation between electrons on different layers are destroyed. Effects due to the finite width of the layers are also considered.

Contents

List of Figures

List of Tables

Abbreviations

2DES	Two-dimensional electron system
CF	Composite fermion
CFC	Composite fermion crystal
CFD	Composite fermion diagonalization
CFFS	Composite fermion Fermi sea
EC	Electron crystal
FQH	Fractional quantum Hall
FQHE	Fractional quantum Hall effect
IQHE	Integer quantum Hall effect
LL	Landau level
LLL	Lowest Landau level
MOSFET	Metal-oxide-semiconductor field-effect transistor
Pf	Pfaffian
QHE	Quantum Hall effect

Dedication

To my late mother, Shulan Wang.

献给我已故去的母亲王淑兰

谁言寸草心

报得三春晖

Chapter 1

Introduction

1.1 Phenomenology

We study in this thesis some types of two dimensional electron system (2DES). As the name suggest, 2DES is a collection of electrons which are constrained to a two dimensional plane. Experimentally, this can be realized by confining the electrons in the interface between two different materials. For instance, 2DES can be confined between semiconductor and insulator in the silicon metal-oxide-semiconductor field-effect transistor (MOSFET), or between two kinds of semiconductors in the GaAs/AlGaAs heterostructure.

Specifically, we are interested in the behavior of a 2DES exposed to a perpendicular magnetic field B. The strength of the magnetic field can be represented by the number of magnetic flux quanta piercing the system

$$N_\phi = \frac{BA}{\phi_0} \tag{1.1}$$

where A is the area of the 2DES and $\phi_0 = hc/e$ is the magnetic flux quantum. It is customary to express all lengths in units of the so-called magnetic length

$$l_{\boldsymbol{B}} = \sqrt{\frac{\hbar c}{eB}} \tag{1.2}$$

The area, in turn, is measure in units of $2\pi l_{\boldsymbol{B}}^2$. In these units, Eq. (1.1) simply tells us that one magnetic flux quantum occupies an area of $2\pi l_{\boldsymbol{B}}^2$. The most important parameter is the filling factor ν which is defined as the ratio between the number of electrons N_e in the 2DES and the number of magnetic flux quanta N_ϕ through it

$$\nu = \frac{N_e}{N_\phi} = \frac{\rho A}{BA/\phi_0} = \frac{\rho\phi_0}{B} \tag{1.3}$$

where ρ is the areal density of the electrons.

The quantum Hall effect (QHE) is observed in transport measurement of 2DES exposed to perpendicular magnetic field. As shown in the inset of Fig. 1.1, a current I_x flows in the x-direction (referred to as longitudinal direction) of the 2DES, and the voltage difference across the y-direction (V_y) and the voltage drop along the x-direction (V_x) are measured. The Hall resistance $R_{xy} = V_y/I_x$ and the longitudinal resistance $R_{xx} = V_x/I_x$ are then determined. In Fig. 1.1, data for both R_{xy} and R_{xx} from an experiment performed in GaAs/GaAlAs heterostructure[1] are shown as functions of the applied magnetic field. The findings of the experiments are: (1) Plateaus form in the R_{xy}-B plot with quantized values $R_{xy}(\nu_0) = \frac{h}{\nu_0 e^2}$ for some special values of ν_0, shown in Fig 1.1. Those special ν_0 fall into two subgroups: integers, and rational fractions $1/3, 2/5, 3/7...$; (2) These plateaus occur around the

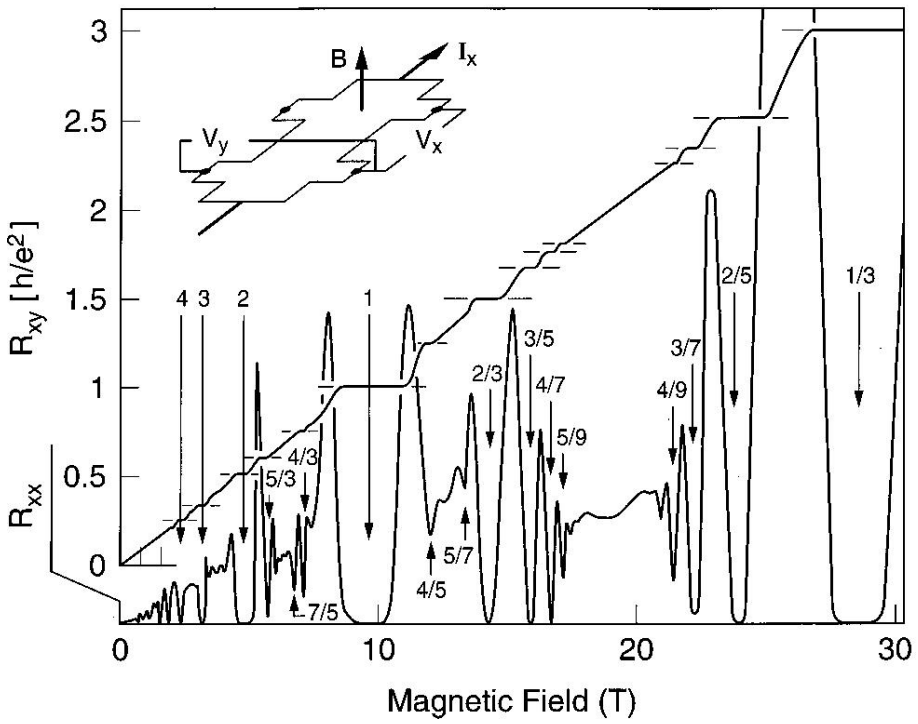

Figure 1.1: The experimental data of quantum Hall effects. The filling factors at which QHE occur are denoted explicitly with a downward arrow pointing into the valley of nearly vanishing, or just minimum for weak QHE states, longitudinal resistance R_{xx}. The corresponding plateaus in the Hall resistance are marked with horizontal bars on the sides for clarity. Source: H. L. Stormer, D. C. Tsui, and A. C. Gossard Rev. Mod. Phys. 71, S298 (1999).

magnetic field at which the filling factor ν of the 2DES equal to the number ν_0 inferred from the resistance value of the corresponding plateau. (3) At the R_{xy} plateaus, the longitudinal resistance R_{xx} drops rapidly, nearly vanishes for cases with a strong effect. We call the phenomenon integer quantum Hall effect (IQHE) when ν_0 is an integer, and fractional quantum Hall effect (FQHE) when ν_0 is a fraction. Historically, the IQHE was discovered in 1980 by von Klitzing et al[2] and the FQHE was first discovered in 1982 by Tsui et al [3].

The integer quantum Hall effect can be understood for a noninteracting 2DES.

The fractional quantum Hall effect, on the other hand, is an intrinsic many-body effect. It would not occur if there were no interactions between electrons. In the next section, we show briefly how the integer quantum Hall effect is explained in terms of one-body quantum physics. Then we move on from there to explain the key ideas to understand the fractional quantum Hall effect in section 1.3.

1.2 The IQHE theory

When an electron is constrained to a two dimensional space and subjected to a magnetic field perpendicular to the plane, its kinetic energy is quantized

$$E_n = \hbar\omega_c \left(n + \frac{1}{2}\right) \tag{1.4}$$

where $\omega_c := eB/m_b$ is the cyclotron frequency of an electron in the magnetic field B(the band mass m_b is used to reflect the fact that all experimentally realized 2DES reside inside some kind of solid). These are the highly degenerate Landau levels(LL). It is found that one state is allowed for each Landau level per unit of magnetic flux quantum. For a noninteracting 2DES with area A, one LL can accommodate $N_\phi = BA/\phi_0$ states. Ignoring the effect of thermal fluctuation, electrons will populate the LLs with the lowest possible kinetic energy. Keep in mind that Pauli's exclusion principle forbids electrons to occupy same state, whcih leads us naturally to the physical meaning of the filling factor ν_0 defined earlier: ν_0 denotes how many LLs are filled at zero temperature.

The Hall plateaus show that R_{xy} takes constant value $h/\nu_0 e^2$ when the filling

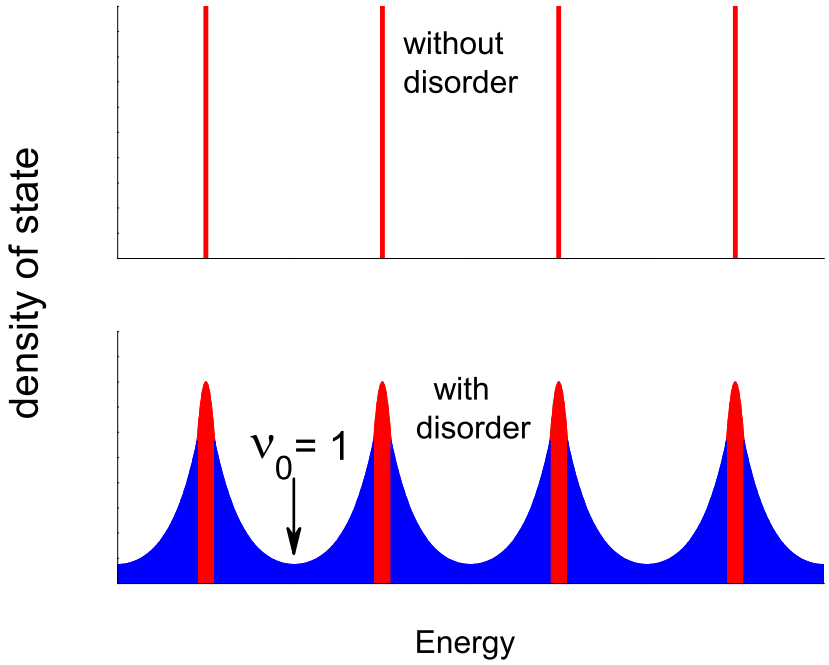

Figure 1.2: The effect of disorder on the density of state for a noninteracting 2DES in perpendicular magnetic field. The red spikes in the top panel denote the Landau levels with huge degeneracy in an disorder free system. The red stripes in the lower panel denotes the disorder broadened LL bands, which consists of delocalized states that are capable of carrying current. The blue region in between LL bands denotes localized states which do not contribute to transport. The position of the Fermi surface for $\nu_0 = 1$ is marked explicitly.

factor ν is varied in a finite range around ν_0. Put differently, addition or removal of a small amount of electrons does not affect the value of the Hall resistance R_{xy} at all. The exponentially small longitudinal resistance R_{xx} when system at $\nu = \nu_0$ indicate that the transport along the edge (along which R_{xx} is measured) is nearly dissipationless. Both features for IQHE can be understood with one-body quantum mechanics. We demonstrate this with the special case $\nu_0 = 1$ as an example in the following.

For an ideal noninteracting 2DES in perpendicular magnetic field, the energy difference between adjacent LLs results in a gap (the cyclotron gap $\hbar\omega_c$) for single particle excitation when the ν is an integer. Fermi energy for such an ideal system is pinned to one of the LL energies. Now we take into account the effect of the disorder, which is always present in a real system. As long as disorder is not very strong, its only effects are to broaden the Landau levels into Landau bands (states within Landau bands are still delocalized and contribute to transport) and produce localized states lying inside the cyclotron gaps (see Fig. 1.2). Only electrons in the delocalized states are responsible for transport, and energy spectrum for them is still gapped (the mobility gap). When the filling factor is close to an integer, e.g. $\nu_0 = 1$ as marked in Fig. 1.2, the Fermi energy lies in the middle of the mobility gap where no delocalized state exists. It is obvious that changing the number of electrons results in shifting Fermi energy. We also know that the transport property of the system is unchanged as long as the Fermi energy still lies inside the mobility gap. Hence, we conclude that altering the filling factor away from $\nu_0 = 1$ by a small amount has no effect on the Hall resistance. This explains the finite width of the Hall plateau at $\nu_0 = 1$. Clearly, similar argument can be made to explain the other IQHE states. In short, the IQHE is just a manifest of the fact that the cyclotron gap survives as a mobility gap when there is mild disorder in the 2DES.

1.3 The FQHE basics

The noninteracting picture given in the last section breaks down in trying to understand the FQHE. For instance, we do not expect a gap in the energy spectrum for a

noninteracting 2DES at $\nu = 1/3$, a FQHE state, even in the absence of disorder. Since all electrons have same kinetic energy, the mismatch between the number of electrons and the LL degeneracy admits enormous many-body states which are degenerate in energy. Apparently, correlation among the motion of electrons due to the electron-electron (e-e) interaction plays an important role in understanding the FQHE. The key is to first find out how a disorder free 2DES at fractional filling factor $\nu_0 = f$ can give rise to a gap in the excitation spectrum then take into consideration the effect of disorder in a manner similar to the IQHE theory: the excitation gap survives as a mobility gap while disorder generates localized states inside the mobility gap.

Historically, the FQHE states at $\nu_0 = 1/m$, where m is an odd integer greater than 1, were understood first. Laughlin proposed a trial wavefunction and showed its lowest excitations have a finite energy [4]. The Laughlin wavefunction was verified to have very high overlap with the exact ground state in small system numerical calculations. This establishes a gap in the many-body energy spectrum in the absence of disorder. Then the idea of the existence of a mobility gap in the presence of mild disorder applies to $\nu_0 = 1/m$ cases as well.

However, FQHE was found experimentally at many other fractional ν_0 which do not belong to this family. Later, Jain put forth the composite fermion (CF) theory which is capable of explaining the FQHE states[5]. The main idea is that each electron in the 2DES captures even number $2p$ of magnetic flux quantum and turns into a composite particle. This new object, which has unit charge and obeys fermionic statistics, is termed composite fermion. Composite fermions experience an

effective magnetic field B^*, which is related to the physical magnetic field via

$$B^* = B - 2p\rho\phi_0 \tag{1.5}$$

Filling factor ν^* for the composite fermion is defined in the same way as the filling factor of electrons

$$\nu^* = \frac{\rho A}{B^* A/\phi_0} = \frac{\rho\phi_0}{B^*} \tag{1.6}$$

but with the effective field B^* in place of the physical magnetic field B. We immediately see the relation between the electron filling factor ν and the CF filling factor ν^*

$$\nu = \frac{\nu^*}{2p\nu^* + 1} \tag{1.7}$$

In principle, B^* can be chosen to be antiparallel to B, in which case, we have $B^* = B - 2p\rho\phi_0$ and $\nu = \frac{\nu^*}{2p\nu^* - 1}$ instead. For the simplicity of presentation, we will always assume B^* and B have same sign in this thesis. Also, we demonstrate the main ideas of composite fermion theory with the simplest and the most important $p = 1$ case.

A natural explanation of the fractional quantum Hall effect emerges from the relations between filling factors of composite fermions and electrons. The integer quantum Hall effect of the composite fermions at ν^*=n, n being an integer, corresponds to the

fractional quantum Hall effect of the electrons at the filling factor

$$\nu = \frac{n}{2n+1} \tag{1.8}$$

Particularly, the IQHE of composite fermions at $\nu^* = 1, 2, 3, ...$ produce the series $\nu = 1/3, 2/5, 3/7, ..$ which are precisely the strongest FQHE states found in experiments (see Fig. 1.1). More specifically, the composite fermions populate their own LLs (termed Λ-levels) with the degeneracy determined by $N_{\phi^*} = B^* A/\phi_0$. For instance, 2/5 FQHE corresponds to the case where composite fermions fill two Λ-levels exactly. The explanation of IQHE we presented in the last section has a natural generalization to the FQHE in composite fermion theory. Just like electrons have to across a cyclotron gap to be excited when the system is at exact integral filling factors, the composite fermions have to across their own cyclotron gap to be excited when an integral number of Λ-levels are filled. Furthermore, the cyclotron gap of composite fermions for disorder free FQHE survives as a mobility gap in the presence of a mild disorder. The finite width of FQHE plateaus are readily explained following reasoning similar to the IQHE case. Namely, the Fermi surface of the composite fermions lies inside one of such mobility gaps and the transport is independent of where exactly the Fermi surface is as long as it does not cross one of the bands of the delocalized states.

Subsequently, the concept of composite fermion was applied successfully to many cases other than bulk FQHE states. For instance, it is found that a Fermi sea of composite fermions develops at $\nu = 1/2$[6]. One can see this by the fact that $B = 2\rho\phi_0$

at this filling factor and the composite fermions experience a zero effective magnetic field B^*.

1.4 Outline of the present work

In this thesis, we study the behavior of three fractional quantum Hall (FQH) systems belong to the category of 2DES in strong perpendicular magnetic field, specially focus on the effect of strong correlation between electrons. After presenting some of the details in theoretical treatment of FQHE physics in chapter 2, a detailed description of these studies is presented with one chapter devoted to each system (chapter 3, 4, 5). In the rest of this section, we give short introductions of those three chapters, each consist of the motivations for studying the particular case and a brief summary of the methods and results.

Chapter 3: It was known long ago that the properties of a doubly connected electron system are periodic in magnetic flux through the region devoid of electrons with periods no greater than one unit of flux quantum[7].For systems with a island of FQHE state at filling factor ν_1 surrounded by another FQHE state at filling factor ν_0, it was predicted that superperiods, periods that are greater than one unit of flux quantum, could occur[8].

The possibility of the superperiods result from the fact that the quasiparticles of the FQHE state are fractionally charged. It was predicted that these fractionally charged quasiparticles obey fractional braiding statistics[9], which was proposed earlier from a pure theoretical viewpoint[10][11] and later formulated in the context of FQHE[9][12]. It regards the change in the Berry phases $\Delta_B = 2\pi\theta^*$ gained upon mov-

ing one particle around a loop, when another identical particle is inserted inside the loop. It is clear that the θ^* would be an even integer if both particles were identical bosons and an odd integer if both particles were identical fermions. It was noticed in Ref. [10] that particles with fractional values for θ^* can exist in principle in two dimensional space. Up to now, the FQHE quasiparticles are still the only candidate as the particles which obey the fractional braiding statistics.

In a very interesting experiment published in 2005[13], observation of quasiperiodic peaks in transport measurement in the FQHE regime was reported. The experimental setup consists of a 2/5 FQHE island surrounded by a 1/3 FQHE sea. The period was identified as a flux change of $5\phi_0$ through the island as a function of the applied magnetic field. In another set of measurements, period of two units of electric charge e was identified as a function of the back gate potential $V_{\mathbf{BG}}$. They interpreted the data as a direct evidence of the existence of the fractional braiding statistics.

We study the resonant tunneling of composite fermions into or from a $\nu_1 = 2/5$ FQH island which are surrounded by a $\nu_0 = 1/3$ FQH bulk state. Composite fermion theory describe the FQHE state in the island as a collection of composite fermions at effective filling factor $\nu_1^* = 2$ and the outside bulk state as composite fermions at $\nu_0^* = 1$. Thus, we could investigate possible transitions inside the island region by studying the possible ways how composite fermions populate their own Landau levels. We find a rich set of such transitions and identify the change of charges in the island and the amount of magnetic flux through the island. Many of these transitions are found to produce superperiods. We also find that creating a $e/5$ charged quasiparticle inside the island always result in another $2e/15$ additional charge at the island edge. Hence

the change of charge in the whole island is $e/3$. This suggest the interpretation[13] of $2e$ charge increment as ten $e/5$ charged quasiparticles is incorrect. Rather, it should be viewed as six $e/3$ charged quasiparticles. Adopting this view, we find that the fractional braiding statistic parameter calculated by using experimental data is inconsistent with the accepted theoretical value. Furthermore, we emphasize that the two types of periods, $5\phi_0$ in flux as a function of the magnetic field and $2e$ as a function of the backgate voltage, are obtained in different type experimental measurements. The measurement of flux period require fixed external potential hence prohibit charge increment in the island. The measurement of charge periods is performed with varying backgate voltage, so there is no restriction on the total amount of charges in the island. This makes it more difficult to extract information about fractional braiding statistics.

chapter 4: We study the two-component quantum dot, which contain only a few electrons,in a perpendicular magnetic field. This model is relevant to various systems which could be realized experimentally. This include the quantum dots made of all kinds of two-component 2DES, for instance, two valley semiconductors (as in the silicon metal-oxide-semiconductor field-effect-transistor), graphene (where electrons reside two inequivalent Dirac points), bilayer 2DES (when the layer separation is small), GaAs/AlGaAs heterostructures with Zeeman energy tuned to be small.

The behavior of quantum dots in a perpendicular magnetic field with spinless electrons was successfully described by composite fermion theory[14], either starting from liquid states and proceeding by CF diagonalization techniques or starting from a solid state with crystal correlation among composite fermions built-in and proceeding by projection on to subspace with well defined quantum numbers.

We show that both approaches can be generalized to the two-component quantum dot. We model the two-component internal degree of freedom by spin. However, no Zeeman coupling between the spin and the magnetic field is included. We first check the efficiency of the mean field theory of composite fermions in predicting the ground states of a two-component quantum dot with four electrons. It is found that mean field theory predicts correct quantum numbers of the ground states for most cases and gives wrong answers for cases where exchange interaction plays an important role. Then we go on to include the effect due to residual interaction between composite fermions by the CF diagonalization (CFD) technique, which is basically a procedure of obtaining the eigenstates of Coulomb interaction within the subspace chosen by mean field consideration. We find that the composite fermion liquid states obtained via CF diagonalization correctly predict most of the ground states and some low-lying excitation states. The exceptions are again the cases where exchange interaction is so strong that some states with high energy in mean field theory is favored when effect beyond mean field consideration is included.

The second type of wavefunctions that we consider have crystal order built-in to begin with. We study these wavefunctions because it is expected that electrons will crystalize in the limit of large angular momentum. First, we write down trial wavefunctions describing electron crystals with spin by generalizing the method of constructing electron crystal wavefunction for spinless systems[15]. These wavefunctions predict all quantum numbers of the ground states correctly and give a good estimate of the energies of the ground states for relatively small angular momentum cases. In large angular momentum range, this kind of elctron crystal wavefunction

can still be written down, but wavefunctions describing crystal formed by composite fermions can be constructed as well. Both type of wavefunctions predict all quantum numbers correctly in large angular momentum cases. By comparing their energies and overlaps to the corresponding exact states, we find that the composite fermion crystal wavefunctions perform better consistently. Furthermore, the residual interaction between composite fermions in two-component model leads to new phenomenon which are unaccessible to the spinless system. In this model with only four electrons, we already see complex nearest- and next-nearest-neighbor spin correlations developed in the crystalline states because of the residual interaction between composite fermions.

Chapter 5: In literature, bilayer FQHE system with a total filling factor $\nu_{\boldsymbol{T}} = 1$ is extensively investigated both theoretically[16, 17, 18, 19, 20, 21, 22, 23, 24, 25, 26] and experimentally[27, 28, 29, 30]. When the separation d between two layers is very small, the $\nu_{\boldsymbol{T}} = 1$ bilayer system ($\nu = 1/2$ for each layer) can be viewed as a collection of excitons, one exciton consists of one electron from one layer and one hole from the other layer. At sufficiently low temperature those excitons condensate into superfluid because they are bosons. At very large d, however, the e-e interaction between electrons in different layers are negligible. Hence no correlation between electrons in different layers are expected. It is understood that $\nu = 1/2$ FQHE system is described by the Fermi sea of composite fermions, so the $\nu_{\boldsymbol{T}} = 1$ system at large d limit is simply two uncorrelated composite Fermi sea.

In this thesis we study the bilayer system at $\nu_{\boldsymbol{T}} = 5$ where phenomenon similar to the $\nu_{\boldsymbol{T}} = 1$ case is expected but with interesting new physics. At small d, we

expect excitonic superfluidity for $\nu_{\boldsymbol{T}} = 5$ system as well. To see this, we first take a look at electrons in one layer. Electrons in the two completely filled LLLs (same spatial states but with opposite spin orientation) can be assumed inert and ignored when analyzing the competing orders of the system. This leaves electrons filling just half of the second LL in each layer. Excitons can be made in the same way as in the $\nu_{\boldsymbol{T}} = 1$ case and similar reasoning for excitonic superfluidity follows. At large d, on the other hand, $\nu_{\boldsymbol{T}} = 5$ system differs from the $\nu_{\boldsymbol{T}} = 1$ system qualitatively. In the former, filling factor for each layer is 5/2. Experimentally, it was found that single layer 2DES at $\nu = 5/2$ show characteristic FQHE features: the quantized Hall resistance $R_{xy} = h/(\frac{5}{2}e^2)$ and reduced longitudinal resistance R_{xx}. In fact, it is the only confirmed FQHE state with filling factor being an even denominator fraction[1]. Lots of studies have focused on the $\nu = 5/2$ state for its potential of being utilized in quantum computation. Theoretically, the most promising candidate wavefunction for $\nu = 5/2$ FQHE state is the so-called Pfaffian wavefunction proposed by Moore and Read[31]. The Pfaffian wavefunction is believed to support quasiparticles which obey non-abelian braiding statistics. Basically, this refers to the observation that multiple degenerate states exist for quasiparticle excitations of Pfaffian wavefunction even if the positions of quasiparticles are fixed. Moving one quasiparticle around another one adiabatically for a complete loop (Braiding quasiparticles) leads to a unitary transformation within the subspace spanned by these degenerate states. It is called nonabelian braiding statistics because two consecutive braiding processes generally lead to different final states when the order of the braiding processes is reversed, i.e.

[1]Recently, evidences of a FQHE state at $\nu = 19/8$ have been reported[32], but it is not conclusive yet.

they do not commute.

Our work concerns the critical value d_C of the layer separation at which interlayer coherence is lost. Specifically, we computed the interaction energies of two wavefunctions, one that show excitonic superfluidity (appropriate for small d systems) and the other with two uncorrelated layers which are both described by the Pfaffian wavefunctions (appropriate for large d systems). For technical reasons, both wavefunctions are constructed within the LLL. To take into account the fact that the relevant electrons reside in the second LL (with $n = 1$) are relevant, we evaluate the interaction energy by calculating the expectation value of an carefully chosen effective interaction with respect to these LLL wavefunctions. The justification of this method is given in chapter 5 and Appendix A and a brief explanation can be found in section 2.3 . The real systems in experiments always have finite width w in the direction perpendicular to the bilayer planes. We included the effect due to the finite layer width by allowing the electron density to be spread in that direction within an infinite depth square well potential with width w. It is of interest to check if Pfaffian state is still the best candidate for $\nu = 2/5$ FQHE when the finite width effect is include. We compared the interaction energy of composite fermion Fermi sea with that of the Pfaffian state and found the latter is favored for systems with w up to 5 magnetic lengths. More importantly, we investigated whether the width of the layers play any role in determining the behavior of the system. Our results indicate that the interlayer coherence is lost when the layer separation exceed a critical value d_C of roughly one magnetic length. This critical layer separation is essentially independent of the width of the layers. Furthermore, we performed exact studies for systems with up to 20 electrons

to verify our prediction. This is necessary because the trial wavefunction approach cannot rule out the possibility that other types of states may become the ground state for systems with intermediate d, which in turn could alter the value d_C. The exact results from these relatively small systems show that interlayer correlations are indeed suppressed rapidly once d exceeds one magnetic length.

Chapter 2

Microscopics of FQHE theory

The microscopic theory is well developed and a comprehensive treatment can be found in the Ref. [33]. Only the concepts which would be used later are given in this chapter.

2.1 Hamiltonian and LLL states

The Hamiltonian for a 2DES with Coulomb interaction between electrons takes the form

$$H = \frac{1}{2m_b}\sum_i \left(\boldsymbol{p} + \frac{e}{c}\boldsymbol{A}\right)^2 + \frac{e^2}{\epsilon}\sum_{i<j}\frac{1}{|\boldsymbol{r}_i - \boldsymbol{r}_j|}, \tag{2.1}$$

where m_b is the band mass of electron and ϵ is the dielectric coefficient. The first term is the kinetic energy and the second term is the Coulomb interaction between electrons. Here we have not included the possible one-body potential and the Zeeman energy term. For the noninteracting 2DES, the second term is absent and the system is fully accounted for by the kinetic energy alone, which gives rise to the famous

Landau levels. The energies of Landau levels are given in Eq. (1.4) with n being the LL index. The wavefunctions of the eigenstates are gauge dependent. It is convenient to study finite size systems using the symmetric gauge $\boldsymbol{A} = B(-y/2, x/2, 0)$. As a result, the angular momentum m is a good quantum number and it can be used to label the degenerated states within the same LL. Also, it is customary to define a complex coordinate $z = (x - iy)/l_{\boldsymbol{B}}$ which is measured in units of the magnetic length $l_{\boldsymbol{B}}$. Then the one-body wavefunction for a n^{th} LL state with angular momentum m is given by

$$\eta_{n,m}(z) = \frac{(-1)^n \sqrt{n!}}{\sqrt{2^{m+1}\pi(m+n)!}} z^m L_n^m \left(\frac{|z|^2}{2}\right) e^{-|z|^2/4} \tag{2.2}$$

where L_n^m is the generalized Laguerre Polynomial. Clearly, $\eta_{n,m}$ generally depend on both z and its complex conjugate z^*. However, the most important case is the LLL one-body wavefunctions

$$\varphi_m(z) \equiv \eta_{0,m}(z) = \frac{1}{\sqrt{2\pi 2^m m!}} z^m e^{-|z|^2/4}. \tag{2.3}$$

and it does not depend on z^* except for the Gaussian factor $e^{-|z|^2/4}$.

In our following discussions, we will always work with electrons residing one single LL. This is justified because the cyclotron gap is typically very large due to the large applied magnetic field. As will be explained in section 2.3, even problems of FQHE in higher LLs can be reformulated as LLL problems with specially chosen effective interactions.

This indicates that the kinetic energy term in the Hamiltonian only contributes

a trivial $\hbar\omega_c/2$ to the energy for each electron and the building blocks for the many-body wavefunction are the LLL one-body wavefunctions. The Gaussian factor in $\varphi_m(z)$ confines the motion of the electron within a finite region. As we can see from Eq. (2.3), the LLL one-body wave function is just a product of the Gaussian factor and a monomial of z. It is found that any many-body LLL wavefunctions has similar property, it must be a product of a polynomial of the complex coordinates z_i of electrons and a Gaussian factor $\exp\{-\sum_i |z_i|^2/4\}$ which confines electrons within a finite region. This provide a guideline in constructing trial wavefunctions for LLL FQH systems, i.e. $\nu < 1$. The simplest many-body wavefunction in LLL with a non-trivial correlation is the celebrated Laughlin wavefunction

$$\Psi_{1/m} = \prod_{i<j} (z_i - z_j)^m e^{-\sum_i |z_i|^2/4} \tag{2.4}$$

for a FQHE system at $\nu = 1/m$, where m is an odd integer.

In practice, for those trial wavefunctions motivated by certain type of explicit correlation between electrons, which contains unwanted z^* in their expressions, a well known projection procedure is performed to get a legitimate wavefunction in LLL[34]. The projection proceeds without changing anything about the Gaussian factor.Firstly, one bring all z^* to the left of all the z. Then replace z^* by a diffraction $2\partial/\partial z$ with the understanding that it do not act on the Gaussian factor.

2.2 Composite Fermion Wavefunctions

Composite fermion theory applies to more general cases outside of Laughlin wavefunction family, e.g. $\nu = 2/5$ bulk 2DES. Recall that a composite fermion consists of an electron and two magnetic flux and electron system at ν can be mapped to composite fermion system at ν^*, determined by Eq. (1.7), we write down trial many body wavefunctions at ν as

$$\Psi_\nu = \mathcal{P}_{\mathrm{LLL}} \Phi_{\nu^*} \prod_{i<j} (z_i - z_j)^2 \tag{2.5}$$

where Φ_{ν^*} is the many-body wavefunction for noninteracting electrons at ν^* and the Jastrow factor $\prod_{i<j}(z_i - z_j)^2$ converts electrons into composite fermions. The LLL projection $\mathcal{P}_{LLL}$ is a standard procedure to project any wavefunction onto the LLL. It is necessary because, Φ_{ν^*} may contain higher LL components because it is written down with the understanding that composite fermions populate Λ-levels. For instance, $\Phi_{\nu^*=2}$ in the expression for the $\nu = 2/5$ FQHE state is made of a Slater determinant with electrons filling two LLs completely. Half of the one-body wavefunctions in the determinant depend on z^* explicitly. The LLL projection [34] proceeds as follows. Firstly, one bring all z^* to the left of all the z within each term without doing anything to the Gaussian factor. Then replace z^* with $2\partial/\partial z$. At the end, evaluate the derivatives with the understanding that they do not act on the Gaussian factor.

It has been verified that composite wavefunctions capture the essence of both the ground states and the excitation states to a surprisingly high precision. Recall from

Eq. (2.3), the angular momentum of the one-body wavefunction is simply the power of the complex coordinates z. In many-body case, the total angular momentum L is given by the summation of the powers of all coordinates $\{z_i\}$. Therefore, the Jastrow factor $\prod_{i<j}(z_i - z_j)^2$ contributes $N_e(N_e-1)$, to L. And we have a relation between the total angular momentum L of the wavefunction Ψ_ν and the total angular momentum L^* of the wavefunction Φ_{ν^*}

$$L = L^* + N_e(N_e - 1) \tag{2.6}$$

2.3 Pseudopotentials

In the case where electrons populate multiple LLs, we assume that the e-e interaction is not strong enough to cause electrons being excited across the cyclotron gap. This is usually a good approximation considering the magnetic field at which FQHE occurs is typically very large. As a result, only the one-body states in the topmost LL are relevant. Haldane has shown that the effects of e-e interaction on a FQH system with many electrons within single LL are completely specified by the so-called pseudopotentials, which concern only two interacting electrons[35]. Pseudopotentials are determined by the relative motion part of the two-body wavefunctions and the type of the e-e interaction in consideration. In the LLL, this can be computed by

$$V_m = \langle \varphi_m(z_r)|V(z_r)|\varphi_m(z_r)\rangle \tag{2.7}$$

where $z_r = z_1 - z_2$ is the complex relative coordinate of the two relevant electrons and m in the relative angular momentum between them. The complex coordinate $Z_c = (z_1 + z_2)/2$ of center of mass is not involved in evaluating the interaction energy. Below we demonstrate how the interaction between electrons within LLL is fully specified by the pseudopotentials V_m.

When the interaction $V(\sum_{i<j} |z_i - z_j|)$ is applied to a many-body state $\Psi(\{z_i\})$, we could always project the wavefunction onto the subspace of the two-body wavefunctions of the i, j -th electrons and exhaust all possible ways $\{i, j\}$ of pairing up electrons. We could further project the resultant two-body wavefunction onto the subspace where the two relevant electrons have definite relative angular momentum m. At the end, we have

$$V(\sum_{i<j} |z_i - z_j|)\Psi(\{z_i\}) = \sum_{i<j} \sum_{m} V_m P_m^{ij} \Psi(\{z_i\}) \tag{2.8}$$

where P_m^{ij} denote the action of the two step projection we just explained.

Similarly, pseudopotentials in the higher LL can be defined the same way as Eq. (2.7) only with the higher LL one-body wavefunctions in place of $\varphi_m(z)$. We will not show the details here. We just give the explicit results for the two cases relevant to our work in chapter 5: the LLL pseudopotentials of Coulomb interaction are given by

$$\left[\frac{1}{r}\right]_m = \frac{\Gamma(m + \frac{1}{2})}{2\Gamma(m+1)} \tag{2.9}$$

and the second LL pseudopotentials of Coulomb interaction are given by

$$\left[\frac{1}{r}\right]_m^{(1)} = \frac{\left(m-\frac{3}{8}\right)\left(m-\frac{11}{8}\right)\Gamma\left(m-\frac{3}{2}\right)}{2\Gamma(m+1)} \tag{2.10}$$

where the notation $[V(r)]_m^{(n)}$ is used to denote the pseudopotentials of the interaction $V(r)$ in the n^{th} LL with relative angular momentum m.

Pseudopotential is particularly useful when we wish to do a calculation with a known type of e-e interaction, say Coulomb interaction $\sum_{i<j} 1/r_{ij}$, and a many-body state Ψ^n in higher LLs. The many-body wavefunctions are most easily constructed in LLL due to the fact that the one-body wavefunctions, in the LLL has much simpler form than their higher LL counterparts. Now suppose we know Ψ^0, the LLL counterpart of Ψ^1, explicitly and we want to calculate the Coulomb energy of the state Ψ^1,

$$\frac{\langle\Psi^1|\sum_{i<j}\frac{1}{r_{ij}}|\Psi^1\rangle}{\langle\Psi^1|\Psi^1\rangle} \tag{2.11}$$

The only thing we need is an effective interaction $V_{\text{eff}}(r)$ which satisfy

$$[V_{\text{eff}}(r)]_m = \left[\frac{1}{r}\right]_m^{(1)} \tag{2.12}$$

for $m = 0, 1, 2, ...$ Namely, all of the LLL pseudopotentials of V_{eff} are equal to respective second LL pseudopotentials of $1/r$. It can be shown that for this effective

interaction

$$\frac{\langle\Psi^1|\sum_{i<j}\frac{1}{r_{ij}}|\Psi^1\rangle}{\langle\Psi^1|\Psi^1\rangle}=\frac{\langle\Psi^0|\sum_{i<j}V_{\text{eff}}(r_{ij})|\Psi^0\rangle}{\langle\Psi^0|\Psi^0\rangle} \tag{2.13}$$

Every thing on the right hand side are known explicitly and the original higher LL problem is casted into a LL problem with an effective interaction.

2.4 Implementation of FQHE wavefunction on spherical surfaces

Up to now, we only talked about the wavefunctions on a disk with a Gaussian factor holds electrons within a finite region. There will always be a edge in such models. To calculate the properties of the bulk 2DES, the ubiquitous edge effects need to be eliminated. This makes the analysis of data very difficult in the disk geometry. A very useful alternative exists for studying the bulk property free from the trouble caused by the edge[35]. We can put electrons on the surface of a sphere which has a magnetic monopole at its center. This way, we have a 2DES free of edge and exposed to perpendicular magnet flux. It was shown by Dirac that the strength of the monopoles are quantized to be an integer[36], denoted by $2Q$ in the following. Wu and Yang[37, 38] have studied in detail the quantum states of a single electron on the surface of a sphere with a monopole of strength $2Q$ at the center. A comprehensive explanation of this issue can be found in Ref. [33] and reference therein. In this thesis, we shall just present it as an alternative of disk geometry for the convenience of calculations. Thus, we are satisfied to just point out how to implement in the spherical

geometry the aforementioned wavefunctions and projection procedure, especially the composite fermion wavefunctions. One body wavefunctions in the LLL in spherical geometry is given by

$$Y_{Qm} = \left[\frac{2Q+1}{4\pi}\frac{2Q!}{(Q+m)!(Q-m)!}\right]^{1/2}(-1)^{Q-m}v^{Q-m}u^{Q+m} \tag{2.14}$$

where the quantum number m can take values $-Q, -Q+1, ..., Q-1, Q$. The "spinor" variables u and v are related to the polar coordinates θ and ϕ via

$$\begin{cases} u = \cos(\theta/2)\, e^{i\phi/2} \\ v = \sin(\theta/2)\, e^{-i\phi/2} \end{cases} \tag{2.15}$$

And the radius R of the sphere on whose surface the 2DES reside is given by $R = \sqrt{Q}l_B$. Now that the surface of the sphere naturally has a finite area $4\pi Q l_B^2$, the degeneracy of each LL is just a finite number, e.g. $2Q+1$ for LLL. In spherical geometry, the wavefunctions no longer have Gaussian factors, for confinement is unnecessary. Any LLL wavefunction is a polynomial of u and v independent of their complex conjugates u^* and v^*, while higher LL states involve u^* and v^* in general. In spherical geometry, projection onto LLL is realized via bringing all u^* and v^* to the left of the u and v then making the replacements $u^* \to \partial/\partial u$ and $v^* \to \partial/\partial v$.

The Jastrow factor in the composite fermion wavefunction now is given by $\prod_{i<j}(u_i v_j - u_j v_i)^2$. Since the magnetic field strength is now denoted by the monopole strength $2Q$, the implementation of the relation between physical magnetic field and effective

magnetic field for composite fermions in the spherical geometry is

$$Q = Q^* + (N_e - 1) \tag{2.16}$$

And the composite fermion wavefunction Ψ_Q is constructed via mapping wavefunction Φ_{Q^*} of a noninteracting system with same number of particles N_e via

$$\Psi_Q = \mathcal{P}_{\mathrm{LLL}} \Phi_{Q^*} \prod_{i<j} (u_i v_j - u_j v_i)^2 \tag{2.17}$$

Chapter 3

Resonant Tunneling in the Fractional Quantum Hall Effect: Superperiods and Braiding Statistics

We study in this chapter the resonant tunneling composite fermions through their quasibound states around a fractional quantum Hall island, and find a rich set of possible transitions of the island state as a function of the magnetic field or the backgate voltage. These have possible relevance to a recent experimental study, and reveal many subtleties involved in deducing fractional braiding statistics.

The work presented in this Chapter was done in collaboration with J.K. Jain. Section 3.1 was reproduced from the paper published in Physical Review Letters[1]. Additional calculations are given in Section 3.2.

[1] J.K. Jain and Chuntai Shi, Phys. Rev. Lett. 96, 136802 (2006)

3.1 Resonant Tunneling in the Fractional Quantum Hall Effect: Superperiods and Braiding Statistics

Properties of an electron system in a doubly connected geometry are periodic in the flux through the region devoid of electrons, with the period being precisely one flux quantum[7] (flux quantum is defined as $\phi_0 = hc/|e|$). An example is Aharonov Bohm oscillations in the resistance of a ring as a function of the magnetic field. Periods smaller than ϕ_0 are in principle possible, and do occur in superconducting rings. It was noted in Ref. [8] that the fractional quantum Hall effect [3] (FQHE) allows for the possibility of superperiods $K\phi_0$ with $K > 1$. The geometry considered therein contains an island of ν_1 FQHE state on the background of a ν_0 FQHE state, and the periodic behavior occurs with respect to the magnetic flux through the island. Given the singly connected geometry, there is no reason, *a priori*, why there ought to be any period, ϕ_0 or otherwise. However, as a result of the incompressibility of the two Hall states, the minimal readjustment of the island is accompanied by a change of an integral number of flux quanta through it, producing, possibly, a superperiod. For example, for a 2/5 island surrounded by the 1/3 sea, a period of $5\phi_0$ was predicted[8].

The unusual period is closely related to the fact that the charge of "quasiparticles" of the FQHE state is fractionally quantized [4]. It is believed that FQHE quasiparticles also obey fractional braiding statistics [10, 11], which refers to the property that the Berry phase associated with a closed loop of a quasiparticle changes, upon insertion of another quasiparticle inside the loop, by $2\pi\theta^*$, with $\theta^* \neq$ integer [39, 12]. Fractional braiding statistics was proposed as a theoretical construct in late 1970's

[10, 11], and FQHE quasiparticles are presently the only viable candidates for its realization. While interesting in its own right, a definitive experimental observation of "abelian" braiding statistics would also appear to be a necessary first step on the way to the more complicated "non-abelian" braiding statistics believed to occur in paired composite fermion states, which has attracted much attention recently [40].

A very interesting experiment of Camino, Zhou, and Goldman[13] has reported quasiperiodic peaks in the FQHE regime. They argue that the peaks occur due to resonant tunneling through quasi-bound states [41] around a 2/5 island surrounded by the 1/3 sea, and estimate that the period corresponds to a flux change of $5\phi_0$ through the island as a function of the magnetic field, and to a change of charge two (in units of the electron charge $e = -|e|$) in the island as a function of the backgate potential $V_{\rm BG}$. They interpret this result as providing a direct observation of fractional braiding statistics. The reasoning, briefly, is as follows[13]. The Berry phase acquired by a "test" quasiparticle for a path encircling the island of area A is assumed to change by 2π between two successive resonant tunnelings. Modeling the test quasiparticle as an object with charge e^* and braiding statistics θ^*, this gives[42], with $\phi_0^* = hc/|e^*| = (|e/e^*|)\phi_0$,

$$-2\pi\frac{\Delta(BA)}{\phi_0^*} + 2\pi\theta^*\Delta N_q = \pm 2\pi \ . \tag{3.1}$$

Here $\Delta(BA)$ is change in the flux and ΔN_q is the change in the number of quasiparticles enclosed by the path between two successive tunneling resonances. Substituting $\Delta(BA) = 5\phi_0$ and $e^*/e = 1/3$ (as appropriate for a negatively charged test quasipar-

ticle in the 1/3 region) gives $\theta^* = 2/(3\Delta N_q)$ or $\theta^* = 8/(3\Delta N_q)$. Identifying charge two with ten charge 1/5 quasiparticles in the 2/5 island ($\Delta N_q = 10$) yields $\theta^* = 1/15$ or 4/15, which was interpreted as the *relative* braiding statistics of the $e^*/e = 1/3$ quasiparticle in the 1/3 state with respect to an $e^*/e = 1/5$ quasiparticle in the 2/5 island.

Our theoretical analysis of the geometry of Ref. [13] shows that, because of a rich set of possible transitions of the island as well as of the island edge effects, an interpretation of the experimental results can be quite subtle and complicated. An alternative theoretical interpretation leads to an unacceptable value for the braiding statistics, and there does not seem to be any fundamental reason why the flux and charge cannot change by the smallest possible units. We speculate, at the end, on one possible scenario for reconciling theory and experiment, but much further work will be needed for a definitive understanding.

Transitions of a FQHE island: The evolution of a FQHE island is rather complicated, but various possibilities can be enumerated in the composite fermion (CF) theory[5]. Composite fermions are bound states of electrons and an even number (taken to be two below) of quantized vortices, and experience a reduced effective magnetic field. They form Landau-like levels in this reduced magnetic field, which will be called "Λ levels."[43] We will consider an island surrounded by the FQHE sea at $\nu_0 = n/(2n+1)$, which has $\nu_0^* = n$ filled Λ levels. The island state will be denoted by $[N_1, N_2, \cdots]$, where N_j is the number of composite fermions in the $(n+j)^{\text{th}}$ Λ level. In particular, $[N_1]$ represents an island of the $\nu_1 = (n+1)/(2n+3)$ (i.e. $\nu_1^* = n+1$) FQHE state. The lowest n Λ levels will be taken to be fully occupied and inert in

Table 3.1: The change in flux, $\frac{\Delta(BA)}{\phi_0}$, the total charge, ΔQ, and the excess charge, Δq, associated with the transition of the FQHE island $[N_1]$ (notation explained in text) into various final states.

final state	$\frac{\Delta(BA)}{\phi_0}$	ΔQ	Δq
$[N_1+1]$	$2n+3$	$n+1$	$1/(2n+1)$
$[N_1,1]$	2	1	$1/(2n+1)$
$[N_1-1]$	$-2n-3$	$-n-1$	$-1/(2n+1)$
$[N_1,-1]$	-2	-1	$-1/(2n+1)$
$[N_1-1,1]$	$-2n-1$	$-n$	0
$[N_1-1,n+1]$	-1	0	$n/(2n+1)$
$[N_1-2,2n+3]$	0	1	1

the entire region of interest, and the number of composite fermions in them (N_0) will be suppressed for notational convenience. We shall assume here the simplest model, neglecting, in particular, the effect of screening at the edge of the island; while one can see such complications destroying simple quasi-periodic behavior, it is difficult to imagine how they could be responsible for it.

A "quasiparticle" of a FQHE state is an *isolated* composite fermion in an excited Λ level, and a "quasihole" is a missing composite fermion from an otherwise full Λ level[5]. The localized charge *excess* (i.e., the charge sticking out of the uniform incompressible state; also called the "local" charge[44]) associated with a CF-quasiparticle of the $\nu_0 = n/(2n+1)$ FQHE state is $1/(2n+1)$ in units of the electron charge [5]. When CF-quasiparticles are far apart, they have well defined fractional braiding statistics with $\theta^* = 2/(2n+1)$ (Refs. [5, 44]). When they are overlapping, however, the braiding statistics is not a meaningful concept; that is intuitively obvious, and also confirmed by explicit calculation [46, 47, 45]. The braiding statistics of CF-quasiparticles is not an additional concept, but a consequence of the physics encoded in the CF theory, and follows from the topological aspect that composite fermions

carry an even number of quantized vortices [45]. The CF theory reproduces the earlier result [12] for quasiholes at $\nu = 1/3$, and enables a microscopic evaluation of θ^* for quasiparticles of 1/3 and other FQHE states [47, 45].

What gives a discrete character to the island state is that it can change only through integral variations in the number of composite fermions occupying various Λ levels. In deducing the corresponding changes in the electronic state, we make use of the following results: In the ν_1 state: (i) the *total* charge per flux quantum is $\nu_1 = (n+1)/(2n+3)$, whereas (ii) the *excess* charge per flux quantum is $\nu_1 - \nu_0 = [(2n+1)(2n+3)]^{-1}$. (iii) From the perspective of the "substrate" FQHE state (ν_0), a composite fermion in any higher Λ level has an *excess* charge of $1/(2n+1)$.

The two "elementary" transitions of a FQHE island are given by the addition of a composite fermion to the island edge ($[N_1] \rightarrow [N_1+1]$) or in a higher Λ level in the island interior ($[N_1] \rightarrow [N_1, 1]$). The excess charge in either case is $\Delta q = 1/(2n+1)$, because a single CF-quasiparticle has been added. The change in the total charge in the island, ΔQ, and the flux passing through it, $\Delta(BA)/\phi_0$, are determined as follows. In the former case the island accommodates the excess charge by expanding to enclose $2n+3$ additional flux quanta, and the total charge increases by $\Delta Q = (2n+3)\nu_1 = n+1$. In the latter case, the excess charge appears in two places: $1/(2n+3)$ in the interior of the ν_1 island, equal to the local charge of the quasiparticle for this state, and $2/[(2n+1)(2n+3)]$ at the boundary. [By definition, when a composite fermion is added in the interior of the island, it shifts the island edge by an amount that encloses two additional flux quanta, giving an excess boundary charge of $2(\nu_1 - \nu_0)$.] The total island charge changes by $\Delta Q = 1$ for the latter case, with $2\nu_1$ coming from the island

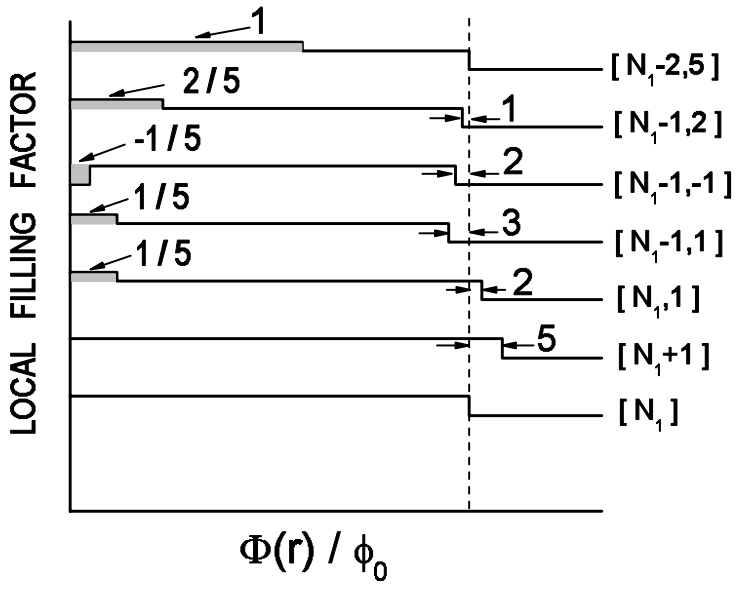

Figure 3.1: Schematic view of several transitions of the 2/5 island discussed in the text. The y-axis labels the local filling factor as a function of the distance r from the center, with different traces offset for clarity (the filling factor on the far right is 1/3 for each trace). The x-axis is the flux through the area enclosed by the disk of radius r ($\Phi(r) = \pi r^2 B$) in units of the flux quantum ϕ_0. The bottom plot labeled $[N_1]$ shows a 2/5 island inside the 1/3 state, with N_1 composite fermions in the second Λ level. Addition of a composite fermion at the boundary in the second Λ level (at the center in the third Λ level) produces $[N_1+1]$ ($[N_1, 1]$), and moving a composite fermion from the boundary to the center results in $[N_1 - 1, 1]$. The top two trace show the density for $[N_1 - 2, 5]$ and $[N_1 - 1, 2]$. The numbers near the shaded regions show the excess charge there. The numbers near the vertical dashed line show the shift in the island edge in units of flux quanta. The density oscillations at the edge and near the charge 1/5 CF-quasiparticle have been suppressed for simplicity. For ease of illustration, the island has been taken to be circularly symmetric, and all quasiparticles are added at the center; changes in area and charge given in the text are more generally valid.

edge and $1/(2n + 3)$ from the interior quasiparticle. The $[N_1] \rightarrow [N_1, 1]$ transition illustrates how apparently simple transitions of composite fermions manifest through rather complicated, nonlocal changes in the electronic state.

$\Delta(BA)$, ΔQ and Δq can be similarly determined due to the removal of a composite fermion from the island edge or interior, or resulting from a combination of several elementary transitions. Many transitions are listed in Table 1 and depicted

schematically in Fig. 1 for the special case of a 2/5 island on the 1/3 substrate. We have also confirmed the basic physics presented in Fig. 1 by extensive calculations with explicit microscopic wave functions for composite fermions.

It may be checked that the transitions in Table 1 are, in general, described by the equation[42]

$$-2\pi\frac{\Delta(BA)}{\phi_0^*} + 2\pi\theta^*\Delta N_q = 2k\pi \ , \tag{3.2}$$

with $\theta^* = 2/(2n+1)$, the braiding statistics of the CF quasiparticles of the ν_0 state[45], and $\Delta N_q = r - s$ for the transition $[N_1] \rightarrow [N_1 - s, r]$. The values of k are given by -1, 0, 1, 0, 1, 1, 2, for the transitions in Table 1, from top to bottom, respectively. The Berry phase change between successive resonant tunnelings can be zero (with the changes in the Aharonov-Bohm and the statistical phases canceling one another), and, under certain constraint, even 4π (an example is given below).

The actual island is likely to be more complicated than that considered above. Depending on the shape of the potential due to confinement *and* disorder, many Λ levels may be occupied and some localized quasiparticles and quasiholes may be present. For example, 3/7 hills or 1/3 lakes can exist inside the 2/5 island. The presence of such non-idealities does not affect the conclusions regarding changes in the size and the charge of the island due to addition or removal of a composite fermion at the edge or in the interior. Also, transfer of a composite fermion from one localized state to another within the interior of the island does not change either its area or its charge.

Relevance to experiment: Returning to the experiment of Ref. [13], the creation of a charge 1/5 particle in the interior of the 2/5 island has associated with it a

charge 2/15 at the island edge, which must also be accounted for in the Berry phase calculation. It is therefore more appropriate to view the charge two as six charge 1/5 quasiparticles in the island interior plus six units of charge 2/15 at the island edge. From the vantage point of the test quasiparticle, this is equivalent to six charge 1/3 quasiparticles. Substituting $e^*/e = 1/3$, $\Delta(BA) = 5\phi_0$, and $\Delta N_q = 6$ into Eq. (3.1) gives $\theta^* = 1/9$ or $4/9$, which now is the braiding statistics for the 1/3 quasiparticles relative to one another. This value in disagreement with the theoretically accepted one. Further insight is gained by noting that, for exterior Berry trajectories, a collection of six charge 1/3 quasiparticles (or, for that matter, ten charge 1/5 quasiparticles) is topologically indistinguishable from two charge one electrons. This points, on the one hand, to a conceptual difficulty with interpreting the result as a measure of the relative braiding statistics of *fractionally charged* quasiparticles; on the other, $\Delta N_q = 2$ produces $\theta^* = 4/3$ or $1/3$ for the braiding statistics of the 1/3 quasiparticle relative to an electron, which also contradicts theoretical result [48].

From a microscopic point of view, the experimental result seems, at first, to correspond to the elementary transition $[N_1] \rightarrow [N_1 + 1]$ (considered in Ref. [8]) for which the island area increases by $5\phi_0$ and its net charge by two units ($\Delta Q = 2$). (Note that $\Delta N_q = 1$ for this transition, because a single composite fermion has been added to the boundary of the second Λ level.) The value $\Delta Q = 2$ appears to be consistent with the observed period in backgate voltage. However, ΔV_{BG} is proportional to the change in the *excess* charge, $\Delta q = 1/3$ (table 1), and not to ΔQ, part of which is due to the increase in the area of the island and counts the charge in the 1/3 substrate that was already present. A change of $\Delta q = 1/3$ between two successive ΔV_{BG} is

presumably too small for the experimental parameters of Ref. [13].

There, however, is no reason why the island transitions as a function of $V_{\rm BG}$ should be the same as those as a function of B, as assumed implicitly above. [Should the transitions be different, only one of ΔN_q and $\Delta(AB)$ in Eq. 3.1 is known for each transition, preventing a determination of θ^*.] The two experiments ought to be analyzed independently. It is also necessary to allow for the possibility of more complex combinations of elementary transitions, which can occur due to energetic considerations arising from the electrostatics of the problem. It seems reasonable that, as a function of B, the charge on the 2/5 island does not change during consecutive transitions (although it is redistributed internally), because that would have a large Coulomb blockade energy associated with it [13]. With what minimum flux change can the island readjust while preserving the total charge inside it? Clearly, that must involve addition of composite fermions in the interior of the island accompanied by removal of composite fermions from its edge. The smallest flux change is ϕ_0, and the associated transition is into $[N_1 - 1, n + 1]$ (table 3.1). Consider next variation of $V_{\rm BG}$. What is the smallest unit of charge that can be added to the island (at a fixed B) without altering its area? One can convince oneself that the transition is into $[N_1 - 2, 2n + 3]$, which implies $\Delta Q = \Delta q = 1$. Both these results are obvious in the compact spherical geometry. The flux through a uniform density ν_1 FQHE state on a sphere (representing the island only) can be changed by ϕ_0 without altering the area or the number of particles, at the cost of creating quasiparticles. Further, a unit charge can surely be added to any FQHE state without changing either the size or the magnetic field (the "electron" goes into a complicated excited state of composite

fermions [49]). In light of this general argument, it is not obvious theoretically why the flux through the island should change in units of $5\phi_0$ and charge in units of two. Incidentally, a transition $[N_1] \rightarrow [N_1 - 2, 2n + 3]$ corresponds to a change of Berry phase by 4π ($k = 2$ in Eq. 2); this "superselection rule" arises from the constraint of fixed area.

We do not know, at this stage, how to reconcile theory and experiment. Several parameters (e.g. the existence or the area of the 2/5 island; the filling factor variation within the island; the relation between $V_{\rm BG}$ and the charge on the island) are deduced indirectly in experiment, making an unambiguous conversion of ΔB and $\Delta V_{\rm BG}$ periods into flux and charge periods difficult. One can therefore ask if the experiment may be consistent with other transitions mentioned above. It is appealing to consider the possibility of the smallest periods. A ϕ_0 period as a function of B would imply, for the experiment of Ref. [13], an island area of $A = 0.2 \times 10^{-8}$ cm^2, which is much smaller than either the lithographic area of the island (3.5×10^{-8} cm^2) or the area corresponding to the ΔB period at $\nu = 1$ (1.5×10^{-8} cm^2). However, a smaller area could perhaps occur either if the peak density in the island is less than the density in the unpatterned sample, or if many disconnected patches of 2/5 exist (as a result of disorder) rather than a singly connected island, with one of them dominating the resonant tunneling process. The smallest period in $V_{\rm BG}$ is produced by the transition $[N_1] \rightarrow [N_1 + 1]$ or $[N_1] \rightarrow [N_1, 1]$, which slightly alters the island area but adds the smallest unit of excess charge ($\Delta q = 1/3$). That corresponds, for the area $A = 0.2 \times 10^{-8}$ cm^2, to $d\rho/dV_{\rm BG} = 1.7 \times 10^8$ cm$^{-2}/V$, which compares favorably to the values at $B = 0$ and $\nu = 1$ (2.4×10^8 cm$^{-2}/V$ and 2.0×10^8 cm$^{-2}/V$,

respectively). Obviously, further work will be needed to clarify the situation. It is noted that possible non-equilibrium or long-time scale effects have been neglected in our analysis.

We close with general comments regarding the relation of such a tunneling experiment to braiding statistics, independent of which transition is responsible for the quasiperiodicity. While all transitions can be consistently interpreted in terms of particles with a braiding statistics of $\theta^* = 2/(2n+1)$ (which is the braiding statistics of CF-quasiparticles of the substrate FQHE state), as evident from the discussion near Eq. 2, one may question, for the following reasons, if any of them can be taken as providing a definitive observation of braiding statistics. For an unambiguous measurement of the braiding statistics it is crucial that the test quasiparticle be well separated from all of the quasiparticles it is encircling. For the transition $[N_1] \rightarrow [N_1+1]$, the composite fermion added at the edge does not qualify as a quasiparticle, but is a part of the ν_1 state (see, for example, the $[N_1+1]$ trace in Fig. 1). For transitions into $[N_1, 1]$ or $[N_1-1, n+1]$, the quasiparticles have an induced part residing at the edge, which interferes with the test composite fermion at the island edge, making the braiding statistics ill-defined[46, 47, 50]. How about the transition $[N_1] \rightarrow [N_1-2, 2n+3]$, where the induced charge at the island boundary has been explicitly removed, leaving only $2n+3$ charge $1/(2n+3)$ quasiparticles in the interior? This also does not enable a measurement of the braiding statistics of quasiparticles because, together, the interior quasiparticles behave as a single electron in their topological properties. It may also be noted that the period can be derived in all cases solely from the knowledge of the values of fractional charges and filling factors in the island and the exterior

regions.

3.2 Addendum

In this section we show the numeric calculations we have done for particular cases outline in previous section.

3.2.1 Addition spectrum in a quantum dot

It is natural to imagine that the Aharonov-Bohm period can be used to measure the fractional local charge of the FQHE quasi-particles, which are composite fermions in an otherwise empty Λ-level. The question was addressed by Goldmann and Renn[52] in mean-field composite fermion theory. In this study, they assumed that composite fermions occupy only two lowest Λ-levels, each of which is filled compactly[55]. And they studied two kinds of quantum dots which are confined by different potentials. In one case the dots are parabolically confined in the sense that every electron subject to a potential quadratic in the position. In the other case they are rigidly confined by a infinite potential barrier of radius R besides a uniformly distributed positive charge. By solving a set of Hartree equations self consistently, they showed that parabolically confined quantum dots displays a $3\phi_0$ period in the chemical potential as the magnetic field changes while sharply confined quantum dots displays $1\phi_0$ period.

As shown in several recent studies[51, 14, 53, 54], the actual ground states of a quantum dot in a high magnetic field is much more complicated and can involve occupation of composite fermions in very high Λ-levels. To see how this affects the results, we have studied small size systems.

The total energy of a specific state in the quantum dot consist of two parts: Coulomb energy and the potential energy from the confinement. These two kind of energy scale differently as the magnetic field changes. Therefore different states get to be the ground state at different magnetic field. The Coulomb energies of composite fermions with different angular momenta are calculated by CF diagonalization. The potential energy is simply related to its angular momentum. By plotting the total energies against the magnetic field for each states(see Fig. 3.2), we could determine the ground state energy of the dot in a range of magnetic field strength. We have calculated the ground state energies of quantum dots with 6,7,8 particles(Only results of 8 particles system is shown in Fig.1). And the chemical potential is simply:

$$\mu(N) = E_g(N) - E_g(N-1) \tag{3.3}$$

which reflects the tunnelling conductance of the system. As we can see from Fig. 3.3 there is no identifiable periodic behavior. Actually, a non-interacting composite fermion theory already implied the possibility of this behavior. In a parabolic potential well. particles with smaller angular momentum has smaller confine energy. Thus a composite fermion might prefer to stay at higher Λ level as long as it gain less energy from effective magnetic field than the confine energy it lowest due to the lower angular momentum. In that case, sometimes composite fermions jump to higher Λ levels when the magnetic field changes and the periodic oscillation in chemical potential is destroyed. This is not in contradiction to the experiment, however,since this $5\phi_0$ superperiod is observed in a sample which contain about 1700 electrons.

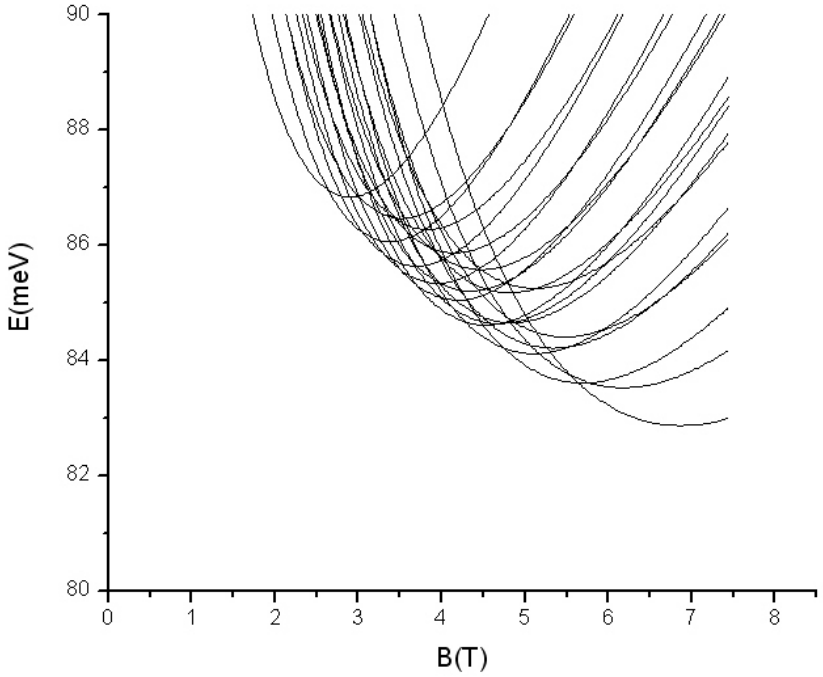

Figure 3.2: Changing of the ground state energy of a 8 electron dot as magnetic field changes. Here a bunch of energy cures corresponding to states with certain angular momentum are plotted. And the Ground state energy at a certain magnetic field is just the lowest energy of all possible states

3.2.2 Superperiod for the 2/5-1/3 geometry

It is likely that the essential physics is being obscured by the presence of the edges of the 1/3 state. To focus on the behavior of the 2/5 island alone, we would like to extend the 1/3 state all the way to infinity. Fortunately, the outer edge can be suppressed by working in the spherical geometry. In this section, we shall not seek the solutions of a Hamiltonian but rather work with composite fermion states of the type $[N_0, N_1]$, which have N_0 composite fermions filling completely the lowest Λ-level, and N_1 composite fermions filling the second Λ-level partially, but compactly, forming a disk surrounding the North Pole. We shall not address the question of what realistic

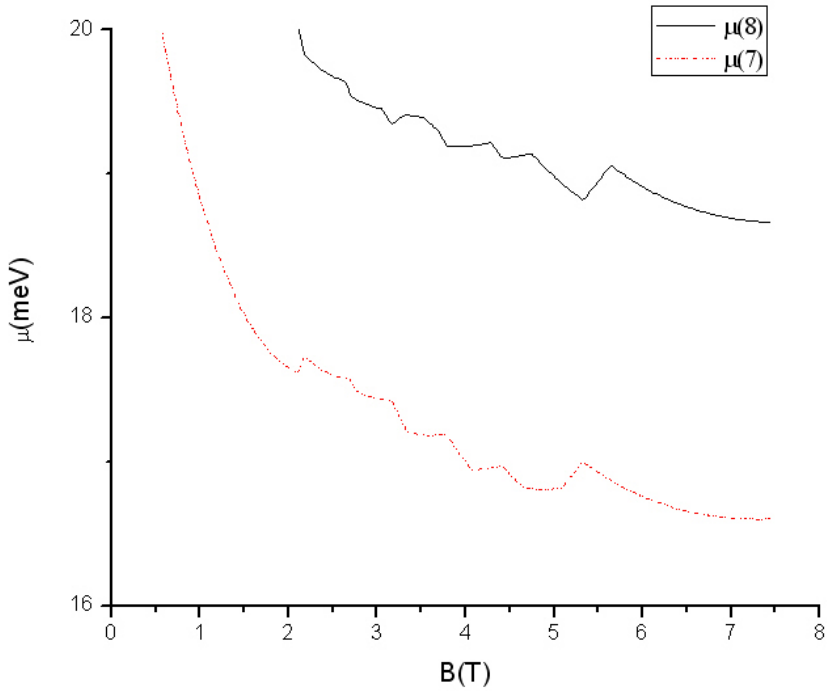

Figure 3.3: Oscillation of Chemical potential for adding the seventh and the eighth particle to the dot as magnetic field changes. Those cusps result from level crossing when the system readjust its charge distribution.

potential would produce such a state, but only investigate what the signature would be. In the next section, we shall slightly relax the restriction.

In the spherical geometry, the degeneracy of the lowest Landau level is 2Q+1 where 2Q is the monopole strength. In Composite fermion theory, each electron captures 2p magnetic flux to convert to composite fermions. Hence the effective magnetic field is reduced to $2q = 2Q - 2p(N-1)$ and the degeneracy of the lowest Λ level is 2q+1. In our calculation, we start from the configuration where the lowest Λ level is completely filled and no composte fermions on the higher levels. Then we prompt composite fermions from lowest Λ level to the second Λ level one by one till the lowest two levels are filled exactly. During this procedure, we always keep the lowest Λ level

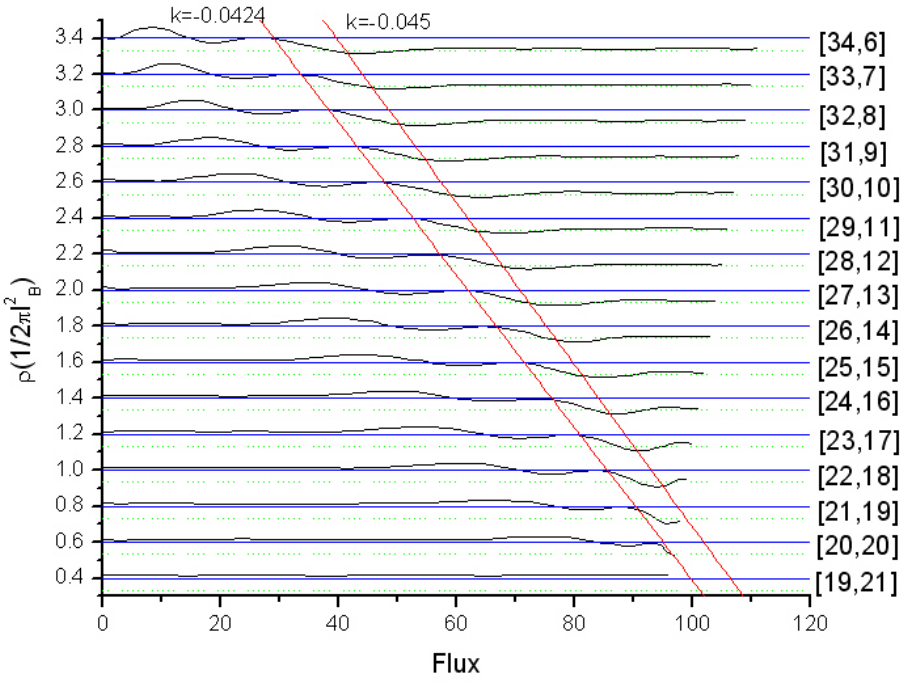

Figure 3.4: Density profiles of a sequence of CF-configurations with one composite fermion is prompted from lowest Λ level to the second level each step. The boundary of the 2/5 island is identified in two ways: the end of 2/5 part of the start of the 1/3(see the text). Each curve is shifted up 0.2 more than the one right beneath it for clarity. Therefore we should see lines with slope $k = 0.2/(-5) = -0.04$ if the increment of the amount of fluxes inside the island in each step is exactly $5\phi_0$.

filled by changing the monopole strength.

For a 40 particles system, the density profiles of the configurations from [34,6] to [19,21] are displayed in Fig. 3.4 . Here the density is in unit of $1/2\pi l_B^2$ and it is plotted against the amount of magnetic fluxes enclosed by a circle around the north pole. In this unit system, the density here could be considered as local filling factors. So we could roughly identify the boundary of the 2/5 island either by the last point where $\rho = 2/5$ or the first point where $\rho = 1/3$. By either criterion, we can see that the amount of magnetic flux inside the island increases $5\phi_0$ approximately each step.

These results demonstrate that prompting one composite fermions from the lowest Λ level to the second Λ level happens under the condition that magnetic field changes a certain amount such that the flux inside the $\nu = 2/5$ island changes by $5\phi_0$. The periodic changing of system configuration in turn result in periodic behavior in its conductance.

3.2.3 Corrections due to CF quasi-particles in higher Λ-levels

In the previous section we assumed that the effect of a variation in the magnetic field is simply to transfer charge from the 1/3 state to the 2/5 island. It may also be possible in experiments that sometimes a composite fermion may go into the third Λ-level, producing states of the form $[N_0, N_1, N_2]$. We now show that so long as such events are rare, regions with well defined period of $5\phi_0$ ought to be identifiable. Specifically, we calculated the system with one, two composite fermions on the third Λ level in addition to the systems studied in last section. As we can see in Fig. 3.5 , the boundary of the island is pushed out in each configuration but the $5\phi_0$ period survives.

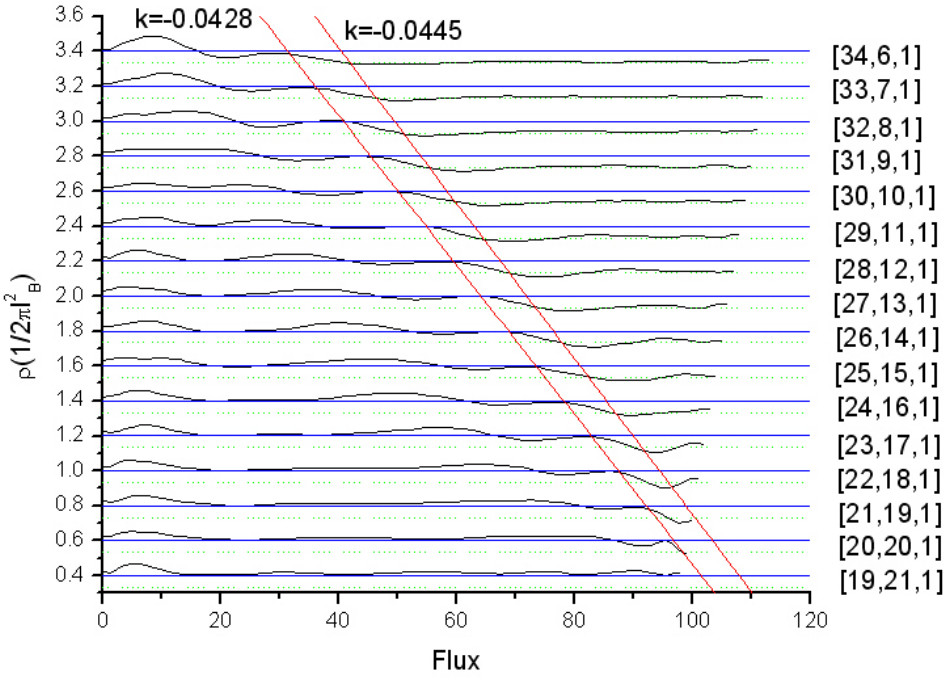

(a)

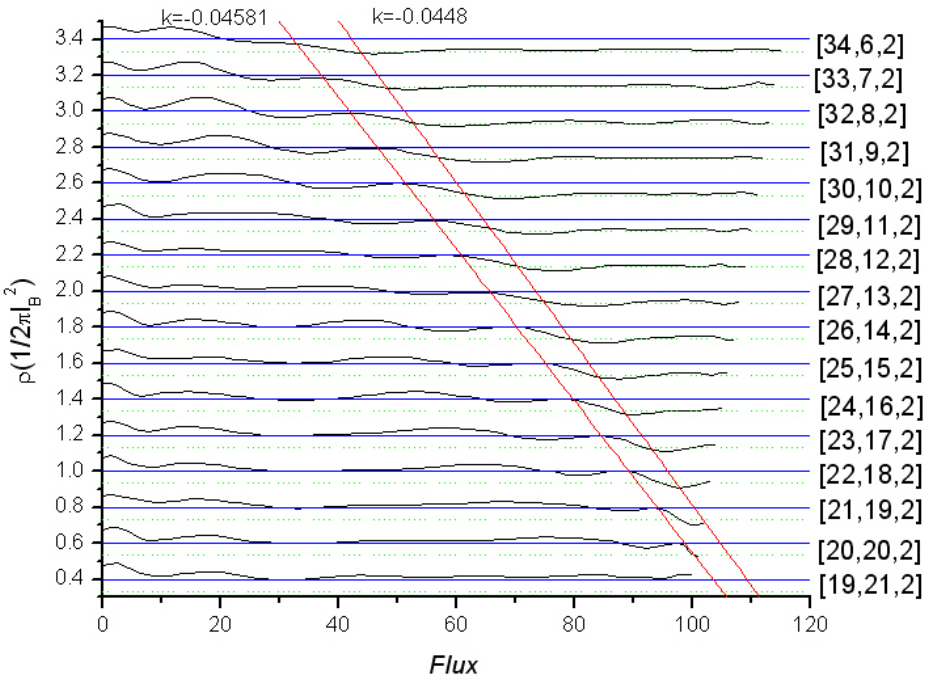

(b)

Figure 3.5: (a)Density profiles of the configurations with one more composite fermions on the third Λ level in addition to those studied in section III.(b)Density profiles of the configurations with two more particles on the third Λ level.

Chapter 4

Composite fermion solid and liquid states in two component quantum dots

In this chapter we consider correlated states of a quantum dot, at high magnetic fields, assuming four electrons with two components. This model has possible relevance to quantum dots in a bilayer system, a two valley system, in graphene, or for ordinary GaAs based quantum dots in the limit of a small Zeeman energy. We show that both the liquid states and crystallites (the latter occurring at large angular momenta) of four electrons are accurately described in terms of composite fermions. The residual interaction between composite fermions is important, however, and causes complex nearest- and next-nearest-neighbor spin correlations in the composite fermion crystallite.

This work was done in collaboration with Gun Sang Jeon and J. K. Jain. The remainder of the chapter is reproduced from the paper published in Physical Review

B[1].

4.1 Introduction

Quantum dots with a few electrons are realized in semiconductor heterostructures by suppressing the lateral size of a two-dimensional electron gas (2DES), and many of their properties have been studied experimentally. [56] Under the application of a sufficiently strong transverse magnetic field, the system becomes fully spin polarized; many theoretical papers have studied this limit by exact diagonalization, [57, 60, 61, 66, 15, 65, 67, 64, 62, 63, 69, 68, 58, 55, 14, 59, 70] by composite fermion (CF) theory, [58, 55, 14, 59, 71] and by other methods. [67, 72, 73, 79, 78, 69, 74, 77, 68, 76, 80, 75, 81, 82]

We ascertain in this chapter the validity of the CF theory for *two*-component electrons confined to a quantum dot, assuming that the Hamiltonian is SU(2) symmetric under rotation in the component space. This model is relevant to several experimentally realizable systems, for example, quantum dots made of semiconductors with two degenerate valleys (for example Si MOSFET), or quantum dots of graphene (where the two components of electrons reside at the different Fermi points). Another system is a bilayer quantum dot, where the layer index plays the role of pseudospin; a perfect SU(2) symmetry is achieved in the limit of vanishing separation between the two layers. The model can also be applicable to the usual GaAs quantum dots at relatively low magnetic fields, because the Zeeman splitting in GaAs is very small – it is approximately 1/70th of the cyclotron energy in the bulk system. (For the

[1]Chuntai Shi, Gun Sang Jeon and Janendra K. Jain, Phys. Rev. B 75, 165302 (2007).

g-factor in quantum dots, we refer the reader to the literature. [83]) Indeed, this observation has motivated a number of previous studies of the zero Zeeman energy limit. [59, 60, 61, 67] The two components are often termed "pseudospins." For economy of language, we will refer to the two components as "spins" in the following; it should be borne in mind, however, that our work applies to any two component system with SU(2) symmetry.

Our principal findings are as follows:

• The mean-field approximation of composite fermions, in which composite fermions are treated as noninteracting fermions with an effective mass, is inadequate for this problem.

• A satisfactory account is achieved when interactions between composite fermions are taken into account through CF diagonalization. In CF diagonalization one usually considers only the CF states with the smallest CF kinetic energy. We find that, for the present problem, it is also necessary to include the fully spin polarized states (even though they may have larger CF kinetic energy). These states are energetically relevant because of their low exchange energy, further indicating the importance of the interactions between composite fermions.

• For large angular momenta, the actual Coulomb ground state of the two-component quantum dot is a crystallite. [60, 61] We show that it is a crystallite of composite fermions. This crystal exhibits complex nearest or next nearest neighbor spin correlations, [60, 61] which can be ferromagnetic or anti-ferromagnetic. The CF theory gives a practically exact account of these spin correlations.

• For fully spin polarized crystals, the crystal symmetry imposes certain con-

straints on the allowed angular momenta. [15, 81] Crystallites are obtained for a larger range of angular momenta when the spin degree of freedom is available.

The validity of the composite fermion theory has been demonstrated for fractional quantum Hall states with partial spin polarization[85], and is intuitively understood because binding of vortices to electrons builds good repulsive correlations. However, that does not necessarily imply similarly good agreement for quantum dots, because of the presence of edges and because of enhanced crystalline correlations in small quantum dots.

The plan of this chapter is as follows. Section II defines the model considered in the rest of the chapter and the composite fermion theory. In Sec. III, mean-field type consideration based on noninteracting composite fermions are discussed. The effect of the residual interaction between composite fermions by means of CF-diagonalization is treated in Sec. IV, where we generalize CF diagonalization to include spin. The crystalline structure is explored in Sec. V, where the exact state is compared with both the CF crystallite and the electron crystallite. This section also contains a derivation of the restrictions on the allowed angular momentum of a crystallite for "spinful" particles, which sheds light on the quantum numbers of the lowest energy states as well as on the spin-spin correlations of the crystalline state.

4.2 Composite fermion theory

The Hamiltonian of interest is given by

$$H = \frac{1}{2m_b}\sum_i \left(\boldsymbol{p} + \frac{e}{c}\boldsymbol{A}\right)^2 + \sum_i V(\boldsymbol{r_i}) + \frac{e^2}{\epsilon}\sum_{i<j}\frac{1}{|\boldsymbol{r}_i - \boldsymbol{r}_j|}, \tag{4.1}$$

where m_b is the band mass of the electron, and the Zeeman energy has been set to zero. The quantity $V(\boldsymbol{r})$ represents the external potential confining the system in the lateral direction, which is modeled below as a parabolic potential, $V(\boldsymbol{r}) = m_b\omega_0^2 r^2/2$. The natural gauge for this problem is the circular gauge, $\boldsymbol{A} = (B/2)(-y, x, 0)$, which is used throughout this work. It is also assumed below that the magnetic field is sufficiently high that it is a good approximation to take electrons to be confined to the lowest Landau level (LLL). This leads to much simplification.

Because of the idealizations, the model is only a first step, and a description of a real quantum dot will likely require a consideration of non-parabolicity of the confinement potential, finite Zeeman energy, and also Landau level mixing. These are outside the scope of our present study. We note that, as shown in Ref. [67], the LLL wave function can be used as an input in a fixed phase Monte Carlo study to investigate the effect of Landau level (LL) mixing.

For a single electron, Eq. (4.1), with parabolic confinement and circular gauge, reduces to the Fock-Darwin Hamiltonian. [86] The single-particle wave function in the LLL can be expressed as

$$\varphi_l(z) = \frac{1}{\sqrt{2\pi 2^l l!}} z^l e^{-|z|^2/4}. \tag{4.2}$$

The complex quantity $z = x - iy$ denotes the position of the electron, l is the angular momentum, and the unit of length is taken as the effective magnetic length $l_B = \sqrt{\hbar/m_b\Omega}$, with $\Omega^2 = \omega_0^2 + (eB/m_bc)^2/4$.

The Coulomb interaction commutes with the total angular momentum L. One therefore investigates the properties of the system as a function of L. The angular momentum of the ground state depends on various parameters, for example the magnetic length or the confinement strength, and level crossings occur as a function of these parameters. Because of the spin degree of freedom, there are twice as many single particle states as for the fully spin polarized problem; as a result, exact diagonalization is possible only for rather small systems. The results below are for four electrons in a quantum dot.

For a two-dimensional electron system exposed to a strong perpendicular magnetic field, the CF theory [87] has been proved to be a very accurate description for fractional quantum Hall systems as well as for lateral quantum dot with only a few electrons. This theory postulates that strongly interacting electrons in the LLL capture an even number of quantized vortices to transform into composite fermions, which are weakly interacting to a good approximation. This suggests the following wave function for interacting electrons

$$\Psi^L = \mathcal{P}\Phi^{L^*}\prod_{i<j}(z_i - z_j)^{2p}. \tag{4.3}$$

Here, Ψ^L is the wave function for interacting electrons at angular momentum L, assuming LLL confinement. Φ^{L^*} is the wave function of weakly interacting electrons

Table 4.1: The dimension of CF Hilbert space, D^*, is compared with the dimension of the full Hilbert space, $D_{\rm ex}$, for a quantum dot containing N=4 particles. The values are tabulated as a function of the total angular momentum L and the total spin S.

	S=0		S=1		S=2			S=0		S=1		S=2	
L	D^*	$D_{\rm ex}$	D^*	$D_{\rm ex}$	D^*	$D_{\rm ex}$	L	D^*	$D_{\rm ex}$	D^*	$D_{\rm ex}$	D^*	$D_{\rm ex}$
18	3	111	3	140	1	34	25	2	270	3	364	0	94
19	3	126	3	165	0	39	26	1	305	0	406	0	108
20	3	148	2	190	0	47	27	1	335	1	455	0	120
21	1	166	1	220	0	54	28	3	375	2	504	0	136
22	1	192	0	250	0	64	29	4	410	4	560	0	150
23	3	214	3	286	0	72	30	7	455	6	616	1	169
24	1	244	1	322	0	84							

at angular momentum L^*, given by

$$L^* = L - pN(N-1)\ ; \tag{4.4}$$

it can have electrons occupying higher LLs. The integer p is chosen to minimize the dimension of Hilbert space of composite fermions at L^*. Physically, $2p$ represent the number of vortices bounded to each electron in a composite fermion. The CF theory thus provides a concrete way to construct correlated wave functions for the electronic state with total angular momentum L. The symbol $\mathcal{P}$ refers to projection of the wave function into the LLL, for which we use the procedure described in Ref. [51].

How does the CF theory help? One considers, at the lowest level of approximation, only the states with the smallest kinetic energy at L^*. The number of such states is much smaller than the total number of LLL basis states $D_{\rm ex}$ at L, leading to an enormous simplification. Upon composite fermionization according to Eq. (4.3), further reduction is sometimes obtained as some of these states are possibly annihilated by LLL projection, and we are left with D^* CF basis states. We tabulate the

Hilbert space dimensions of both CF and exact diagonalizations in Table 4.1 for a range of L and S quantum numbers.

When only a single state is available at L^*, the CF theory provides a unique wave function for the interacting electron ground state. When many states have the same kinetic energy at L^*, it is necessary to diagonalize the Coulomb Hamiltonian in this basis to obtain the low energy states. This is referred to as the "CF diagonalization" (CFD), [51, 88] and incorporates the effect of the residual interactions between composite fermions. CF diagonalization has been performed previously for fully spin polarized electrons [88] and has been shown to give very good results for "single component" quantum dots in strong magnetic fields. [14]

In the following, we include the electron spin into the CFD method. While the essential idea is the same as for the system without spin, one must keep track of the larger dimension of the CF-Hilbert space. To illustrate, we consider the example of a quantum dot with four electrons at total angular momentum $L = 23$. According to Eq. (4.4), this maps into a weakly interacting CF system at angular momentum $L^* = -1$ with $p = 2$. There are six configurations which all have total angular momentum $L^* = -1$, $S_z = 0$, and two units of CF "kinetic energy," as seen in Fig. 4.1. For each configuration in Fig. 4.1, we write a Slater determinant wave function at L^*, and then construct the CF basis according to Eq. (4.3). The CF basis functions constructed in this manner are eigenstates of S_z, but not of the total spin operator. CF diagonalization will produce eigenstates of spin, but we find it convenient to begin with states at L^* that are eigenfunctions of both S_z and $\boldsymbol{S}^2$. Such states are linear

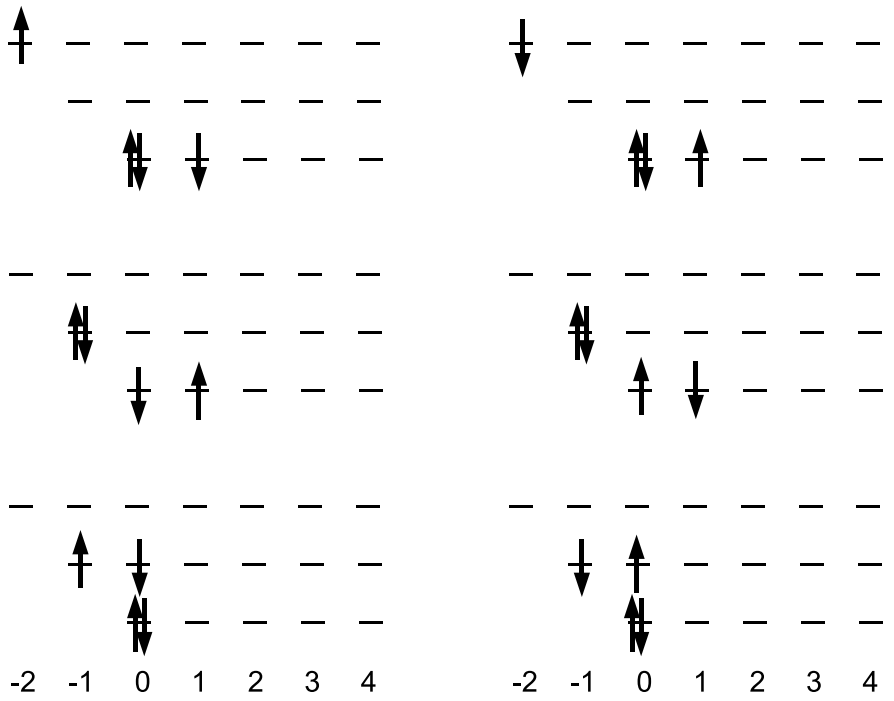

Figure 4.1: The system of four composite fermions at $L^* = -1$, which corresponds to interacting electrons at L=23. In the sector with S_z=0, the six configurations with the lowest CF cyclotron energy ($2\hbar\omega^*$) are shown in this figure. The numbers on the x-axis show the angular momentum of the state, and the different rows in each panel correspond to different CF-LLs. Spin-up (spin-down) composite fermions are shown as $\uparrow$ ($\downarrow$). The total CF cyclotron energy of each configuration is the sum of the CF-LL indices of all electrons.

superpositions of states of the type shown in Fig. 4.1:

$$\Phi^{L^*,S} = \sum_a C_S^a \Phi_a^{L^*}. \tag{4.5}$$

The coefficients of superposition can be determined by either group theoretical methods, or by diagonalizing the Coulomb interaction at L^*; we follow the latter approach. Then, multiplying by the Jastrow factor $\prod_{i<j}(z_i - z_j)^{2p}$ and projecting onto the LLL

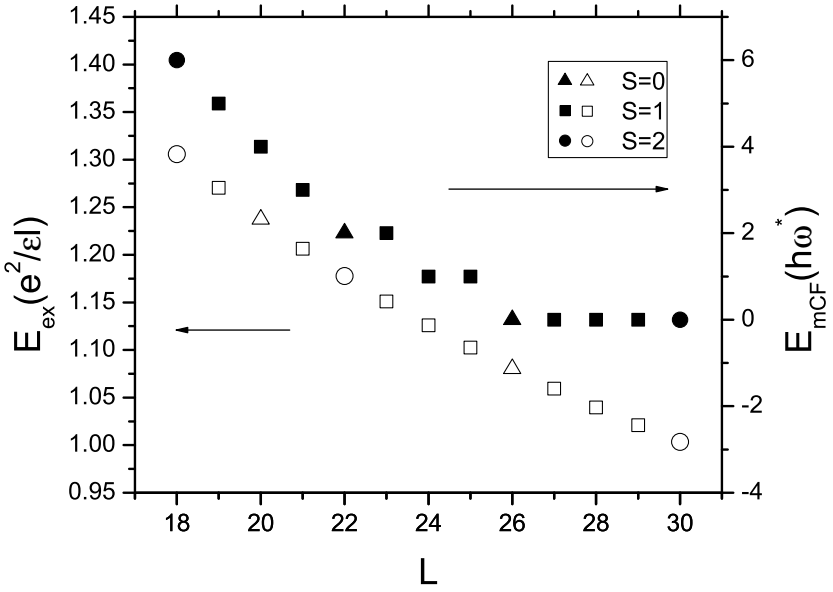

Figure 4.2: The exact ground state energy ($E_{\rm ex}$, left axis, open symbols) and the prediction from the CF mean-field approximation ($E_{\rm CF-MF}$, right axis, solid symbols) as a function of the angular momentum L for N=4 particles. The triangles, squares, and circles denote the total spin (S) values of 0, 1, and 2, respectively. $E_{\rm ex}$ is given in units of $e^2/\epsilon l_B$, while $E_{\rm CF-MF}$ is quoted in units of the CF cyclotron energy $\hbar\omega^*$. For the CF mean-field approximation, whenever there are many candidate ground states with different S, the largest S is assigned to the ground state. $E_{\rm ex}$ is the Coulomb interaction energy; interaction with the background is not included.

gives the wave functions with angular momentum L and total spin S:

$$\Psi^{L,S} = \mathcal{P} \sum_a C_S^a \Phi_a^{L^*} \prod_{i<j} (z_i - z_j)^{2p}. \tag{4.6}$$

In what follows, we perform CF diagonalization with these basis states.

4.3 Mean-field approximation

In the CF theory, it is customary to begin with the simplest approximation, in which the interaction between composite fermions is neglected completely. The interacting electron system then maps into a system of free composite fermions with an effective mass, with the interaction energy between electrons transforming into the "kinetic energy" of composite fermions. The lowest kinetic energy of free fermions at L^* can be evaluated straightforwardly in units of the CF cyclotron energy, shown in Fig. 4.2 by solid symbols for N=4 for a range of L values. When the CF mean-field approximation gives degenerate "ground states" with several S, we assign, guided by Hund's rule, [59] the largest S to the ground state. This figure also shows the exact energy of the Coulomb ground state (open symbols), along with its total spin quantum number, S.

The CF mean-field approximation is generally successful in predicting the ground state spin. L=20 and 22 are exceptions, but even in these cases the spin of a first-excited state, which is almost degenerate with a ground state, is in agreement with the CF mean-field prediction. However, the CF mean-field approximation fails to capture the variation in the ground state energy as a function of L. For example, it predicts cusps at L=22, 24, and 26, while exact E vs. L curve is essentially smooth. This indicates that the CF mean-field approximation is not adequate for our problem, and CF diagonalization is necessary.

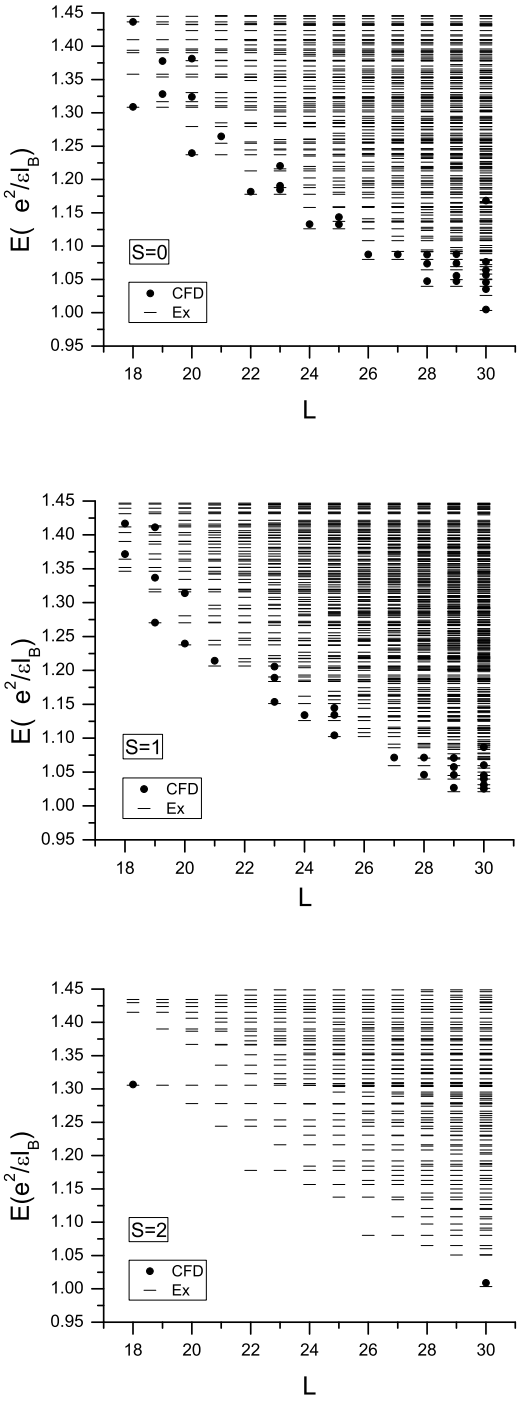

Figure 4.3: Low-energy Coulomb spectrum (dashes) for four electrons as a function of the total angular momentum, L. States with different total spin (S) values are shown in different panels. The predictions from CF diagonalization are shown as solid dots.

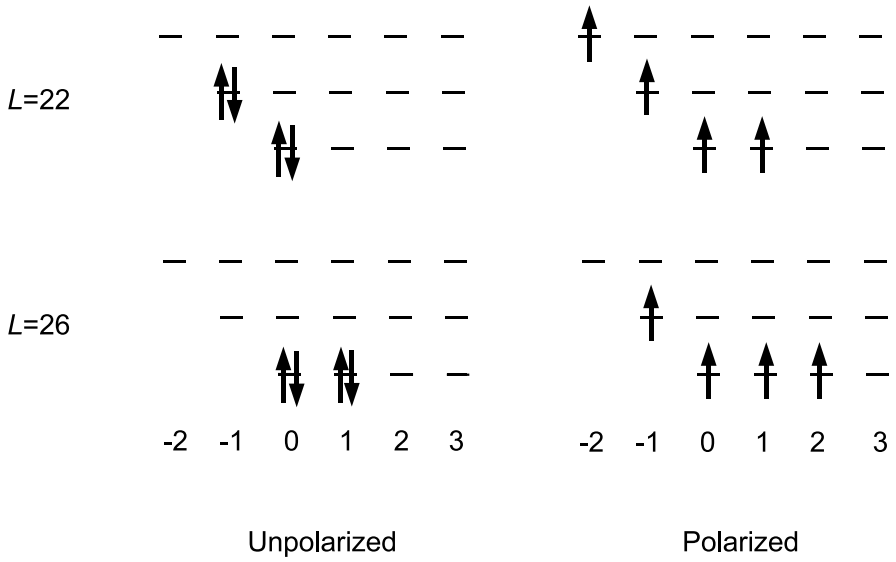

Figure 4.4: For N=4 particles with total angular momentum L=22 and 26 (L^*=−2 and 2 respectively), the mean-field approximation gives unpolarized states (sketched on the left) as the ground states, which have kinetic energies $2\hbar\omega^*$ (for L=22) and zero (for L=26). The fully spin polarized CF states (sketched on the right) at these two angular momenta have kinetic energies $3\hbar\omega^*$ and $\hbar\omega^*$, respectively. Microscopic calculation shows that these fully spin polarized states have similar energies as the unpolarized ones because of exchange effect.

4.4 CF diagonalization results

Figure 4.3 shows how the lowest-order CF diagonalization compares with the exact results in the angular momentum range $18 \leq L \leq 30$. The CF theory accurately reproduces the exact ground-state energies, and also correctly gives the ground state spin.

It is instructive to compare different S sectors separately, as shown in Fig. 4.3. For S=0 and 1, CFD produces positions as well as ground state energies for the cusp states accurately. For L=20 it gives two almost degenerate states, one with S=0 and the other with S=1, as obtained by exact diagonalization method; indeed such a pair

of quasi-degenerate states appear at L=$4n$, which is reproduced in CFD results. In S=2 sector, however, the description is unsatisfactory. While the energies of the states at L=18 and 30 are accurately obtained, the cusp states at L=22 and 26 are missing. We attribute this to the neglect, in the lowest order CF theory, of the exchange interaction between composite fermions, which favors states with larger total spin. As shown in the past, [51, 14] results of fully spin polarized CF-diagonalization agree well with the exact diagonalization results. These states, however, have higher total "kinetic energy" than the ones we used in present calculations (see Fig. 4.4). A good description is thus given by the CF theory for each S, provided that one includes the lowest kinetic energy states in that spin sector for each L. That would produce missing ground states at $S = 2$. (In Fig. 4.3 only the CF states with the *globally* minimum kinetic energy are considered at each L.)

4.5 Composite fermion crystallite

At large angular momenta, electrons form a crystalline structure to minimize the interaction energy [14, 60, 89, 15, 90] The Hartree-Fock crystal of electrons is obtained by placing electrons in the LLL at the positions of a classical crystal, and then anti-symmetrizing the wave function. The maximally localized wave packet of an electron at position Y is given by [91]

$$\Phi(z, Y) = \frac{1}{\sqrt{2\pi}} e^{-\frac{1}{4}(|z|^2+|Y|^2)} e^{\frac{1}{2}zY^*} . \tag{4.7}$$

This should be an increasingly better wave function as the distance between nearest neighbor electrons becomes large compared to the magnetic length. Such a wave function does not have a definite total angular momentum, however. In fact, each Gaussian is a coherent superposition of all states in the LLL (the only exception being when $Y = 0$, which simply produces the state with angular momentum $l = 0$). Thus, the Hartree-Fock wave function can be expanded as a superposition of states with various L values. Following Yannouleas and Landman, [15] we take the projection of this wave function onto a definite L value as the electron crystal (EC) trial wave function. Because of the rotational symmetry, the crystal structure is not apparent in the density in the projected wave function, but is revealed in the pair correlation function.

For four electrons, the classical analysis shows that four particles with Coulomb interaction form a crystal which has four particle on the corners of a square. The quantum electron crystal consists of four Gaussians in LLL centered at the complex coordinates R, iR, $-R$, and $-iR$, denoted as $Y_j, j = 1, 2, 3, 4$ respectively

$$\Phi(z, Y_j) = \frac{1}{\sqrt{2\pi}} e^{-\frac{1}{4}(|z|^2+R^2)} e^{\frac{1}{2}zR(-i)^{j-1}}. \tag{4.8}$$

For fully spin polarized electrons, the many body wave function can be expanded

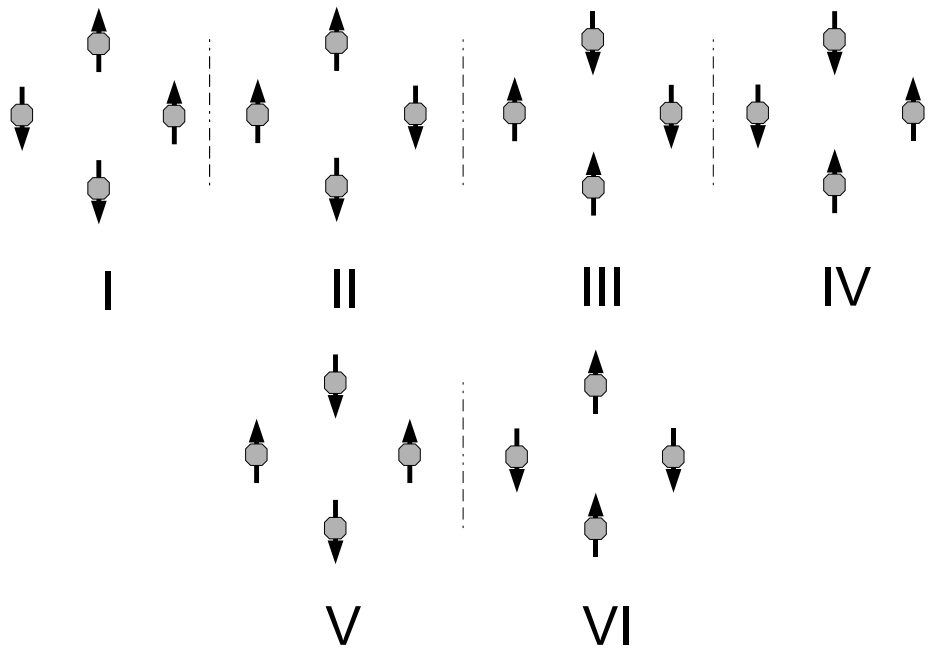

Figure 4.5: At large angular momenta, the particles (represented by fill dots) tend to form a crystal. For four particles, they localize on the corners of a square. [81] The six configurations with S_z=0 are shown. The last two have antiferromagnetic nearest neighbor correlations, whereas the rest have a combination of ferromagnetic and antiferromagnetic nearest neighbor correlations.

using the basis state $D(l_1, l_2, l_3, l_4)$, defined as

$$D(l_1, l_2, l_3, l_4) \equiv \begin{vmatrix} \varphi_{l_1}(z_1) & \varphi_{l_1}(z_2) & \cdots & \varphi_{l_1}(z_4) \\ \varphi_{l_2}(z_1) & \varphi_{l_2}(z_2) & \cdots & \varphi_{l_2}(z_4) \\ \vdots & \vdots & \ddots & \vdots \\ \varphi_{l_4}(z_1) & \varphi_{l_4}(z_2) & \cdots & \varphi_{l_4}(z_4) \end{vmatrix} . \tag{4.9}$$

The resulting wave function, which is projected onto the subspace with total

angular momentum L, is given by [15]

$$\begin{aligned}
\Psi^L(z_i) &= \sum_{l_1,l_2,l_3,l_4}{}' D(l_1,l_2,l_3,l_4)\frac{1}{\sqrt{2^L l_1!l_2!l_3!l_4!}} \\
&\quad \times R^L e^{-2R^2} 1^{l_1} i^{l_2} (-1)^{l_3} (-i)^{l_4} \\
&= \frac{1}{\sqrt{2^L}} R^L e^{-2R^2} \sum_{l_1<l_2<l_3<l_4}{}' D(l_1,l_2,l_3,l_4) \\
&\quad \times \frac{1}{\sqrt{l_1!l_2!l_3!l_4!}} \begin{vmatrix} 1^{l_1} & 1^{l_2} & \cdots & 1^{l_4} \\ i^{l_1} & i^{l_2} & \cdots & i^{l_4} \\ \vdots & \vdots & \ddots & \vdots \\ (-i)^{l_1} & (-i)^{l_2} & \cdots & (-i)^{l_4} \end{vmatrix},
\end{aligned} \tag{4.10}$$

where the prime denotes the restriction

$$\sum_{i=1}^{4} l_i = L. \tag{4.11}$$

We generalize this method to take into account the spin degree of freedom. Just as in exact diagonalization, we set the z-component of total spin, S_z, equal to zero without any loss of generality, which amounts to taking two electrons with spin up and two with spin down. The six resulting configurations are shown in Fig. 4.5. (This should be contrasted with the fully spin polarized crystal, which produces a single configuration.) The antisymmetrized wave function is given by (taking two spin up states, $\varphi_{l_1}\alpha$ and $\varphi_{l_2}\alpha$, and two spin down states, $\varphi_{l_3}\beta$ and $\varphi_{l_4}\beta$; α and β are spinors)

$$D(l_1,l_2;l_3,l_4)= \begin{vmatrix} \varphi_{l_1}(z_1)\alpha_1 & \varphi_{l_1}(z_2)\alpha_2 & \cdots & \varphi_{l_1}(z_4)\alpha_4 \\ \varphi_{l_2}(z_1)\alpha_1 & \varphi_{l_2}(z_2)\alpha_2 & \cdots & \varphi_{l_2}(z_4)\alpha_4 \\ \varphi_{l_3}(z_1)\beta_1 & \varphi_{l_3}(z_2)\beta_2 & \cdots & \varphi_{l_3}(z_4)\beta_4 \\ \varphi_{l_4}(z_1)\beta_1 & \varphi_{l_4}(z_2)\beta_2 & \cdots & \varphi_{l_4}(z_4)\beta_4 \end{vmatrix} . \tag{4.12}$$

Projection of each of these states onto a definite L can be handled similarly to the fully spin polarized case. For example, the projection of the configuration I of Fig. 4.5 onto subspace with total angular momentum L is

$$\begin{aligned} \Psi_I^L(z_i) &= N(L,R) \sum_{l_1,l_2,l_3,l_4}{}' D(l_1,l_2;l_3,l_4) \frac{1}{\sqrt{l_1!l_2!l_3!l_4!}} \\ &\quad \times 1^{l_1} i^{l_2} (-1)^{l_3} (-i)^{l_4} \\ &= N(L,R) \sum_{l_1<l_2;l_3<l_4}{}' D(l_1,l_2;l_3,l_4) \frac{1}{\sqrt{l_1!l_2!l_3!l_4!}} \\ &\quad \times \begin{vmatrix} 1^{l_1} & 1^{l_2} \\ i^{l_1} & i^{l_2} \end{vmatrix} \times \begin{vmatrix} (-1)^{l_3} & (-1)^{l_4} \\ (-i)^{l_3} & (-i)^{l_4} \end{vmatrix} , \end{aligned} \tag{4.13}$$

where $N(L,R)$ is the normalization factor and the prime above the summation still represent the restriction that $\sum_{i=1}^{4} l_i = L$.

In the fully spin polarized case, [15] the projection vanishes except for certain periodically spaced "magic angular momenta," which correspond to cusp states in the exact spectrum. [81] With spin we have more than one candidate state for a crystal, as shown in Fig. 4.5 for N=4. At least one of these states survives the projection at any value of total angular momentum L. In fact, the projection often

produces more than one nonvanishing state, and we diagonalize Coulomb matrix in the space spanned by the states and obtain the energy $E_{\rm EC}$ and the wave function $\Psi^L_{\rm EC}$ for EC state. Although none of the candidate states we started with is an eigenstate of the total spin operator, the states obtained after diagonalization are eigenstates of the total spin operator since the Hamiltonian and the total spin operator commute. The expectation value of the spin operator $\boldsymbol{S}^2$ for the eigenstates is calculated by expressing it in terms of the matrix elements of $\boldsymbol{S}^2$ relative to the Slater determinant states of Eq. (4.12).

We find that for odd L the crystal has S=1, whereas for even L crystals with two different spins are obtained (with S=0, 1 for L=4n, and S=0, 2 for L=4n+2). The total spin values for $18 \leq L \leq 30$ are tabulated in Table 4.2, which agree with the spins of the nearly degenerate ground states in the exact spectrum, also studied in Ref. [60].

4.5.1 Composite fermion crystal

It has been shown that for fully spin polarized electrons in a quantum dot at high magnetic fields, the crystallite is a crystallite of composite fermions. [14, 90, 71] It is interesting to check if that also holds in the zero Zeeman energy limit. In the spin-polarized case, the wave function for a CF crystal, $\Psi^L_{\rm CFC}$, at angular momentum L is constructed by composite-fermionizing the electron crystal wave function, $\Psi^{L^*}_{\rm EC}$, at angular momentum L^*:

$$\Psi^L_{\rm CFC}(z_i) = \Psi^{L^*}_{\rm EC}(z_i) \prod_{j<k} (z_j - z_k)^2 \,. \tag{4.14}$$

Table 4.2: The values of total spin (S) for which an electron crystal (EC) wave function exists for a given L.

L	18	19	20	21	22	23	24	25	26	27	28	29	30
S	2,0	1	0,1	1	2,0	1	0,1	1	2,0	1	0,1	1	2,0

Table 4.3: Comparison of the CF crystal (CFC) and electron crystal (EC) wave functions with the exact Coulomb ground states in the angular momentum range $20 \leq L \leq 22$ for several values of the total spin S. The quantities $E_{\rm ex}$, $E_{\rm CFC}$, and $E_{\rm EC}$ are the Coulomb energies of the exact, CF crystal, and electron crystal states. (The energies are in units of $e^2/\epsilon l_B$.) $\mathcal{O}_{\rm EC} = |\langle\Psi_{\rm EC}|\Psi_{\rm ex}\rangle|/\sqrt{\langle\Psi_{\rm EC}|\Psi_{\rm EC}\rangle\langle\Psi_{\rm ex}|\Psi_{\rm ex}\rangle}$ and $\mathcal{O}_{\rm CFC} = |\langle\Psi_{\rm CFC}|\Psi_{\rm ex}\rangle|/\sqrt{\langle\Psi_{\rm CFC}|\Psi_{\rm CFC}\rangle\langle\Psi_{\rm ex}|\Psi_{\rm ex}\rangle}$ are the overlaps of the electron crystal and the CF crystal wave functions with the exact ground state wave function.

L	S	$\mathcal{O}_{\rm EC}$	$\mathcal{O}_{\rm CFC}$	$E_{\rm ex}$	$E_{\rm EC}$	$E_{\rm CFC}$
20	0	0.9512	0.991	1.237174	1.250724	1.2388
20	1	0.9551	0.993	1.237642	1.251980	1.2390
21	1	0.9569	0.993	1.206434	1.218274	1.2088
22	2	0.9627	0.994	1.177793	1.187545	1.1792
22	0	0.9580	0.996	1.177882	1.189561	1.1782

When the spin degree of freedom is allowed, we first transform all candidate states in Fig. 4.5 onto CFC basis states and then obtain the CFC state by diagonalizing the Hamiltonian.

We have compared the electron and CF crystals with the exact ground state as a function of L. Figure 4.6 shows the ground state energy as a function of L in the angular momentum range $6 \leq L \leq 30$, along with the ground state energies of the electron and CF crystals. The energy expectation value for the CF crystal state is obtained by Monte Carlo method. The crystal description is seen to become better with increasing L. Figure 4.6 shows the energies separately for each S sector, and Table 4.3 shows the interaction energies of these wave functions and their overlaps with the exact wave functions $\Psi_{\rm ex}$, evaluated by the Monte Carlo method. The CF

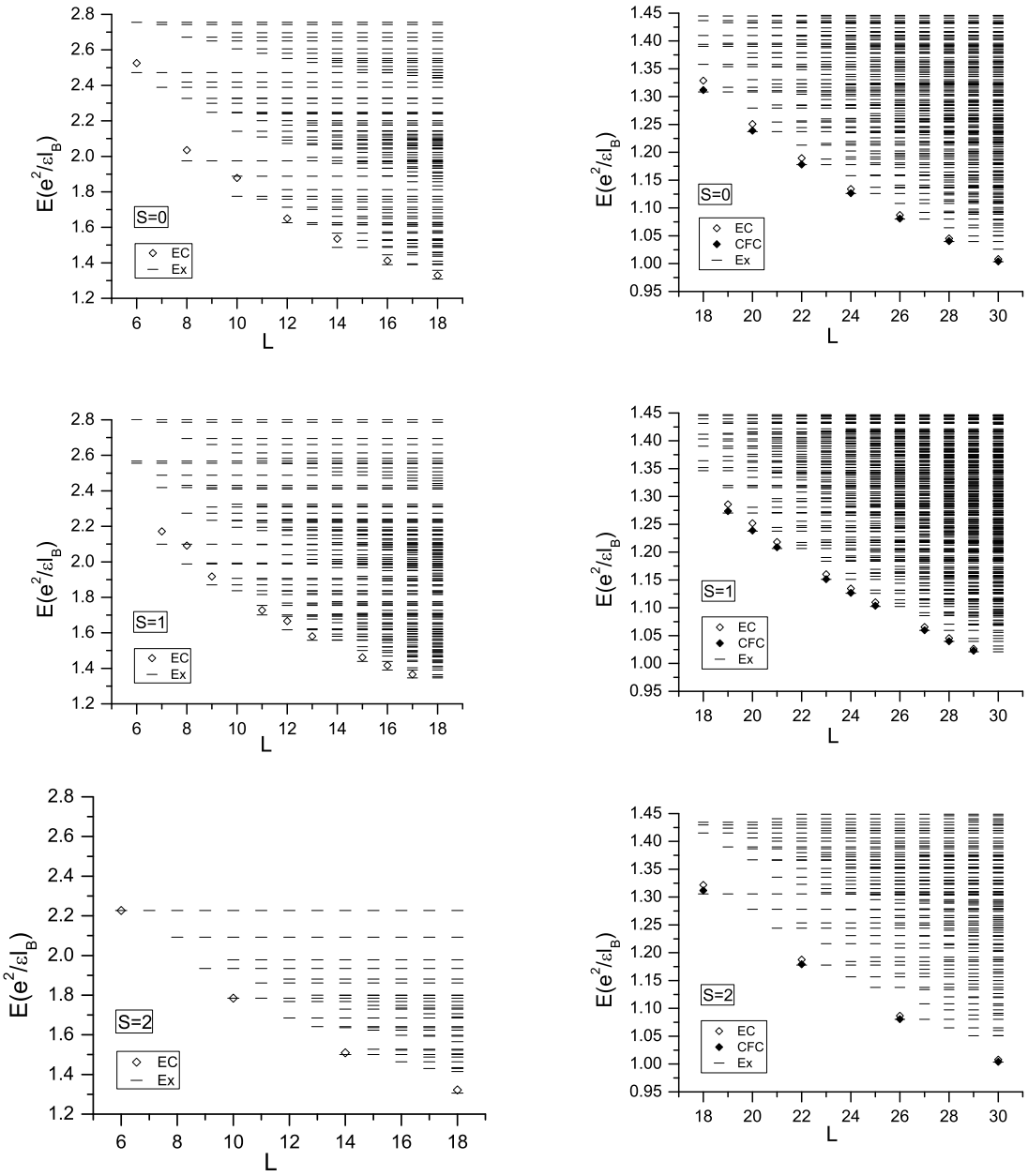

Figure 4.6: The exact Coulomb spectra are given as a function of L (dashes) for four electrons. The energies of the electron crystal (EC) wave functions (open diamonds), and CF crystal (CFC) wave functions (solid dots) are also given. The total spin S is shown on the graphs. The CF crystal cannot be created in the angular momentum range $\nu > 1/3$ (i.e., for $L < 18$ for $N = 4$.)

crystal provides an almost exact account of the actual state, and is always superior to the electron crystal.

The correlations between the spins of the electrons of the crystallite are of interest. We might expect that the strong Coulomb interaction induces antiferromagnetic correlation between neighboring electrons. We have computed spin-spin correlation for exact and CFC states, defined by

$$\begin{aligned} g_{\uparrow\uparrow}(\boldsymbol{r};\boldsymbol{R}) &\equiv \sum_{\chi_3,\chi_4=\alpha,\beta}\int d^2\boldsymbol{r}_3 d^2\boldsymbol{r}_4 \\ &\quad \times \left|\Psi(\boldsymbol{R}\alpha_1,\boldsymbol{r}\alpha_2,\boldsymbol{r}_3\chi_3,\boldsymbol{r}_4\chi_4)\right|^2, \\ g_{\uparrow\downarrow}(\boldsymbol{r};\boldsymbol{R}) &\equiv \sum_{\chi_3,\chi_4=\alpha,\beta}\int d^2\boldsymbol{r}_3 d^2\boldsymbol{r}_4 \\ &\quad \times \left|\Psi(\boldsymbol{R}\alpha_1,\boldsymbol{r}\beta_2,\boldsymbol{r}_3\chi_3,\boldsymbol{r}_4\chi_4)\right|^2. \end{aligned} \tag{4.15}$$

The functions $g_{\uparrow\uparrow}(\boldsymbol{r};\boldsymbol{R})$ and $g_{\uparrow\downarrow}(\boldsymbol{r};\boldsymbol{R})$ represent the probability of finding, respectively, an up-spin and a down-spin particle at $\boldsymbol{r}$ given an up-spin particle at $\boldsymbol{R}$. The position $\boldsymbol{R}$ is chosen as a point on $+x$ axis where the density of the wave function has a maximum. For CFC crystals, the integrals in Eq. (4.15) are evaluated by Monte Carlo method.

Figures 4.7–4.9 show spin correlations of exact and CFC wave functions at L=20, 21, and 22. For L=20 and 22, where two states are almost degenerate, we also plot the spin-correlations for first-excited states. At all angular momenta the spin-correlations of exact states are reproduced by the CFC states, which again reflects the accuracy of CFC wave functions. Remarkably, most of correlations are different from the naively expected nearest-neighbor antiferromagnetic correlations. Only for S=1 at L=20

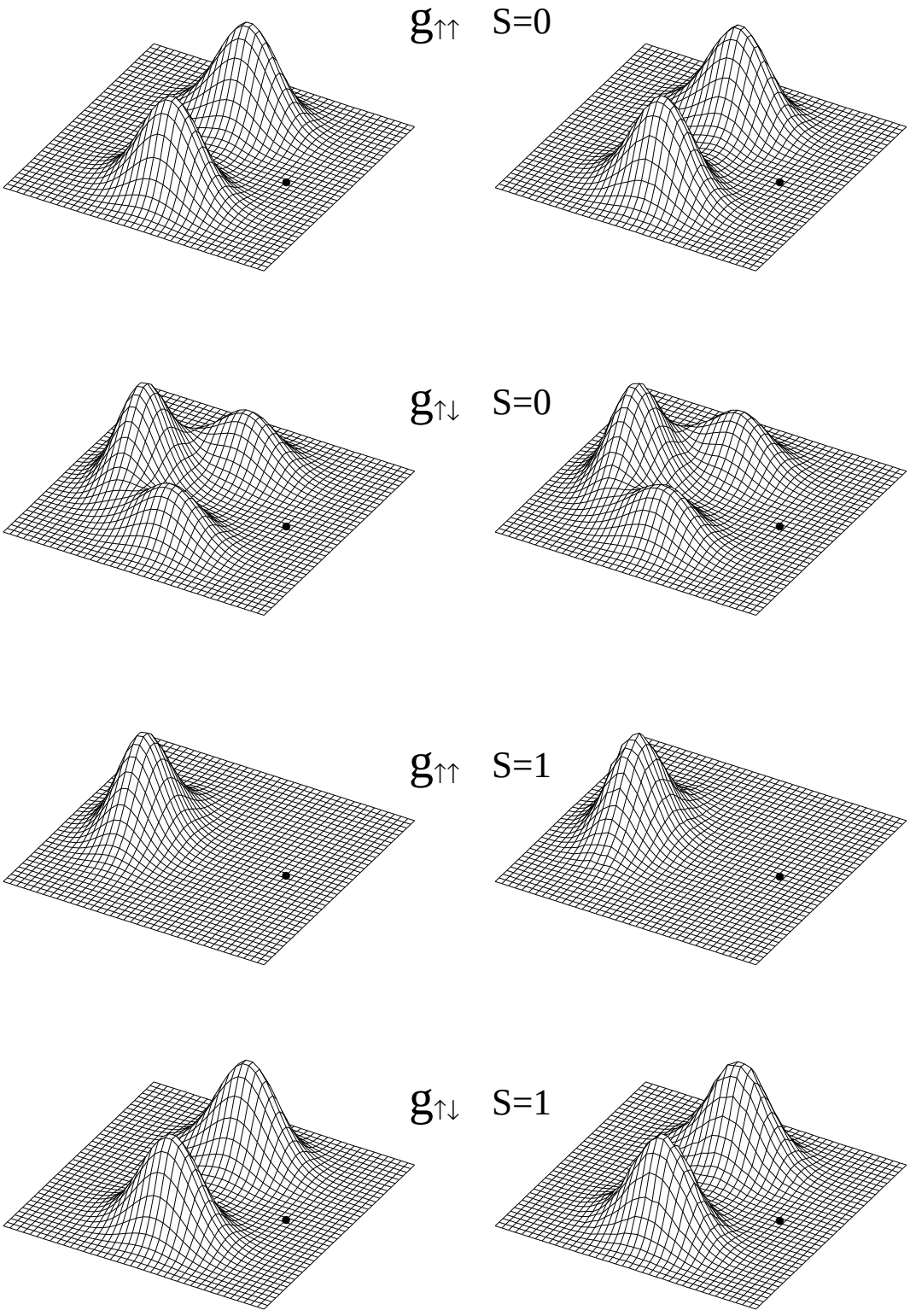

Figure 4.7: Spin-spin correlations for four electrons in a quantum dot at angular momentum L=20. The quantity $g_{\uparrow\uparrow}$ ($g_{\downarrow\uparrow}$) gives the probability of finding an up-spin (down-spin) particle as a function of the position in the quantum dot, given that one particle with spin up is held fixed at the position marked by the dot. Results are shown for both the ground state (S=0) and the almost degenerate first-excited state (S=1). The left column shows the exact correlation function, and the right one shows the CFC prediction.

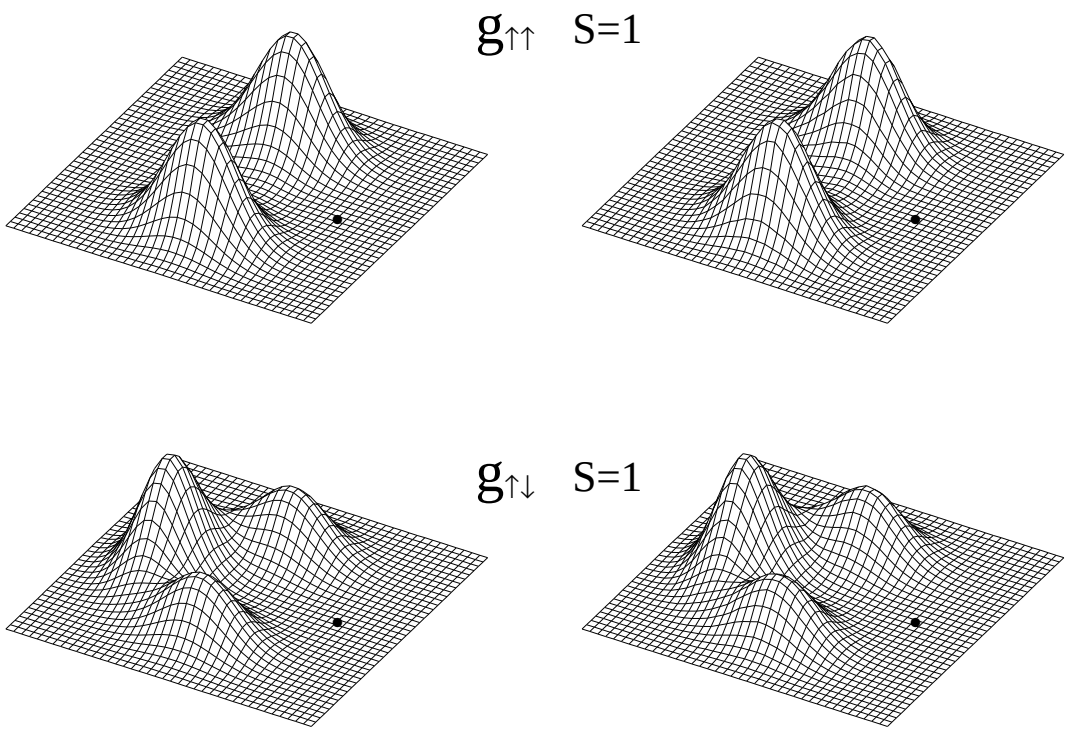

Figure 4.8: Same as in Fig. 4.7 for the ground state at L=21.

do we find perfect antiferromagnetic correlations between neighboring electrons. The state with S=0 at L=22 also exhibits nearest-neighbor antiferromagnetic correlations but the antiferromagnetism is not perfect. On the other hand, for S=0 at L=20, the neighboring spins are uncorrelated whereas the next nearest neighbor spins have ferromagnetic correlations. Spin correlations at L=21 (Fig. 4.8) and L=23 (not shown) are almost the same as for the state with S=0 at L=20. Note that the ground states both at L=21 and L=23 have total spin S=1 in contrast to the state at L=20. All the spin-correlation behaviors observed for $20 \leq L \leq 23$ are repeated with the periodicity of four as L increases.

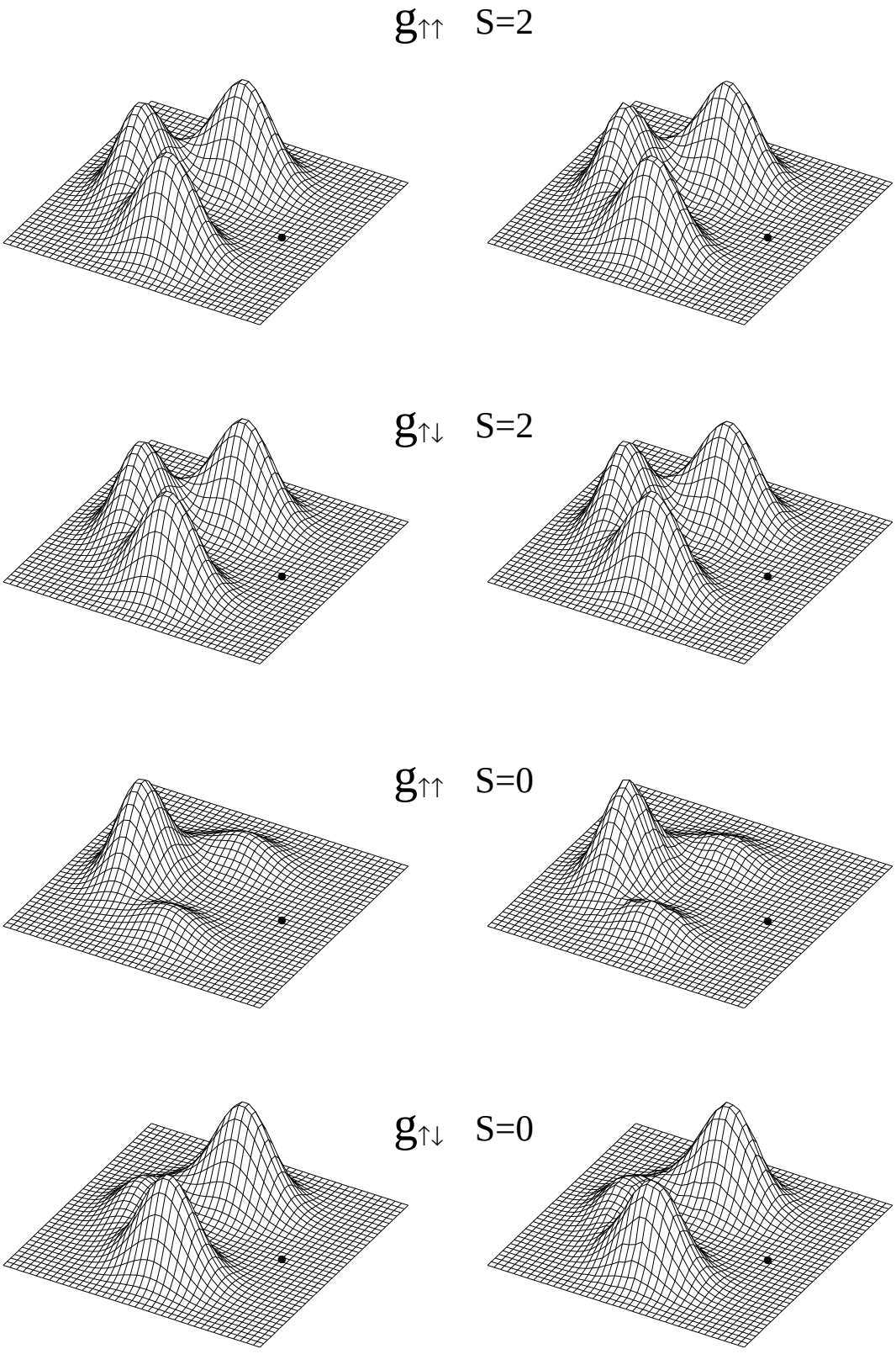

Figure 4.9: Same as in Fig. 4.7 for ground state (S=2) and almost degenerate first excited state (S=0) at L=22.

4.5.2 Symmetry analysis

A symmetry analysis similar to fully polarized case [81] sheds light on our understanding of angular-momentum dependence of spin correlations as well as the total spin. For a fully spin polarized crystal of four electrons, the phase factor produced by rotation by $\pi/2$ around the origin can be calculated in two ways. First, it is equivalent to an odd permutation, which implies a phase factor $-1 = \exp[i(2n+1)\pi]$. Alternatively, the total angular momentum L determines the phase to be $(\pi/2)L$. This restricts the angular momentum values to be L=$4n$+2; these are also the angular momentum values where cusps appear (for large angular momenta, where the crystal description is valid).

With the spin degree of freedom allowed, more (in fact, all) values of L are allowed because we have an additional contribution. Since the rotation operator $R(\theta{=}\pi/2)$ commutes with spin operator, we can obtain the simultaneous eigenstates of $R(\pi/2)$ and $\boldsymbol{S}^2$. Accordingly, eigenstates can be represented by two quantum numbers, total spin S and the phase factor associated with $\pi/2$ rotation. The phase factor due to rotation $R(\pi/2)$ is defined as $\pi/2L + \Theta$, where the first term is the contribution of the total angular momentum. Unlike the spin-polarized case, we have an additional phase Θ since each eigenstate is now a combination of different spin configurations. In the space spanned by the six states shown in Fig. 4.5, (here we assume each site provides a single-particle state localized at the site with spin degrees of freedom) the

six eigenstates are given by

$$\begin{aligned}
|S{=}0,\Theta{=}0\rangle &= \frac{1}{2\sqrt{3}}\left(|\mathrm{I}\rangle+|\mathrm{II}\rangle+|\mathrm{III}\rangle+|\mathrm{IV}\rangle\right.\\
&\qquad \left.+2|\mathrm{V}\rangle+2|\mathrm{VI}\rangle\right),\\
|S{=}0,\Theta{=}\pi\rangle &= \frac{1}{2}\left(-|\mathrm{I}\rangle+|\mathrm{II}\rangle-|\mathrm{III}\rangle+|\mathrm{IV}\rangle\right),\\
|S{=}1,\Theta{=}\pi\rangle &= \frac{1}{\sqrt{2}}\left(-|\mathrm{V}\rangle+|\mathrm{VI}\rangle\right),\\
|S{=}1,\Theta{=}\frac{\pi}{2}\rangle &= \frac{1}{2}\left(-|\mathrm{I}\rangle-i|\mathrm{II}\rangle+|\mathrm{III}\rangle+i|\mathrm{IV}\rangle\right),\\
|S{=}1,\Theta{=}-\frac{\pi}{2}\rangle &= \frac{1}{2}\left(-|\mathrm{I}\rangle+i|\mathrm{II}\rangle+|\mathrm{III}\rangle-i|\mathrm{IV}\rangle\right),\\
|S{=}2,\Theta{=}0\rangle &= \frac{1}{\sqrt{6}}\left(-|\mathrm{I}\rangle-|\mathrm{II}\rangle-|\mathrm{III}\rangle-|\mathrm{IV}\rangle\right.\\
&\qquad \left.+|\mathrm{V}\rangle+|\mathrm{VI}\rangle\right). \qquad (4.16)
\end{aligned}$$

The total phase factor associated with $\pi/2$ rotation is now seen to be $(\pi/2)L+\Theta$ for each eigenstate. The allowed crystals at each angular momentum are

$$\begin{aligned}
|S{=}0,\Theta{=}\pi\rangle, |S{=}1,\Theta{=}\pi\rangle &\quad \text{for } L{=}4n,\\
|S{=}1,\Theta{=}\frac{\pi}{2}\rangle &\quad \text{for } L{=}4n{+}1,\\
|S{=}0,\Theta{=}0\rangle, |S{=}2,\Theta{=}0\rangle &\quad \text{for } L{=}4n{+}2,\\
|S{=}1,\Theta{=}-\frac{\pi}{2}\rangle &\quad \text{for } L{=}4n{+}3.
\end{aligned}$$

These quantum numbers agree well with those of the states in the lowest-energy band. Furthermore, the states given in Eq. (4.16) explain the spin correlations of exact states at all angular momenta. For example, $|S{=}0,\Theta{=}\pi\rangle$, which survives at $L{=}4n$, predicts

no correlation between neighboring spins. On the other hand, $|S{=}0, \Theta{=}0\rangle$ at $L{=}4n{+}2$ shows partial antiferromagnetic correlations between neighboring spins (the correlation is not perfect because of the contribution from the components $|\mathrm{I}\rangle, |\mathrm{II}\rangle, |\mathrm{III}\rangle, |\mathrm{IV}\rangle$).

4.6 Chapter Conclusion

We have studied the correlated quantum dot states for electrons with two degenerate components, for example, the up and down spins in the absence of the Zeeman energy, and shown that the CF theory provides a satisfactory account. In particular, the state at high angular momenta is well described as a CF crystal, which has complex nearest neighbor and next-nearest neighbor spin-spin correlations.

Chapter 5

Phase diagram for bilayer quantum Hall effect at total filling $\nu_T = 5$

In this chapter we evaluate the phase diagram of the bilayer quantum Hall effect at total filling $\nu_T = 5$, which is a bilayer phase coherent state at small separations and two uncoupled 5/2 states at large separations. Based on a combination of variational and exact calculations, we estimate that the transition between these states occurs at a layer separation of approximately one magnetic length. The composite fermion Fermi sea is not found to be relevant for any parameters.

This work was done in collaboration with Shivakumar Jolad, Nicolas Regnault and Jainendra K. Jain. The remainder of the chapter is reproduced from the paper published in Physical Review B.[1]

[1]Chuntai Shi, Shivakumar Jolad, Nicolas Regnault and Jainendra K. Jain, Phys. Rev. B 77, 155127 (2008).

5.1 Introduction

The fractional quantum Hall effect[3] (FQHE) in bilayer systems exhibits new structure not available in single layer FQHE. In particular, the bilayer state at total filling $\nu_T = 1$ has attracted interest due to the possibility of interlayer phase coherence. At sufficiently small separations, interlayer interactions stabilize the so-called 111 wave function [9]:

$$\Psi_{111} = \prod_{i<j}(z_i - z_j) \prod_{\alpha<\beta}(w_\alpha - w_\beta) \prod_{i,\alpha}(z_i - w_\alpha), \tag{5.1}$$

Here $z_i = x_i - iy_i$ labels electrons on one layer while $w_\alpha = x_\alpha - iy_\alpha$ labels electrons on the other. The ubiquitous Gaussian factor $\exp[-\sum_j |z_j|^2/4 - \sum_\alpha |w_\alpha|^2/4]$ has been suppressed in the above equation and the rest of the chapter, and the lengths are expressed in units of the magnetic length $\ell = \sqrt{\hbar c/eB}$. Interpreting the layer index as a pseudospin, this wave function is fully pseudospin polarized. (The electrons' spin is assumed to be fully polarized, and therefore not explicitly considered. Only the spatial part of the wave function is explicitly shown; the full wave function is obtained by antisymmetrizing the product of the spatial and pseudo-spinor wave functions.) It can be interpreted as a condensate of excitons composed of electrons in one layer and holes in the other [16]. Experiments have seen clear evidence for superfluid-like behavior in the counterflow channel in bilayer systems [29, 30]. We stress that the interlayer correlations leading to incompressibility are caused by Coulomb interactions alone, not requiring any interlayer tunneling (which is neglected throughout this work). At large separations, two uncorrelated $\nu = 1/2$ layers are obtained, each well described

as a Fermi sea [6] of composite fermions[5] (CFs). The composite fermion Fermi sea (CFFS) wave function for a single layer is given by

$$\Psi_{\mathrm{CFFS}} = \mathcal{P}_{\mathrm{LLL}} \Phi_{\mathrm{eFS}} \prod_{j<k} (z_j - z_k)^2, \tag{5.2}$$

where Φ_{eFS} is the electron Fermi sea at zero magnetic field, and $\mathcal{P}_{\mathrm{LLL}}$ is the lowest Landau level (LL) projection operator. The bilayer wave function at large separations, denoted by CFFS^2, is simply a product of two single layer CFFS wave functions. Many articles have investigated transition between the 111 wave function and the uncoupled CFFSs both theoretically[16, 17, 18, 19, 20, 21, 22, 23, 24, 25, 26] and experimentally[27, 28, 29, 30].

Not much attention has been paid so far to the bilayer state at total filling of $\nu_T = 5$. In the first approximation it is reasonable to treat the lowest Landau level in each layer as completely full and inert, which corresponds to a filling of two in each layer. Considering only the electrons in the second Landau level, the problem becomes analogous to that of electrons at $\nu_T = 1$, but with an interaction that simulates the second Landau level Coulomb interaction. (This is how electrons at $\nu_T = 5$ are modeled below in our variational and exact calculations.) The goal of this chapter is to ascertain the parameters for which exciton condensation can be expected at $\nu_T = 5$. An interesting difference from $\nu_T = 1$ is that in the large separation limit, each layer is expected to assume a 5/2 FQHE state rather than a CF Fermi sea. A

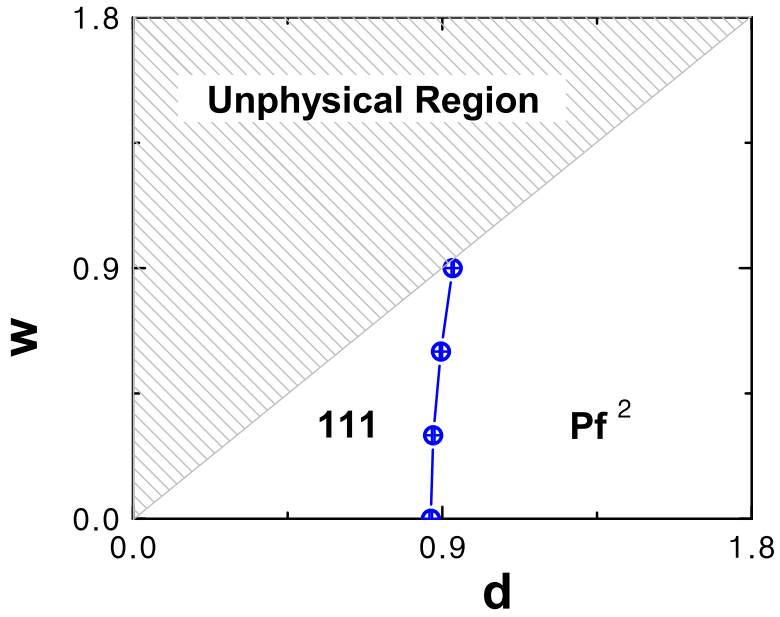

Figure 5.1: Phase diagram in the $w - d$ plane for a bilayer system, where w is the width of each layer and d is the interlayer separation (measured from center to center), both given in units of the magnetic length. The transition from the 111 wave function to the Pf^2 wave function (see text for definition) occurs at $d \sim 0.9$ magnetic length, almost independent of the layer width. The region with $d < w$ is unphysical.

promising wave function for the former is the so-called Pfaffian wave function [31]:

$$\Psi_{\mathrm{Pf}} = \mathrm{Pf}\left(\frac{1}{z_l - z_m}\right)\prod_{j<k}(z_j - z_k)^2 \tag{5.3}$$

where the Pfaffian of an antisymmetric matrix is defined,apart from an overall factor, as

$$\mathrm{Pf}\left(M_{ij}\right) = \mathcal{A}\left[M_{12}M_{34}...M_{2N-1,2N}\right], \tag{5.4}$$

$\mathcal{A}$ being the antisymmetrization operator. The wave function $\Psi_{\rm Pf}$, which can be written only for an even number of electrons, is interpreted as a paired state of composite fermions, because the Pfaffian factor is a BCS-like p-wave paired state of electrons and the Jastrow factor converts electrons into composite fermions. Variational [92] as well as exact diagonalization [93, 94] studies have shown that $\Psi_{\rm Pf}$ provides a reasonable approximation for the exact ground state of the half filled second Landau level. As a result, we expect at $\nu_T = 5$ a transition from the 111 wave function at small separation to the Pf^2 wave function at large separations. Two questions immediately arise: At what separation does the transition occur? Do other states (e.g. the CFFS) become relevant at intermediate separations? These questions have acquired added importance because of recent proposals for using the quasiparticles of the 5/2 state, which are thought to obey nonabelian braiding statistics, for quantum computation[95].

This chapter presents on our variational and exact diagonalization calculations on this problem. We study the competition between three wave functions: 111, CFFS^2, and Pf^2, as a function of the layer separation d for several quantum well widths. Interlayer tunneling has been neglected, as also the possibility of real spin reversal. (It is possible to prepare bilayer systems for which the interlayer tunneling is extremely small[27].) The principal prediction of our work is the phase diagram of the bilayer state at $\nu_T = 5$, shown in Fig. 5.1. The 111 wave function is stabilized for separations less than ~ 1 magnetic length, and Pf^2 elsewhere; the CFFS^2 is not found to be relevant anywhere. While the critical separation appears smaller than that for the 111 wave function at $\nu_T = 1$, we should recall that for a given sample the

magnetic length at $\nu_T = 5$ is larger by a factor of $\sqrt{5}$ than that at $\nu_T = 1$.

We note that bilayers also exhibit interesting physics at filling factors other than $\nu_T = 1$. A FQHE has been seen [96, 97] at $\nu_T = 1/2$ (where each layer has $\nu = 1/4$) at an intermediate value of d, described by the so-called 331 wave function [9]

$$\Psi_{331} = \prod_{i<j}(z_i - z_j)^3 \prod_{\alpha<\beta}(w_\alpha - w_\beta)^3 \prod_{i,\alpha}(z_i - w_\alpha). \tag{5.5}$$

The phase diagram containing a rich array of phases has been predicted at several other filling factors using the composite fermion theory, with wave functions of the form [17]

$$\Psi = \prod_{j,\alpha}(z_j - w_\alpha)^m \; \psi_{\overline{\nu}}[\{z_k\}] \; \psi_{\overline{\nu}}[\{w_\alpha\}], \tag{5.6}$$

where the fully antisymmetric wave function $\psi_{\overline{\nu}}$ describes a single layer CF state at filling factor $\overline{\nu}$, and m is either an even or an odd integer. The bilayer wave function Ψ describes a CF state at $\nu_T = 2\overline{\nu}/(1 + m\overline{\nu})$, which can be either compressible or incompressible, depending on whether $\psi_{\overline{\nu}}$ is compressible or incompressible. The state at large d has no interlayer correlations ($m = 0$); the integer m increases in unit steps as d is decreased.

Previously, Refs. [98, 99] have studied transition at $\nu_T = 5$ from the 111 to a charge/pseudospin density wave state, either a stripe phase[100] or a Wigner crystal, as a function of the layer separation. They use a Hartree-Fock approximation, which is well suited for these states, but cannot deal with the FQHE state relevant at large separations. On the other hand, we do not consider the density wave states in our variational studies below. Given that a single layer at $\nu = 5/2$ does not show any

evidence for the stripe phase, we believe that the stripe phase is unlikely to be relevant for the bilayer system at $\nu_T = 5$ as well, although we cannot rule it out completely. We note that an experiment [101] reports anisotropic transport in a bilayer system in the presence of a parallel magnetic field. This may be related to a similar tilted field induced stripe phase observed in a single layer[102, 103]. Our model does not consider interlayer tunneling or a parallel magnetic field.

The plan of this chpater is as follows. In Section II we briefly discuss the effective interaction, leaving many details to the Appendices. Sections III and IV show our results from variational and exact calculations. Section V concludes the chapter.

5.2 Effective Interaction

One of our goals is to evaluate the energies of the wave functions in Eqs. (5.1)-(5.3) to determine which one is most favorable. For this purpose, we employ the spherical geometry, which considers N electrons on the surface of a sphere, with $2Q$ flux quanta (a flux quantum is defined as $\phi_0 = hc/e$) penetrating its surface. The single particle wave functions are called monopole harmonics, denoted by $Y_{Q,l,m}(\theta, \phi)$, where θ and ϕ are angular coordinates and the quantum numbers l and m are the angular momentum and its z coordinate. It is convenient to define

$$u = \cos(\theta/2)e^{i\phi/2}\,, v = \sin(\theta/2)e^{-i\phi/2}. \tag{5.7}$$

For wave functions in the spherical geometry, the Jastrow factor $\prod_{j<k}(z_j - z_k)$ is replaced by $\prod_{j<k}(u_j v_k - u_k v_j)$. Further details on the spherical geometry, the wave

functions, and lowest LL projection can be found in the literature.[37, 38, 35, 104, 105].

The 111, CFFS, and Pf wave functions are most easily constructed in the lowest Landau level. In principle, it is possible to construct analogous wave functions in the second Landau level, but, in practice, it is more convenient to follow an alternative approach which constructs an effective interaction that simulates the second Landau level physics in the lowest Landau level [92].

The interaction energy of electrons within a single LL is completely specified by the pseudopotentials[35] $[V(r)]_m^{(n)}$, defined as the interaction energy of two particles with relative angular momentum m in the n^{th} Landau level. (In the following, the lowest and the second Landau levels refer to $n = 0$ and $n = 1$, and the superscript n is suppressed for the lowest Landau level). We define an effective interaction $V_{\text{eff}}(r)$ such that it has the same pseudopotentials in the lowest Landau level as the Coulomb interaction does in the second ($n = 1$) Landau level:

$$\left[\frac{1}{r} \right]_m^{(1)} = [\ V_{\text{eff}}(r)\ ]_m \tag{5.8}$$

for $m = 0, 1, 2, \cdots$. This implies

$$\frac{\langle \Psi^{(1)}|\ \frac{1}{r}\ |\Psi^{(1)}\rangle}{\langle \Psi^{(1)}|\Psi^{(1)}\rangle} = \frac{\langle \Psi^{(0)}|\ V_{\text{eff}}(r)\ |\Psi^{(0)}\rangle}{\langle \Psi^{(0)}|\Psi^{(0)}\rangle}, \tag{5.9}$$

where $|\Psi^{(1)}\rangle$ is the $n = 1$ LL counterpart of the lowest Landau level wave function $|\Psi^{(0)}\rangle$.

For the bilayer system, we have two sets of pseudopotentials, both intra and inter layer. For zero thickness, the effective interactions, denoted by $V_{\text{inter}}(r\ ; d)$ and

$V_{\rm intra}(r)$, are defined by the equations

$$\begin{aligned} \left[\frac{1}{\sqrt{r^2+d^2}} \right]_m^{(1)} &= [\ V_{\rm inter}(r\ ;d)\ ]_m \\ \left[\frac{1}{r} \right]_m^{(1)} &= [\ V_{\rm intra}(r)\ ]_m \end{aligned} \tag{5.10}$$

for all m. These expressions can be generalized to include the effect of finite width (Appendix A).

There are two simplifications specific to the wave functions of our interest. (i) The wave functions CFFS^2 and Pf^2 do not have any interlayer correlations, and their energies per particle (including the interaction with the positively charged jellium background; see Appendix B for details) are identical to the energies per particle for the single layer CFFS and Pf wave functions. (ii) The 111 wave function is fully antisymmetric, so only odd m pseudopotentials are relevant even for the inter-layer interaction.

The effective interactions we work with has the complicated form given in Eq. (A.17), which is motivated in the Appendix A. While it is not exact, it is extremely accurate, and, in particular, exactly captures the long distance part of the actual interaction. A simpler and less accurate form for the effective interaction was used in Ref. [92], but a reliable comparison between inter and intra layer energies requires a more accurate interaction.

We note that we determine the effective interaction in the planar geometry, which we then use in our spherical geometry calculations. In principle, the effective interaction can be determined in the spherical geometry directly, but then one must deal

with the complication that the interaction pseudopotentials in this geometry vary with the system size, requiring a different effective interaction for each system. With the planar effective interaction, the energies computed for individual spherical systems differ from what would be obtained in a genuine spherical geometry calculation, but accurate thermodynamic value is obtained when extrapolation to $N \to \infty$ is taken. (Certain subtleties associated with the evaluation of the thermodynamic limit are discussed in Appendix B.)

To confirm the validity of our procedure as well as the accuracy of the form of our effective interaction, we note that our computed energy of the 111 wave function for $d = 0$ (-0.4696(16)) compares very well with the analytical result for the energy of the fully occupied second Landau level, $-(3/4)\sqrt{\pi/8} = -0.4700$. Also, our energy of single layer Pfaffian wave function, namely $-0.3631(22)$, is consistent with an earlier variational result[92] $-0.362(2)$, and close to the number -0.366 obtained from an extrapolation of the exact energies of small systems[93]. (All these numbers assume $w = 0$.) This also supports the approximate validity of the $\nu_T = 5$ bilayer phase diagram obtained by our variational calculation.

5.3 Variational study

We first proceed to evaluate the interaction energies of the 111, CFFS^2, and Pf^2 wave functions as a function of the layer separation d and the layer width w. The inter and intra-layer effective interactions are given in Eqs. (A.17) and Eq. (A.18). For the Pf^2 and CFFS^2 wave functions, it is sufficient to evaluate the energies for a single layer, as these wave functions have no interlayer correlations built into them. The

interaction energies

$$E = \frac{\langle \Psi | V | \Psi \rangle}{\langle \Psi | \Psi \rangle} \tag{5.11}$$

are evaluated for the variational wave function Ψ by the standard Metropolis Monte Carlo method[106, 104, 105], with the inter and intralayer interactions V defined in Eqs. (A.17) and (A.18). Thermodynamic limits are obtained by the procedure given in Appendix B. As shown in Fig. 5.2, the Pfaffian wave function has lower energy in the entire range of parameters considered in our calculations.[107] (Ref. [17] had demonstrated the opposite result in the lowest Landau level.)

For the 111 wave function, the total energy consists of two parts, intra-layer energy among electrons within same layer and inter-layer energy between electrons in different layers. For the inter-layer part, the effective interaction $V_{\rm inter}(r\ ; w, d)$, defined in Eq. (A.17), is used to simulate the Coulomb interaction $1/\sqrt{r^2+d^2}$ in $n = 1$ LL, while $V_{\rm intra}(r\ ; w)$ is used for the intra-layer part. (Here, r refers to the projection of the distance between two electrons in the two-dimensional plane.) Fig. 5.3 shows the 111 and Pf^2 energies for two different quantum well widths. The Pf^2 wave function has lower energy beyond a critical layer separation, which is around 0.9 magnetic length for $w = 0$. The critical layer separation is only weakly dependent on the width. The resulting phase diagram is shown in Fig. 5.1.

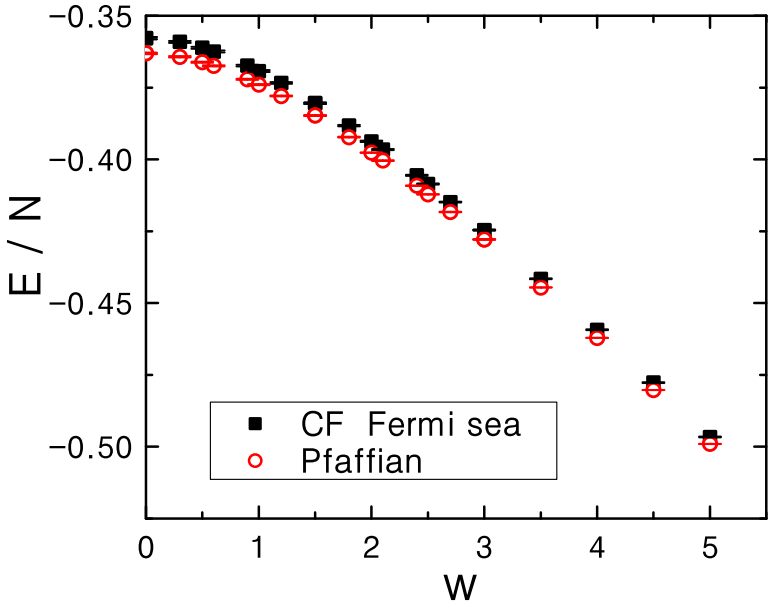

Figure 5.2: Thermodynamic values of the interaction energies of the Pfaffian and the CF Fermi sea wave functions are shown as functions of w, the width of the layer. The former has lower energy in the entire parameter range considered. We have used the interaction in Eq. (A.18) with three adjustable parameters.

5.4 Exact diagonalization

The variational approach is as good as the variational wave functions. An unsatisfactory aspect of the wave functions considered here is their lack of adjustable parameters: no interlayer correlations develop between the two Pfaffian wave functions as d is reduced, and neither does a softening of interlayer correlations take place for 111 as d is increased. Further, this approach cannot rule out other possible states at intermediate layer separations. We have therefore also performed exact diagonalization studies. These, in turn, suffer from their limitation to small systems with

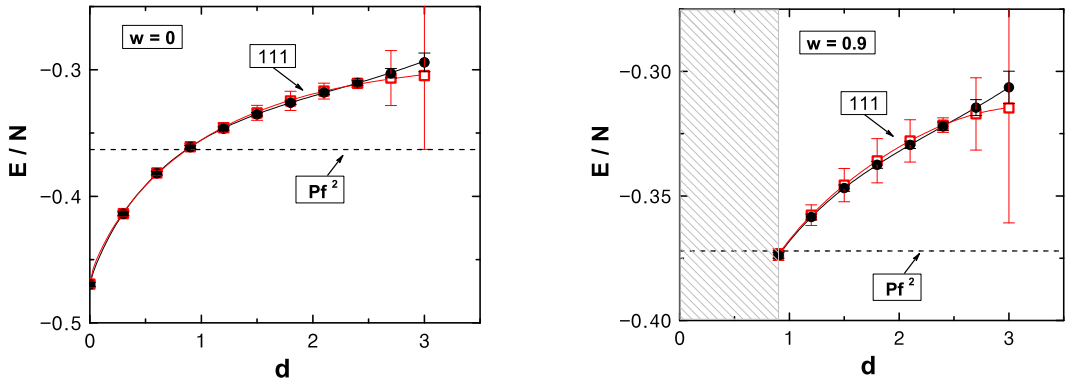

Figure 5.3: Thermodynamic limit of the energy per particle of the 111 wave function (curve) as a function of the layer separation d for two values of width $w = 0$ and 0.9 magnetic length. The energies have been computed for two approximations (with three and four adjustable parameters, shown by black dots and boxes, respectively), which are indistinguishable for $d \sim 1$. The energy of the Pfaffian wave function Pf^2 (dashed horizontal line) is independent of layer separation. Pf^2 has lower energy for d greater than approximately one magnetic length.

very few electrons, because the Hilbert space grows exponentially with the number of electrons. However, the two approaches taken together provide a consistent picture.

It is natural to study the overlap of 111 and Pf^2 wave functions with the corresponding true ground state wave functions at various values of layer separations d to ascertain the nature of the true state at d. We employ the spherical geometry for our calculations. The fact that 111 and Pf^2 occur at different monopole strengths, given by $2Q = 2N - 1$ and $2N - 3$ respectively, makes the analysis somewhat difficult, but nonetheless useful information can be gleaned. We show here results for 16 and 20 particles (eight and ten particles in each layer). To give an idea of the scale of the calculation, we note that for twenty particles at $2Q = 19$, the dimension of the Hilbert space in the $L_z = 0$ and $S_z = 0$ sector is 719541996; exploiting two discrete

symmetries, namely invariance under global S_z and L_z flip, it reduces to 179948926, which is what we work with. We have used the Lanczos algorithm to compute the system ground state. Calculations were performed on a PC cluster with 24 cores (AMD Opteron 265) and 48 Gb of memory. Each Lanczos iteration has required up to 16 hours of cpu time for the largest Hilbert space.

Fig. 5.4 depicts the overlaps of the 111 and the Pf^2 wave functions with the corresponding exact ground state wave functions for 16 and 20 particles as a function of d. The overlap for the 111 state decreases from close to unity at $d = 0$ to zero at large d, with the crossover taking place at $d \approx 1$, consistent with our variational estimate of the critical layer separation. The squared overlap between Pf^2 and the exact ground state increases is nearly zero at $d = 0$, but approaches a sizable value (0.75 for 16 particles and 0.70 for 20 particles, consistent with the values quoted in the literature [94]) at large d. For the larger system, the transition again takes place at $d \approx 1$, although there seem to be stronger finite size effects for Pf^2. We treat the 111 results as being more reliable for determining the transition position, because the 111 state is essentially exact at $d = 0$; the Pf^2 wave function is a less good approximation of the exact wave function at $d = \infty$, which we believe is the reason for stronger finite size effects seen in the overlap results.

We have also compared the exact ground state with the CFFS^2 wave function. For the CF Fermi sea, we use the ground state of the lowest Landau level pseudopotentials (which has been known to have almost perfect overlap with the CF Fermi sea wave function) in each layer. The overlap between the exact second Landau level ground state and the CFFS^2 is shown in Fig. 5.5 for $2N = 16$ and 18 at various values of

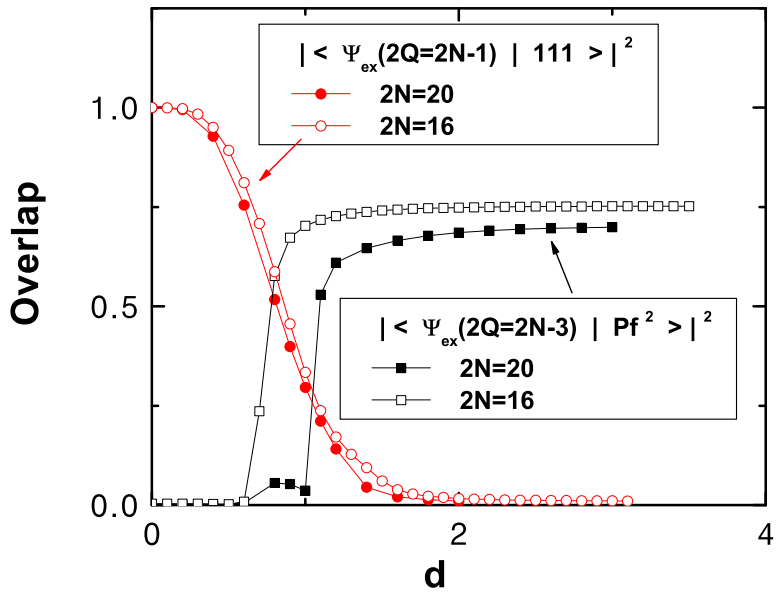

Figure 5.4: Overlaps of variational bilayer wave functions with the exact ground state wave functions as a function of the layer separation for sixteen and twenty electrons. Pf^2 is compared to the exact ground state at $2Q = 2N-3$, and the 111 wave function to the ground state at $2Q = 2N - 1$. The layer thickness is set to $w = 0$ in these calculations.

d. The overlap is always less than 0.1, confirming our conclusion in section III that $CFFS^2$ is irrelevant for a bilayer system at $\nu_T = 5$.

The expectation value of the total pseudo-spin operator $\boldsymbol{S}^2$ is shown in Fig. 5.6 for both $2Q = 2N - 3$ and $2N - 1$ systems. At zero layer separation, the pseudo-spin is a good quantum number. The 111 wave function here is fully pseudospin polarized, with $S = 2N/2$, as seen on the figure for $2Q = 2N - 1$. For small d the exact wave function continues to be close to fully pseudospin polarized, but the pseudospin polarization decays rapidly at around $d = 1$. For completeness, we have

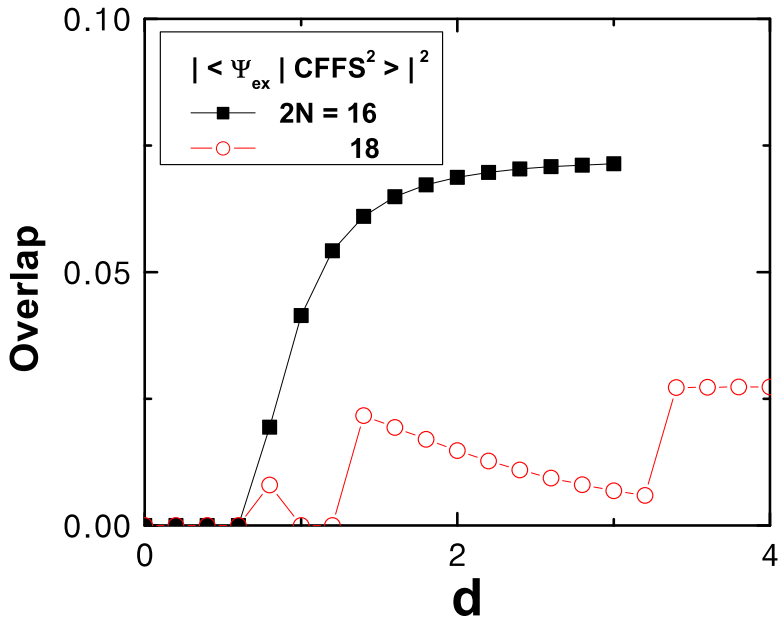

Figure 5.5: Overlaps of CF fermi sea wave function with the exact ground state wave function as a function of the layer separation for 16 and 18 electrons. The layer thickness is set to $w = 0$ in these calculations. For $2N = 18$ particles, the CF Fermi sea in each layer has $L = 0$, because we have a filled shells state (with 1+3+5 particles in the lowest three Λ levels). For $2N = 16$, the state has one CF-hole in the third Λ level, giving $L = 2$. The non-monotonic behavior of the overlap for $2N = 18$ indicates nearly degenerate ground states in the exact solution, which was also confirmed by the long convergence times for the Lanczos procedure. Please note that the y-axis scales are different in Figs. 5.5 and 5.4.

also shown the expectation value of $\boldsymbol{S}^2$ at $2Q = 2N - 3$. Here, at $d = 0$ we expect the maximum value for the pseudospin, i.e. $S = (2N - 4)/2$ ($2N - 2$ electrons with one pseudo-spin direction, and 2 electrons with opposite pseudo-spin orientation), as confirmed by numerical calculations. Again, the pseudospin polarization is destroyed at approximately one magnetic length separation.

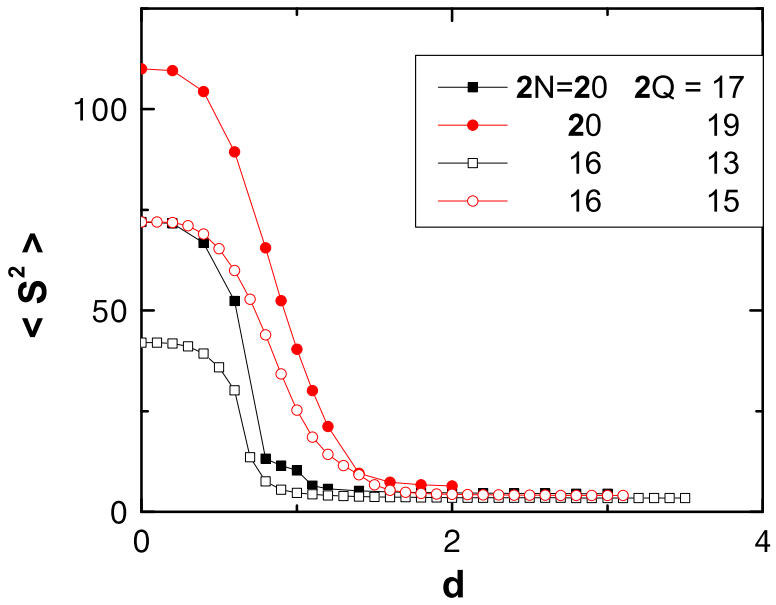

Figure 5.6: Expectation values of the pseudo-spin operator $\boldsymbol{S}^2$ of the true ground states as a function of the layer separation d for $2Q = 2N - 3$ and $2Q = 2N - 1$.

5.5 Chapter Conclusions

We have determined the phase diagram of a bilayer system at total filling $\nu_T = 5$, neglecting interlayer tunneling and spin fluctuations. Variational calculations show that there is a transition between the interlayer phase-coherent 111 state and two uncoupled Pfaffian wave functions at an interlayer separation of ~ 1 magnetic length. The critical separation is only weakly dependent on the quantum well width. Exact diagonalization results for a bilayer system with up to 20 electrons are consistent with this phase diagram.

Chapter 6

Summary and outlook

In the previous three chapters, we have shown our study of correlations in fractional quantum Hall systems. Here we summarize what have been done and what could be investigated along the lines of the present works.

In chapter 3, we studied the resonant tunneling of composite fermions in a system consists of a $\nu_1 = 2/5$ FQH island and a $\nu_0 = 1/3$ sea surrounding it. A rich set of possible transitions are found and the periods in both the flux and the charge for each transition are identified. We then discussed the related experiments with the help of our new findings. We pointed out the difficulties in identifying the transitions which are responsible for the observed periods and the inconsistence between experimentally extracted values for the periods and the theoretical value of the fractional braiding statistic parameter. Based on these analysis, we concluded that important information are still missing for a direct observation of the fractional braiding statistics among FQHE quasiparticles.

To get a better understanding of this topic, more efforts, both theoretical and

experimental, are needed to clarify a number of key issues. On the theory side, we need to understand whether the some of the assumptions we have made can be relaxed without destroying the qualitative predictions. For instance, we have explored the mean field theory of composite fermions to derive the periods (both in flux and in charge) of all sorts of transitions. It is interesting to see whether the residual interaction between composite fermions is strong enough to destroy all these periodic behavior. Another important issue is whether the boundary of the island is as sharply defined as we assumed. If a non-FQHE state region exists in between the 2/5 island and the 1/3 bulk, those transitions we found will be modified and the periods even the very existence of periodic behavior need to be checked. The other aspect would be to find special situation where certain transition is favored over others. Knowing which transition occurs and observing the periods it produces will lead to clear evaluation of the possible effects of fractional braiding statistics.

In chapter 4, we demonstrated the accuracy of the composite fermion wavefunctions, both liquid and crystal, in capturing the properties of the ground states of a four electron two-component quantum dot. Especially, residual interaction between composite fermions was found to cause interesting spin-spin correlations, which are the precursor of ferromagnetic/antiferromagnetic correlations for a large system.

As the number of electrons in the dot and/or the total angular momentum of the dot increase, the exact calculation of its properties become impractical even impossible. The types of wavefunctions we have tested in this thesis, however, can be handled for a large system at large angular momentum. Calculations with those wavefunctions can predict measurable parameters, e.g. the spin of the ground states. The composite

fermion liquid wavefunctions already produced many low-lying excitations in addition to the ground states by treating the CF-CF residual interaction to the lowest order, as our calculations have shown. If necessary, higher order calculations can be carried out to give a better description of the relevant quantum dot. Composite fermion solid wavefunctions, on the other hand, produce the ground states only. It is interesting to find how the low-lying excitations could be incorporated in a generalized method of constructing crystal wavefunctions. Another issue worth noticing is whether those spin-spin correlations do show up in quantum dots with more electrons. If they do, it is interesting to study the conditions for certain type of correlation to occur.

In chapter 5, we study the transition from an excitonic superfluid state at small d to a state without interlayer correaltion at large d for a bilayer FQHE system at $\nu_{\boldsymbol{T}} = 5$. By using proper trial wavefunctions, we find the critical value of d below which system have interlayer correlation to be $0.9l_B$. Furthermore, we have shown that the layer width do not affect this critical value. Exact study in small systems are performed to further confirm our prediction.

Since $\nu_{\boldsymbol{T}} = 1$ system is extensively studied in literature, future work in $\nu_{\boldsymbol{T}} = 5$ can borrow lots of ideas and computing techniques to deal with the issues which are common to both systems. More important aspect is the issues related to the fact that $\nu_{\boldsymbol{T}} = 5$ system turns into FQHE state at large d limit. For instance, one can look into the possible observable consequences which do not appear in $\nu_{\boldsymbol{T}} = 1$ case. In our work, the spin degree of freedom is ignored completely. We know that $\nu_{\boldsymbol{T}} = 5$ system would be realized in a relatively lower magnetic field, spin could play a more important role here than in the $\nu_{\boldsymbol{T}} = 1$ system. This enlarges the relevant Hilbert

space, and renders the possibility of a more interesting phase diagram.

Appendix A

Effective interaction

A.1 Intralayer interaction

To find an explicit form for the effective interactions by blindly solving Eq. (5.10) is impractical. In fact, there is no unique solution to these equations. Our approach is to construct an effective interaction with variational parameters that capture the correct long distance behavior, and then fix the parameters to match the short distance pseudopotentials. We demonstrate in this subsection how to construct an effective interaction for the intralayer interaction for $d = 0$. Generalization to interlayer interaction and finite transverse with is presented in the next subsection.

The differences in the $n = 1$ LL and $n = 0$ LL Coulomb pseudopotentials are large and irregular for small m, but relatively small and smooth for large m, as shown by open squares in the Fig. A.1). One may conclude that the effective interaction can be approximated by $1/r$ plus some short range functions to take care of the short

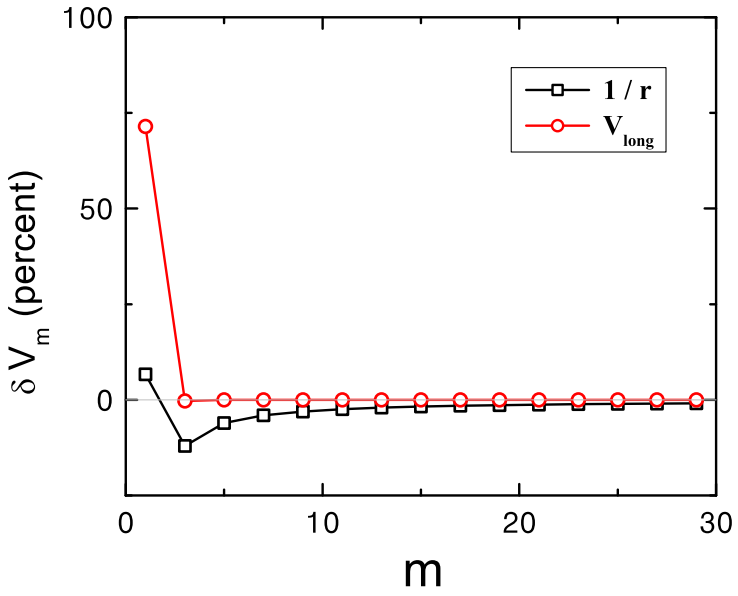

Figure A.1: Open squares show the percent difference between $n = 0$ LL and $n = 1$ LL pseudopotentials of Coulomb interaction. Open circles show the percent differences between $n = 0$ LL pseudopotentials of $V_{\rm long}(r)$ and $n = 1$ LL pseudopotentials of Coulomb interaction. Only pseudopotentials with odd m are considered here.
.

distance deviation. Ref. [92] takes the following expression

$$V_{\rm p}(r) = \frac{1}{r} + C_1 e^{-\alpha_1 x^2} + C_2 e^{-\alpha_2 x^2} \tag{A.1}$$

with the free parameters fixed by the equations

$$[\ V_{\rm p}\ ]_m = \left[\ \frac{1}{r}\ \right]^{(1)}_m \qquad m = 1, 3, 5, 7. \tag{A.2}$$

While the $n = 1$ LL pseudopotentials for $m = 1, 3, 5, 7$ are reproduced exactly, the

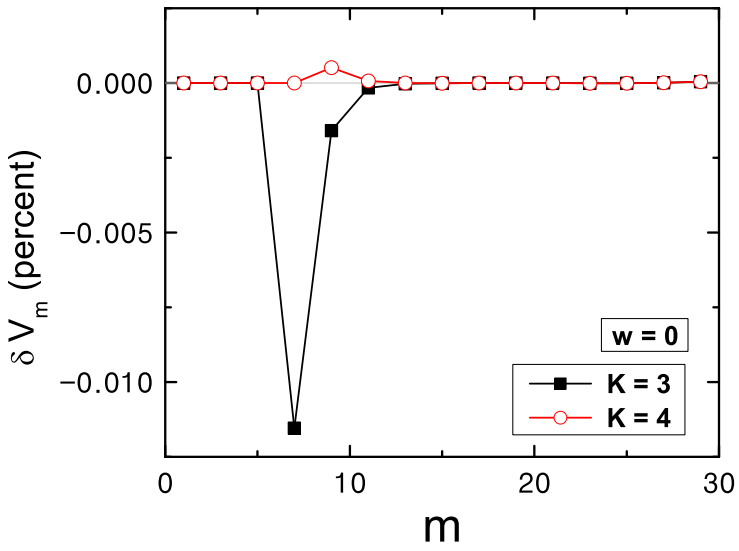

Figure A.2: Percent difference between $n = 0$ LL pseudopotentials of V_{eff} and $n = 1$ LL pseudopotentials of the Coulomb interaction with 3 and 4 adjustable parameters.
.

differences for larger m still remain, because while $[V_p]_m - [1/r]_m$ decays exponentially as a function of m, $[1/r]_m^{(1)} - [1/r]_m$ decays only as a polynomial function of m. To see this, we begin with the expression of the pseudopotentials[35] $[1/r]_m^{(n)}$

$$\left[\frac{1}{r}\right]_m^{(n)} = \int \frac{d^2\boldsymbol{q}}{(2\pi)^2}\frac{2\pi}{q}e^{-q^2}L_m(q^2)[L_n(q^2/2)]^2, \tag{A.3}$$

where $2\pi/q$ is the Fourier transform of $1/r$ and L_n are the Laguerre polynomials. This follows from that fact that the pseudopotentials for an interaction $V(q)$ in the nth LL are the same as those of $V(q)[L_n(q^2/2)]^2$ in the lowest Landau level [35, 33].

Eq. (5.8) is satisfied for an interaction that has the Fourier transform

$$V^{(1)}(q) = \frac{2\pi}{q}[L_1(q^2/2)]^2 = \frac{2\pi}{q}\left(1 - \frac{q^2}{2}\right)^2 \tag{A.4}$$

Unfortunately, the corresponding $V^{(1)}(r)$

$$V^{(1)}(r) = \frac{1}{r} + \frac{1}{r^3} + \frac{9}{4r^5} \tag{A.5}$$

is not integrable in two-dimensional space; $[1/r^3]_m$ is not well defined for $m = 0$ and $[1/r^5]_m$ is not well defined for $m = 0, 1$. Nevertheless, for $m \geq 2$, both $[1/r^3]_m$ and $[1/r^5]_m$ have finite values, and one has the identity

$$\left[\ \frac{1}{r}\ \right]_m^{(1)} \equiv \left[\ \frac{1}{r} + \frac{1}{r^3} + \frac{9}{4r^5}\ \right]_m \qquad\qquad m \geq 2, \tag{A.6}$$

demonstrating that the long range part of the $n = 1$ LL effective interaction differs from the Coulomb interaction through the term $1/r^3 + 9/4r^5$. To avoid the nonintegrability, we approximate the long range part of the interaction by the form

$$V_{\rm long}(r) = \frac{1}{r} + I_3 + \frac{9}{4}I_5 \tag{A.7}$$

$$\equiv \frac{1}{r} + \frac{1}{\sqrt{r^6 + A_3}} + \frac{9}{4}\frac{1}{\sqrt{r^{10} + A_5}} \tag{A.8}$$

which is legitimate in two dimensional space. The constants A_3 and A_5 must be nonzero, but otherwise chosen to maximize the efficiency of the calculations. Fig. A.1 demonstrates that the pseudopotentials of $V_{\rm long}$ with $A_3 = 1$ and $A_5 = 10$ capture

the long distance behavior accurately. The full form of the effective interaction that we have used is

$$V_{\text{eff}}(r) = \frac{1}{r} + \sum_{k=0}^{K-1} C_k r^{2k} e^{-r^2} + \frac{1}{\sqrt{r^6+1}} + \frac{9}{4\sqrt{r^{10}+10}} \tag{A.9}$$

with K free parameters. C_k are determined by matching the first K pseudopotentials with odd m. As shown in Fig. A.2, all odd m pseudopotentials of $n = 1$ LL Coulomb interaction are well approximated by $n = 0$ LL pseudopotentials of $V_{\text{eff}}(r)$ with both three and four fitting parameters.

A.2 Interlayer interaction and finite width

The intra- and inter- layer interactions in the general case of a bilayer system with the layer separation d, and with each layer having a finite thickness w, are obtained similarly. We model the confinement potential of each individual layer by an infinite square well of width w along the transverse direction. The wave function along the transverse direction

$$\varphi(y) = \sqrt{\frac{2}{w}} \cos\left(\frac{y\pi}{w}\right) \qquad -\frac{w}{2} \leqslant y \leqslant \frac{w}{2} \tag{A.10}$$

A w and d dependent interaction $V(r\ ;w,d)$ results from integrating the transverse coordinates (r is now the projection of the distance on the two-dimensional plane):

$$\begin{aligned} V(r\ ;w,d) := \int_{-w/2}^{w/2} dy_1 \int_{-w/2}^{w/2} dy_2 \frac{1}{\sqrt{r^2+(y_1-y_2-d)^2}} \\ \cos^2\left(\frac{y_1\pi}{w}\right)\cos^2\left(\frac{y_2\pi}{w}\right)\left(\frac{2}{w}\right)^2 \end{aligned} \tag{A.11}$$

In the limit of large r, the expansion of the interaction in powers of $1/r$ (up to $o(1/r^7)$) is given as

$$V(r\ ;w,d) \simeq \frac{1}{r} + D_3(w,d)\frac{1}{r^3} + D_5(w,d)\frac{1}{r^5} + D_7(w,d)\frac{1}{r^7} \tag{A.12}$$

where the coefficients $D(w,d)$ are functions of w and d, whose explicit forms can be determined by expanding integrand in Eq. (A.11) and then evaluating the integration analytically:

$$\begin{aligned} D_3(w,d) =& -\frac{d^2}{2} + w^2\left(\frac{1}{2\pi^2} - \frac{1}{12}\right) \\ D_5(w,d) =& \frac{3}{8}d^4 + w^4\frac{1}{80\pi^4}\left(135 - 30\pi^2 + 2\pi^4\right) \\ &+ w^2d^2\frac{3}{8}\left(1 - \frac{6}{\pi^2}\right) \\ D_7(w,d) =& -\frac{5}{16}d^6 + w^6\frac{5}{448\pi^6}\left(1260 - 315\pi^2 + 28\pi^4 - \pi^6\right) \\ &+ w^4d^2\frac{5}{128\pi^4}\left(540 - 120\pi^2 + 8\pi^4\right) \\ &+ w^2d^4\frac{75}{32\pi^2}\left(-6 + \pi^2\right) \end{aligned} \tag{A.13}$$

With the help of

$$\left[\ \frac{1}{r^p}\ \right]_m^{(1)} = \left[\ \frac{1}{r^p} + p^2\frac{1}{r^{p+2}} + (\frac{p}{2}+1)^2p^2\frac{1}{r^{p+4}}\ \right]_m, \quad p \text{ is odd and} \geqslant 1,\ m \geqslant \frac{p-1}{2}, \tag{A.14}$$

one can express the $n = 1$ LL pseudopotentials of $V(r\ ; w, d)$ as a summation of $n = 0$ LL pseudopotentials of $1/r^p$ with odd p (for large m only):

$$\begin{aligned}[V(r\ ; w, d)]_m^{(1)} = &\left[\frac{1}{r} - \frac{d^2}{2}\frac{1}{r^3} + \frac{3d^4}{8}\frac{1}{r^5} - \frac{5}{16}d^6\frac{1}{r^7}\right]_m \\ &+ [B_3(w,d)\frac{1}{r^3} + B_5(w,d)\frac{1}{r^5} + B_7(w,d)\frac{1}{r^7}]_m.\end{aligned} \tag{A.15}$$

The expression in the first square bracket on the right hand side is the large r expansion of the inter-layer Coulomb interaction $1/\sqrt{r^2+d^2}$, with the remaining in the second square brackets. The coefficients $B_p(w, d)$ are given by

$$\begin{aligned}B_3(w,d) =& 1 + \frac{w^2}{12\pi^2}(6-\pi^2) \\ B_5(w,d) =& \frac{9}{4} - \frac{9d^2}{2} + \frac{3w^2}{4\pi^2}(6-\pi^2) + \frac{3w^2d^2}{8\pi^2}(-6+\pi^2) \\ &+ \frac{w^4}{80\pi^4}(135 - 30\pi^2 + 2\pi^4) \\ B_7(w,d) =& -\frac{225d^2}{8} + \frac{75d^4}{8} + \frac{75w^2}{16\pi^2}(6-\pi^2) \\ &+ \frac{5w^4}{16\pi^4}(135 - 30\pi^2 + 2\pi^4) + \frac{75w^2d^2}{8\pi^2}(-6+\pi^2) \\ &+ \frac{75w^2d^4}{32\pi^2}(-6+\pi^2) + \frac{5w^4d^2}{32\pi^4}(135 - 30\pi^2 + 2\pi^4) \\ &+ \frac{5w^6}{448\pi^6}(1260 - 315\pi^2 + 28\pi^4 - \pi^6)\end{aligned} \tag{A.16}$$

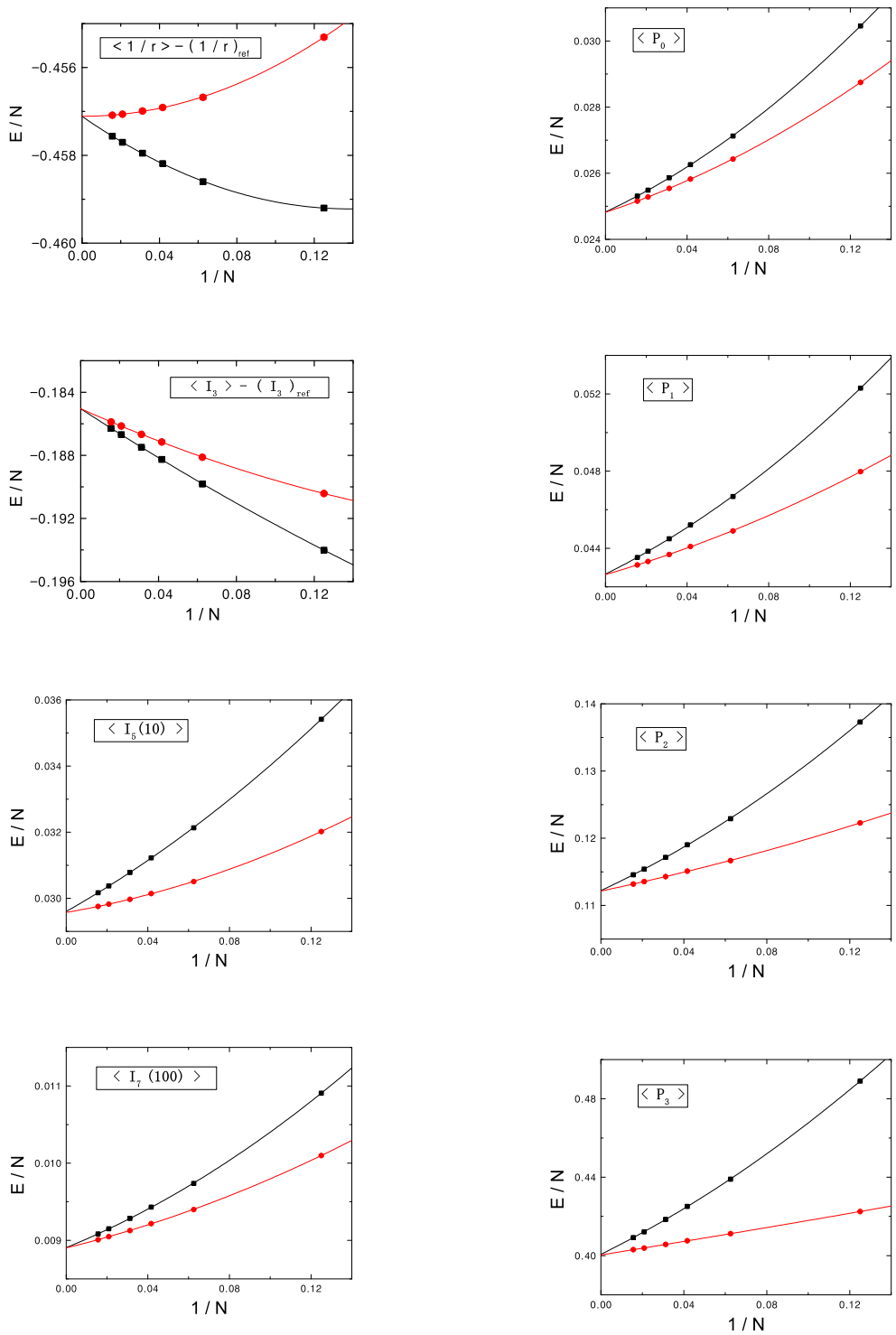

Figure A.3: Thermodynamic extrapolation ($1/N \to 0$) of three individual terms in V_{eff}. I_3,I_5 and I_7 are defined in text, and $P_i = r^{2i}e^{-r^2}, i = 0, 1, 2, 3$. The black squares (red dots) are obtained with the inter-particle distance defined as the chord (great circle arc) distance between their coordinates on the sphere. The curves represent best quadratic fits. Similar fits are obtained for other terms in the interaction.

Table A.1: The parameters C_k and $B_i(w,0)$ in the expression of $V_{\rm intra}(r\ ;w)$ with $K=3$ for selected width w, up to 3 magnetic length.

	short range			long range		
w	C_0	C_1	C_2	B_3	B_5	B_7
0	-20.94019	12.98214	-1.53215	1	2.25	0
0.6	-19.12945	11.61398	-1.35504	0.98824	2.1447	-0.64764
1.2	-15.88768	9.4912	-1.08432	0.95295	1.83554	-2.42498
1.8	-12.48823	7.57305	-0.82555	0.89414	1.3427	-4.85138
2.4	-9.19725	5.80427	-0.55603	0.81181	0.69985	-7.17964
3	-6.21799	4.07031	-0.26737	0.70595	-0.04589	-8.4768

The interaction in Eq. (A.15) describes the long range part of interlayer Coulomb interaction $1/\sqrt{r^2+d^2}$ in $n=1$ LL fairly well but diverts from it significantly at small r. As before, we use the following form for interlayer effective interaction:

$$\begin{aligned} V_{\rm inter}(r\ ;w,d) =& \frac{1}{\sqrt{r^2+d^2}} + \sum_{k=0}^{K-1} C_k r^{2k} e^{-r^2} \\ &+ B_3(w,d)\frac{1}{\sqrt{r^6+1}} + B_5(w,d)\frac{1}{\sqrt{r^{10}+10}} \\ &+ B_7(w,d)\frac{1}{\sqrt{r^{14}+100}}, \end{aligned} \tag{A.17}$$

where the choice of parameters in the last three terms is dictated by numerical efficiency. Setting $d=0$ in this equation, $V_{\rm inter}$ reduces to the intralayer effective interaction with finite width w:

$$V_{\rm intra}(r\ ;w) = V_{\rm inter}(r\ ;w,d=0) \tag{A.18}$$

The free parameters C_k in Eq. (A.17) and (A.18) are determined, as before, by matching the first three or four odd pseudopotentials. We show as an example in Table

A.1 the parameters C_k and $B_i(w, 0)$ for $V_{\text{intra}}(r\ ; w)$. The full interaction is found to be extremely accurate in the region of interest; near the phase boundary, the pseudopotentials are obtained correctly to within 0.02%.

Appendix B

Thermodynamic extrapolation

For a proper thermodynamic limit, interaction with a uniform positively charged background must also be included to define the total energy:

$$E = E_{ee} + E_{eb} + E_{bb} \tag{B.1}$$

where the subscripts e and b refer to electron and background. The interaction between the electrons is given by $V_{\text{eff}}(r)$, but the electron-background and background-background interaction is the Coulomb interaction $1/r$. This equation can be rewritten as

$$E = E_{ee} - E_{\text{ref}}, \tag{B.2}$$

where E_{ref} is the interaction energy of a "classical" reference system with the same charge density as the electron system but without any exchange correlation; the interaction considered for the reference system is the Coulomb interaction $1/r$. (The

previous equation follows because $E_{\rm ref} + E_{eb} + E_{bb} = 0$.)

For large N, the energy per particle E/N for the *lowest* ($n = 0$) Landau level fractional quantum Hall states has been found to behave as (see, for instance, Ref.[108])

$$\frac{E}{N} = \frac{E_\infty}{N} + \frac{E_1}{N^2} + \frac{E_2}{N^3} + o\left(\frac{1}{N^3}\right), \tag{B.3}$$

where E_∞/N is the thermodynamic limit of the energy per particle. However, for our effective interaction for the $n = 1$ Landau level, we also obtain a term proportional to $N^{-3/2}$ because of the presence of the term proportional to $I_3 = 1/\sqrt{r^6+1}$. This can be seen by noting that for a finite system, the interaction range is limited by the size of the system, which leads to a discrepancy between the thermodynamic limit and its finite size counterpart given by

$$\Delta E = \int_R^\infty \frac{1}{\sqrt{r^6+1}} r dr \sim \frac{1}{R} \sim \frac{1}{\sqrt{N}}. \tag{B.4}$$

An extrapolation with a modified Eq. (B.3) is in principle possible, but in practice shows strong variation at large N, producing large uncertainty in the thermodynamic limit. We find it convenient to add an additional interaction term $\sim 1/\sqrt{r^6+1}$ to the energy of the reference system, and evaluate the thermodynamic limit of $\langle I_3\rangle - (I_3)_{\rm ref}$. The error due to this unphysical term in the reference system is corrected after the thermodynamic limit is obtained. In other words, the thermodynamic value of $\langle I_3\rangle$ is calculated as

$$\lim_{N\to\infty} \langle I_3\rangle = \lim_{N\to\infty} \left[\langle I_3\rangle - (I_3)_{\rm ref}\right] + \lim_{N\to\infty} (I_3)_{\rm ref}. \tag{B.5}$$

The quantity $(I_3)_{\rm ref}$ is obtained by numerical integration for finite as well as thermodynamic systems.

The energy expectation value of each term in the effective interactions Eq. (A.17) and (A.18) is evaluated by importance sampling algorithm. We obtain the total energy by extrapolating each term separately to the thermodynamic limit. All finite system energies are multiplied by a size-dependent density factor[108] $\sqrt{2Q/\nu N}$ ($\nu = 1/2$ in our study) to account for the fact that charge density of finite systems divert from that of an ideal $\nu = 1/2$ system. As an additional check, we calculate the energies using both the chord and arc distances for the interparticle separation r, which give different results for finite N, but the same thermodynamic limits. Some representative extrapolations are shown in Fig. A.3 for the single layer Pfaffian wave function.

Bibliography

[1] J.P. Eisenstein and H.L. Stormer, Science **248** 1510 (1990).

[2] K.v. Klitzing, G. Dorda, and M. Pepper, Phys. Rev. Lett.**45**, 494 (1980).

[3] D.C. Tsui, H.L. Stormer, and A.C. Gossard, Phys. Rev. Lett. **48**, 1559 (1982).

[4] R.B. Laughlin, Phys. Rev. Lett.**50**, 1395 (1983).

[5] J.K. Jain, Phys. Rev. Lett. **63**, 199 (1989); J.K. Jain, Phys. Rev. B **41**, 7653 (1990), Phys. Rev. B **40**, R8079 (1989).

[6] B.I. Halperin, P.A. Lee, and N. Read, Phys. Rev. B **47**, 7312 (1993).

[7] N. Byers and C.N. Yang, Phys. Rev. Lett. **7**, 46 (1961).

[8] J.K. Jain, S.A. Kivelson, and D.J. Thouless, Phys. Rev. Lett.**71**, 3003-3006 (1993).

[9] B.I. Halperin, Helv. Phys. Acta **56**, 75-102 (1983).

[10] J.M. Leinaas and J. Myrheim, Nuovo Cimento B **37**, 1 (1977).

[11] F. Wilczek, Phys. Rev. Lett. **49**, 957 (1982).

[12] D. Arovas, J.R. Schrieffer, and F. Wilczek, Phys. Rev. Lett. **53**, 722 (1984).

[13] F.E. Camino, W. Zhou, and V.J. Goldman, Phys. Rev. B **72**, 075342 (2005).

[14] G.S. Jeon, C-C. Chang, and J.K. Jain, Phys. Rev. B **69**, 241304(R) (2004); J. Phys: Condens. Matter **16**, L271 (2004).

[15] C. Yannouleas and U. Landman, Phys. Rev. B**66**, 115315 (2002); *ibid.* **68**, 035326 (2002).

[16] S.M. Girvin and A.H. MacDonald in *Perspectives in Quantum Hall Effects*, edited by S. Das Sarma and A. Pinczuk (Wiley, New York, 1997).

[17] V.W. Scarola and J.K. Jain, Phys. Rev. B **64**, 085313 (2001).

[18] X. G. Wen and Z. Zee, Phys. Rev. B **47**, 2265 (1993); Z. F. Ezawa and A. Iwazaki, ibid. **48**, 15189 (1993).

[19] H. A. Fertig, Phys. Rev. B 40, 1087 (1989).

[20] D. Yoshioka, A.H. MacDonald and S.M. Girvin, Phys. Rev. B **39**, 1932 (1989).

[21] K. Nomura and D. Yoshioka, Phys. Rev. B **66**, 153310 (2002).

[22] K. Yang, K. Moon, L. Zheng, A. H. MacDonald, S. M. Girvin, D. Yoshioka, and S.-C. Zhang, Phys. Rev. Lett. **72**, 732 (1994).

[23] K. Moon, H. Mori, K. Yang, S.M. Girvin, A.H. MacDonald, L. Zheng, D. Yoshioka, and S.C. Zhang, Phys. Rev. B **51**, 5138 (1995).

[24] D. Sheng, L. Balents, and Z. Wang, Phys. Rev. Lett. **91**, 116802 (2003).

[25] Steven H. Simon, E. H. Rezayi, and Milica V. Milovanovic, Phys. Rev. Lett. **91**, 046803 (2003).

[26] G. S. Jeon and J. Ye Phys. Rev. B **71**, 035348 (2005).

[27] S. Q. Murphy, J. P. Eisenstein, G. S. Boebinger, L. N. Pfeiffer, and K. W. West, Phys. Rev. Lett. **72**, 728 (1994); T. S. Lay et al., Phys. Rev. B **50**, 17725 (1994).

[28] I. B. Spielman, J. P. Eisenstein, L. N. Pfeiffer, and K. W. West, Phys. Rev. Lett. **84**, 5808 (2000).

[29] M. Kellogg, J. P. Eisenstein, L. N. Pfeiffer, and K. W. West, Phys. Rev. Lett. **93**, 036801 (2004).

[30] E. Tutuc, M. Shayegan, and D. A. Huse, Phys. Rev. Lett. **93**, 036802 (2004).

[31] G. Moore and N. Read, Nucl. Phys. B **360**, 362 (1991).

[32] J. S. Xia, W. Pan, C. L. Vicente, E. D. Adams, N. S. Sullivan, H. L. Stormer, D. C. Tsui, L. N. Pfeiffer, K. W. Baldwin, and K. W. West, Phys. Rev. Lett. **93**, 176809 (2004).

[33] J.K. Jain, *Composite Fermions*,Cambridge university press 2007.

[34] S.M. Girvin and T. Jach, Phys. Rev. B**29** 5617 (1984).

[35] F.D.M. Haldane, Phys. Rev. Lett. **51**, 605 (1983); F.D.M. Haldane in *The Quantum Hall Effect*, 2nd ed., edited by R.E. Prange and S.M. Girvin, Spinger-Verlag, Berlin,1990.

[36] P.A.M. Dirac Proc.Roy.Soc.(London) **133** 60 (1931).

[37] T.T. Wu and C.N. Yang, Phys. Rev. D **12**, 3845-3857 (1975).

[38] T.T. Wu and C.N. Yang, Nucl. Phys. B **107**, 365-380 (1976).

[39] B.I. Halperin, Phys. Rev. Lett. **52**, 1583 (1984).

[40] See, for example, Physics Today **58** (10), 21 (2005).

[41] J.K. Jain and S.A. Kivelson, Phys. Rev. Lett. **62**, 231 (1989).

[42] S. Kivelson, Phys. Rev. Lett. **65**, 3369 (1990).

[43] These are also called quasi- or CF-Landau levels.

[44] A.S. Goldhaber and J.K. Jain, Phys. Lett. A **199**, 267 (1995).

[45] G.S. Jeon, K.L. Graham, J.K. Jain, Phys. Rev. Lett. **91**, 036801 (2003); Phys. Rev. B **70**, 125316 (2004).

[46] H. Kjønsberg and J. Myrheim, Int. J. Mod. Phys. A **14**, 537 (1999).

[47] H. Kjønsberg and J.M. Leinaas, Nucl. Phys. B **559**, 705 (1999).

[48] The relative statistics of a charge 1/3 quasiparticle with respect to an electron is $\theta^* = 2$, following the arguments of Ref. [45], or from Eq. 2 for the bottom transition in Table 1. Equating the electron to five charge 1/5 quasiparticles allows a determination of the relative braiding statistics of a charge 1/3 quasiparticle in the 1/3 state with respect to a charge 1/5 quasiparticle in the 2/5 state to be $\theta^* = 2/5$.

[49] J.K. Jain and M.R. Peterson, Phys. Rev. Lett. **94**, 186808 (2005).

[50] A.S. Goldhaber, J.K. Jain, and G.S. Jeon, Phys. Rev. Lett. **93**, 169705 (2004).

[51] J.K. Jain and R.K. Kamilla, Int. J. Mod. Phys. **B11**, 2621 (1997); Phys. Rev. B **55**, R4895 (1997).

[52] Eyal Goldmann and Scot Renn,Phys. Rev. B**56** 13269 (1997).

[53] S.S. Mandal and J.K. Jain, Solid State Commun. **118**, 503 (2001); Phys. Rev. Lett. **89**, 096801 (2002).

[54] S.S. Mandal, M.R. Peterson, and J.K. Jain, Phys. Rev. Lett. **90**, 106403 (2003).

[55] J.K. Jain and T. Kawamura, Europhys. Lett. **29**, 321 (1995).

[56] P.L. McEuen, E.B. Foxman, U. Meirav, M.A. Kastner, Y. Meir, N.S. Wingreen, and S.J. Wind, Phys. Rev. Lett.**66**, 1926 (1991); P.L. McEuen, E.B. Foxman, J. Kinaret, U. Meirav, M.A. Kastner, N.S. Wingreen, and S.J. Wind, Phys. Rev. B**45**, 11419 (1992); R.C. Ashoori, H.L. Störmer, J.S. Weiner, L.N. Pfeiffer, S.J. Pearton, K.W. Baldwin, and K.W. West, Phys. Rev. Lett.**68**, 3088 (1992); R.C. Ashoori, H.L. Störmer, J.S. Weiner, L.N. Pfeiffer, K.W. Baldwin, and K.W. West, *ibid.* **71**, 613 (1993); T.H. Oosterkamp, J.W. Janssen, L.P. Kouwenhoven, D.G. Austing, T. Honda, and S. Tarucha, *ibid.* **82**, 2931 (1999).

[57] P.A. Maksym and T. Chakraborty, Phys. Rev. Lett.**65**, 108 (1990); S.M. Reimann, M. Koskinen, and M. Manninen, Phys. Rev. B**62**, 8108 (2000); S.-R. Eric Yang, A.H. MacDonald, and M.D. Johnson, Phys. Rev. Lett.**71**, 3194 (1993).

[58] G. Dev and J.K. Jain, Phys. Rev. B**45**, 1223 (1992).

[59] J.K. Jain and X.G. Wu, Phys. Rev. B**49**, 5085 (1994).

[60] S.M. Reimann, M. Koskinen, Y. Yu, and M. Manninen, New J. Phys. **8**, 59 (2006).

[61] M. Koskinen, S.M Reimann, J.-P. Nikkarila, and M. Manninen, cond-mat/0605321.

[62] P.A. Maksym, Phys. Rev. B**53**, 10871 (1996).

[63] M. Toreblad, M. Borgh, M. Koskinen, M. Manninen, and S.M. Reimann, Phys. Rev. Lett.**93**, 090407 (2004).

[64] A. Cappelli, C. Mendez, J. Simonin, and G.R. Zemba, Phys. Rev. B**58**, 16291 (1998).

[65] X.C. Xie, S. Das Sarma, and S. He, Phys. Rev. B**47**, 15942 (1993).

[66] C. Yannouleas and U. Landman, Phys. Rev. Lett.**82**, 5325 (2002).

[67] A.D. Güçlü, J.-S. Wang, and H. Guo Phys. Rev. B**68**, 035304 (2002); A.D. Güçlü and C.J. Umrigar *ibid.* **72**, 045309 (2003); A.D. Güçlü, G.S. Jeon, C.J. Umrigar, and J.K. Jain, *ibid.* **72**, 205327(2005); G.S. Jeon, A.D. Güçlü, C.J. Umrigar, and J.K. Jain, *ibid.* **72**, 245312(2005).

[68] M. Manninen, S. Viefers, M. Koskinen, and S.M. Reimann, Phys. Rev. B**64**, 245322 (2001).

[69] M. Manninen, S.M. Reimann, M. Koskinen, and B. Mottelson, Eur. Phys. J. D **16**, 381 (2001).

[70] M.B. Tavernier, E. Anisimovas, and F.M. Peeters, Phys. Rev. B**74**, 125305 (2006).

[71] H. Yi and H.A. Fertig, Phys. Rev. B**58** 4019 (1998); R. Narevich, G. Murthy, and H.A. Fertig, *ibid.* **64**, 245326 (2001).

[72] M. Ferconi and G. Vignale, Phys. Rev. B**50**, 14722 (1994).

[73] A. Harju, V.A. Sverdlov, R.M. Nieminen, and V. Halonen, Phys. Rev. B**59**, 5622 (1999).

[74] S.M. Reimann, M. Koskinen, J. Helgesson, P.E. Lindelof, and M. Manninen, Phys. Rev. B**58**, 8111 (1998).

[75] D.G. Austing, S. Sasaki, S. Tarucha, S.M. Reimann, M. Koskinen, and M. Manninen, Phys. Rev. B**60**, 11514 (1999).

[76] M. Manninen, S. M. Reimann, M. Koskinen, Y. Yu, and M. Toreblad, Phys. Rev. Lett.**94**, 106405 (2005).

[77] S.M. Reimann, M. Koskinen, M. Manninen, and B.R. Mottelson, Phys. Rev. Lett.**83**, 3270 (1999).

[78] J.H. Han and S.-R. Eric Yang, Phys. Rev. B**58**, R10163 (1998).

[79] P. Hawrylak, Phys. Rev. Lett.**71**, 3347 (1993).

[80] M. Koskinen, M. Manninen, and S.M. Reimann, Phys. Rev. Lett.**79**, 1389 (1997).

[81] W.Y. Ruan, Y.Y. Liu, C.G. Bao, and Z.Q. Zhang, Phys. Rev. B**51**, R7942 (1995); W.Y. Ruan and H.-F. Cheung, J. Phys.: Condens. Matter **11**, 435 (1999).

[82] For a recent review on both experiment and theoretical aspects of quantum dot, see S.M Reimann and M. Manninen, Rev. Mod. Phys. **74**, 1283 (2002).

[83] R. Hanson, B. Witkamp, L.M.K. Vandersypen, L.H.W. van Beveren, J.M. Elzerman, and L.P. Kouwenhoven, Phys. Rev. Lett. **91**, 196802 (2003); S. Lindemann, T. Ihn, T. Heinzel, W. Zwerger, K. Ensslin, K. Maranowski, and A.C. Gossard, Phys. Rev. B **66**, 195314 (2002).

[84] P. Pfeffer and W. Zawadzki, Phys. Rev. B **74**, 115309 (2006); A. Malinowski and R.T. Harley, *ibid.* **62**, 2051 (2000).

[85] X.G. Wu, G. Dev, and J.K. Jain, *Phys. Rev. Lett.* **71**, 153 (1993); K. Park and J.K. Jain, *Phys. Rev. Lett.* **80**, 4237 (1998).

[86] V. Fock, Z. Phys. **47**, 446 (1928); C.G. Darwin, Proc. Cambridge Philos. Soc. **27**, 86 (1930).

[87] J.K. Jain, Phys. Rev. Lett.**63**, 199 (1989); Physics Today **53**(4), 39 (2000); *Composite Fermions* (Cambridge University Press, 2007).

[88] S.S. Mandal and J.K. Jain, Phys. Rev. B**66**, 155302 (2002).

[89] V.M. Bedanov and F.M. Peeters, Phys. Rev. B**49**, 2667 (1994); V.A. Schweigert and F.M. Peeters, *ibid.* **51**, 7700 (1995); F. Bolton and U. Rössler, Superlatt.

Microstruct. **13**, 139 (1993); A.V. Filinov, M. Bonitz, and Y.E. Lozovik, Phys. Rev. Lett.**86**, 3851 (2001).

[90] C.-C. Chang, G.S. Jeon, and J.K. Jain, Phys. Rev. Lett.**94**, 016809 (2005).

[91] K. Maki and X. Zotos, Phys. Rev. B**28**, 4349 (1983).

[92] K. Park, V. Melik-Alaverdian, N.E. Bonestel, and J.K. Jain, Phys. Rev. B **58**, R10167 (1998).

[93] R.H. Morf, Phys. Rev. Lett. **80**, 1505 (1998).

[94] V.W. Scarola, J.K. Jain and E.H. Rezayi, Phys. Rev. Lett. **88**, 216804 (2002).

[95] S. Das Sarma, M. Freedman, and C. Nayak, Phys. Rev. Lett. **94**, 166802 (2005); A. Stern and B. I. Halperin, *ibid.*, **96**, 016802 (2006).

[96] Y. W. Suen, L. W. Engel, M. B. Santos, M. Shayegan, and D. C. Tsui, Phys. Rev. Lett. **68**, 1379 (1992).

[97] J.P. Eisenstein, G.S. Boebinger, L.N. Pfeiffer, K.W. West, and S. He, Phys. Rev. Lett. **68**, 1383 (1992).

[98] L. Brey and H.A. Fertig, Phys. Rev. B**62**, 10268, (2000).

[99] D.-W. Wang, E. Demler and S. Das Sarma, Phys. Rev. B**68**, 165303 (2003).

[100] A.A. Koulakov, M.M. Fogler, and B.I. Shklovskii, Phys. Rev. Lett. **76**, 499 (1996).

[101] G.M. Gusev, A.K. Bakarov, T.E. Lamas and J.C. Portal, Phys. Rev. Lett.**99** 126804 (2007).

[102] M.P. Lilly, K. B. Cooper, J.P. Eisenstein, L.N. Pfeiffer, and K. W. West Phys. Rev. Lett. **83**, 824 (1999).

[103] W. Pan, R.R. Du, H.L. Stormer, D.C. Tsui, L.N. Pfeiffer, K.W. Baldwin, and K.W. West, Phys. Rev. Lett. **83**, 820 (1999).

[104] J.K. Jain and R.K. Kamilla, Phys. Rev. B **55**, R4895 (1997).

[105] J.K. Jain and R.K. Kamilla, Int. J. Mod. Phys. B **11**, 2621 (1997).

[106] N. Metropolis, A. Rosembluth, M. Rosembluth and A. Teller, J. Chem. Phys. **21**, 1087-1092 (1953).

[107] We have performed calculations with two different approximations for the interaction, containing three and four parameters (Eqs. A.18). While both are accurate, the latter is slightly better, but gives significantly larger uncertainty in the energy for a given number of Monte Carlo sampling steps. We find that the energies obtained from these interactions are indistinguishable in the parameter region of interest (i.e., near the phase boundary). For very large widths ($w \approx 4.5$), the energy differences between the two methods are larger, but still do not affect the energy ordering of various wave functions. (For example, at $w = 4.5$, the interaction with three free parameters gives $E = -0.47768(13)$ and -0.48029(3) for the CFFS and Pf wave functions, while the interaction with four free parameters interaction gives $E = -0.4780(11)$ and -0.48027(56) respectively.)

[108] R. Morf, and B.I. Halperin Z.Phys.B **68** 391 (1987).

Vita

Chuntai Shi

Education

- B.S. Physics, Nankai University, Tianjin, China, 1999.
- M.S. Physics, Institute of Theoretical Physics, Chinese Academy of Sciences, Beijing, China, 2002.
- Ph.D. Physics, The Pennsylvania State University, University Park, PA, USA, *expected* 2009.

Publications

- Jainendra K. Jain and Chuntai Shi, Resonant Tunneling in the fractional Quantum Hall Effect: Superperiods and Braiding Statistics, Phys. Rev. Lett. 96, 136802 (2006).
- Chuntai Shi, Gun Sang Jeon, and Jainendra K. Jain, Composite fermion solid and liquid states in two component quantum dots , Phys. Rev. B 75, 165302 (2007)
- Chuntai Shi, Shivakumar Jolad, Nicolas Regnault, and Jainendra K. Jain, Phase diagram for bilayer quantum Hall effect at total filling ν_T=5 , Phys. Rev. B 77, 155127 (2008)
- Csaba Tőke, Chuntai Shi, and Jainendra K. Jain, States of interacting composite fermions at the Landau level filling ν=2+3/8 , Phys. Rev. B 77, 245305 (2008).
- Jian Wang, Chuntai Shi, Mingliang Tian, Qi Zhang, Nitesh Kumar, J. K. Jain, T. E. Mallouk, and M. H. Chan, Proximity-Induced Superconductivity in Nanowires: Minigap State and Differential Magnetoresistance Oscillations, Phys. Rev. Lett. 102, 247003 (2009).